Représentation reconstruction adaptative des hologrammes numériques

Kartik Viswanathan

Thèse

UNIVERSITE
BRETAGNE
LOIRE

THESE INSA Rennes
sous le sceau de l'Université Bretagne Loire
pour obtenir le titre de
DOCTEUR DE L'INSA RENNES
Spécialité : Traitement du signal et de l'image

présentée par

Kartik VISWANATHAN

ECOLE DOCTORALE : *MATISSE*
LABORATOIRE : *IETR UMR 6164*

Représentation et reconstruction adaptative des hologrammes numériques

Thèse soutenue le 01.12.2016
devant le jury composé de :

Atilla BASKURT
Professeur des Universités, INSA Lyon / Président
Frédéric DUFAUX
Directeur de recherche CNRS, L2S, Gif-sur-Yvette/ Rapporteur
Marc ANTONINI
Directeur de Recherche CNRS, I3S, Sophia Antipolis/ Rapporteur
Patrick GIOIA
Ingénieur de Recherche, Orange Labs Rennes / Encadrant de thèse
Luce MORIN
Professeur des Universités, INSA Rennes / Directrice de thèse

Représentation et reconstruction adaptative des hologrammes numériques

Kartik VISWANATHAN

Orange Labs, Rennes

INSTITUT NATIONAL DES SCIENCES APPLIQUEES DE RENNES

Adaptive representation and reconstruction of digital holograms

by

Kartik Viswanathan

A thesis submitted in partial fulfillment for the
degree of Doctor of Philosophy

in the
INSTITUT D'ELECTRONIQUE ET DE TELECOMMUNICATIONS DE RENNES

December 2016

Declaration of Authorship

I, Kartik Viswanathan, declare that this thesis titled, 'Adaptive representation and reconstruction of digital holograms' and the work presented in it are my own. I confirm that:

- This work was done wholly or mainly while in candidature for a research degree at this University.
- Where any part of this thesis has previously been submitted for a degree or any other qualification at this University or any other institution, this has been clearly stated.
- Where I have consulted the published work of others, this is always clearly attributed.
- Where I have quoted from the work of others, the source is always given. With the exception of such quotations, this thesis is entirely my own work.
- I have acknowledged all main sources of help.
- Where the thesis is based on work done by myself jointly with others, I have made clear exactly what was done by others and what I have contributed myself.

Signed: _____

Date: _____

"People are wonderful one at a time. Each one of them has an entire hologram of the universe somewhere within them"

George Carlin

INSTITUT NATIONAL DES SCIENCES APPLIQUEES DE RENNES

Abstract

INSTITUT D'ELECTRONIQUE ET DE TELECOMMUNICATIONS DE RENNES

Doctor of Philosophy

by Kartik Viswanathan

With the increased interest in 3D video technologies for commercial purposes, there is renewed interest in holography for providing *true*, *life-like* images. Mainly for the hologram's capability to reconstruct all the parallaxes that are needed for a truly immersive views that can be observed by anyone (human, machine or animal). But the large amount of information that is contained in a hologram make it quite unsuitable to be transmitted over existing networks in real-time. In this thesis we present techniques to effectively reduce the size of the hologram by *pruning* portions of the hologram based on the position of the observer. A large amount of information contained in the hologram is not used if the number of observers of an immersive scene are limited. Under this assumption, parts of the hologram can be pruned out and only the requisite parts that can cause a diffraction at an observer point can be retained. For reconstructions these pruned holograms can be propagated numerically or optically. Wavelet transforms are employed to capture the localised frequency information from the hologram. The selection of the wavelets is based on the localisation capabilities in the space and frequency domains. Gabor and Morlet wavelets possess good localisation in space and frequency and form good candidates for the view based reconstruction system. Shannon wavelets are also employed for this cause and the frequency domain based application using the Shannon wavelet is shown to provide fast calculations for real-time pruning and reconstruction.

Acknowledgements

Throughout the history of human civilisation, we humans have learnt, evolved and built our understanding of the universe and everything around us based on the works of millions of ancestors and most importantly the teacher. In my ethinic culture a prayer goes as follows:

Guru Brahma Gurur Vishnu Guru Devo Maheshwaraha Guru Saakshat Para Brahma
Tasmai Sree Gurave Namaha

which translates as, a Guru(teacher) is verily the representative of Brahma, Vishnu and Shiva. He creates, sustains knowledge and destroys the weeds of ignorance.

For years I have mumbled this *mantra* without realising its true importance. Today as a guardian to two young souls I recognise its true meaning.

In this context I would like to dedicate this thesis to all teachers and thank all of them for shaping my life into what it is now. I would like to thank my parents who are my first teachers and who put up with all my idiosyncracies no matter what. I would like to thank all my professors in school and college for their duty bound efforts. A special thanks to all the teachers on Youtube who provide lectures for free, without whom this thesis would not have been possible.

Pertaining to this thesis, I would like to thank Prof. Luce MORIN (INSA, IETR) and Dr. Patrick GIOIA (Orange Labs) for their support and guidance in this work. I special thanks to Prof. Levent ONURAL (Bilkent University, Turkey) for hosting me for 3 months as a visiting student.

I would also like to thank Orange Labs and INSA for giving me this opportunity.

Contents

List of Figures

List of Tables

Dedicated to Prof. Hoshang Moogat (1934 - 2013)

Chapter 1

Introduction

Holographic three-dimensional display technology is an exciting field that attracts a lot of attention of scientists and public alike. The expectation of observing the real *life-like* world through a recording medium has piqued the interest of many a people, and scientists have since a long time tried to provide a solution to this need.

One of the interesting recent developments that is used commercially in movie theatres and high end televisions is the concept of stereoscopic vision. But this technique is very jarring to the human visual system as the depth parallax perceived by the brain and the eye is never consistent. This causes discomfort and eye strain in a large number of people. Yet this technology, even though not true 3D in nature is widely accepted as a commercial product. This shows the immense interest in the 3D display field by the public.

Over the years, there have been great improvements in the understanding of the behavior of light and using this, scientists and engineers have been able to reproduce the physical properties of light filling up a volume. This in essence is the *true* or immersive 3D technology. Holography is one of the most sophisticated true 3D imaging technologies, where we can record and replay any 3D scene with all the relevant physical properties of light. What this means, is that the reconstruction from a hologram would be so *life-like*, that irrespective of the observer (human, animal, camera etc.), they can perceive the scene as if it were really there.

Holographic displays are not as mature as stereoscopic displays today, but we feel that the former are more superior and desirable, even though the technology is more challenging. Moreover there is the inherent issue of bandwidth limitations. Today when digital copies of media fly through the wired pathways of networks and the Internet, there is always a concern on the cost of transmitting such information. This dissertation

is dedicated to overcome the challenges of transmitting digital holograms by *pruning* certain portions of the hologram based on certain physical parameters like position of the observer and reconstructing the part at the observer end.

The development of such a holographic display needs an understanding of the physical properties of light. How light propagates through space and how light is reflected and diffracted and refracted from a 3D object. This scattering of light carries the geometric and optical information of the 3D object and fills the 3D space. The physical properties of this *light field* that fills the 3D space need to be captured to regenerate the same light field at another place and another time. This captured information is *large* and needs to be efficiently reduced (pruned and compressed) before it can be used for today's networks for transmission.

This dissertation focusses on the efficient pruning of the holograms based on the position of the observer using wavelet transforms. The choice of the wavelet transforms is unique since conventional wavelets are not suitable for this type of display system. Our proposed display system emphasizes on the use of well-localized wavelets in space and frequency, and hence special wavelets need to be considered.

1.1 Contributions of this thesis

The following contributions are made in this thesis

- *A proposition of a display setup for a view based representation and reconstruction setup for holograms*: We propose a framework for a display setup which produces reconstructions based on the position of the observer by pruning portions of the hologram.
- *A comparison between Gabor wavelets and Fresnelets with respect to their usage for view based representation*: We provide a comparative analysis between Fresnelets and Gabor wavelets and show that Gabor wavelets are more suited for view-dependent representation of holograms.
- *Modification of the Gabor basis function to form the Morlet wavelet*: We modify the Gabor basis function to form the Morlet wavelet and show its implementation and evaluation in the view based system.
- *Proposition of the Shannon wavelet for the view based system*: We propose the use of Shannon wavelets for the view-based representation system, and show an implementation and evaluation of the same.

- *Fast implementation of the Shannon wavelet for generating the sub-holograms and reconstructing them in real-time*: We propose an optimized method of implementing the Shannon wavelet for obtaining real-time encoding and decoding of holograms for the view based representation system.
- *GUI for demonstrating the view based system*: We provide a GUI interface for loading, wavelet transforming and displaying the reconstructions based on the position of the observer.

1.2 Organization of the thesis

The organization of the thesis is as follows:

- Chapter 2 provides a history of holography. We shall discuss in brief the advent of Optical holography, Digital holography and Digital holographic displays. We shall provide a short overview of scalar diffraction theory which forms the mathematical backbone for the numerical reconstructions in this thesis.
- Chapter 3 we present the State of the art in the compact representation of holographic data. We shall see the conventional methods of compression being used for holograms (lossy and lossless methods). We will see the various wavelets that are used for compressing the holograms and introduce the view-dependent approach of representing holograms. We shall provide the requirements for such a view-based representation and formulate some basic requirements for the wavelets that need to be used for a view-based representation system. In the next chapters we shall discuss and use three wavelets for our view-based system namely
- Chapter 4 discusses Gabor wavelets for view based representation of holograms and compare it Fresnelets on the basis of localization in space and frequency.
- Chapter 5 discusses the Morlet wavelets and their implementation in a view based representation and reconstruction setup.
- Chapter 6 discusses Shannon wavelets and the increase in computational performance achieved by their usage in our implementation.
- Chapter 7 we will provide the real-time setup and GUI of the software we developed and some results to validate our claims. We end with Chapter **??** to elaborate the conclusions and future work.

1.3 List of Publications

The following publications were done during the course of this thesis.

Publication-I K.Viswanathan, P.Gioia, L.Morin, "*Wavelet compression of holograms: Towards view-dependent frameworks*," SPIE Applications in digital image processing, 36(8856):1-10, October 2013

Publication-II K.Viswanathan, P.Gioia, L.Morin, "*Morlet wavelet transformed holograms for numerical adaptive view-based reconstruction*," SPIE Optics and Photonics for Information Processing, 8(9216):1-14, October 2014

Publication-III K.Viswanathan, P.Gioia, L.Morin, "*A framework for View-dependent hologram representation and adaptive reconstruction*," IEEE ICIP , September 2015

1.4 Patents

- Procede de traitement d'une sequence d'images holographiques en vue d'une transmission d'un angle de vue particulier de la scene holographique
- Holographic data representation using Shannon wavelets for view based systems

Chapter 2

Introduction to Holography

In this chapter we will present a historical background of holography (2.1). We shall then in the following sections of this chapter discuss briefly some of the methods that are used for hologram generation and reconstruction, for Optical holography (2.2), Digital holography (2.3.1) and Computer Generated Holograms (2.3.2). We shall then mention some existing hologram display technologies in (2.3.3). The last section of this chapter will give the basics of scalar diffraction theory (2.4) that forms the basis for all numerical reconstruction algorithms used in the thesis.

2.1 Short history of holography

This section has been written from the survey paper [1] by Yaras et al.. Holography was first presented in 1948 by Denis Gabor to avoid aberrations in electron microscopy by recording and reconstructing amplitude and phase of a wave field [2–4]. He created the word *hologram* from the Greek word 'holos' meaning whole and 'graphein' meaning to write.

The interference pattern between a wave fields scattered from the object and a coherent, monochromatic reference wave results in a holographical image that can be recorded photographically or otherwise. It contains information from the entire three-dimensional wave field i.e. all the depth cues [5] perceivable are present. *Hologram Generation* is the process of recording a wave field as a 2D interference pattern. The object wave can be reconstructed by illuminating the hologram with the reference wave again. This reconstructed wave is identical to the original object wave. *Hologram reconstruction* refers to this process of regenerating a 3D wave field from the hologram.

However at that time the monochromatic coherent light sources were not present, hence the quality of the images obtained were unsatisfactory. Gabor illuminated in his original setup the hologram by a parallel beam through a mostly transparent object. The axes of the object wave and reference wave were parallel. This is called *inline* holography. The reconstruction of this hologram results in the real image superimposed by undiffracted part of the reconstruction wave and the so called *virtual* image lying on the optical axis. People began to lose interest in holography in general. After the development in laser technologies, holography came to the forefront again. In 1962 Yuri Denisyuk in the Soviet Union and Emmett Leith and Juris Upatnieks at the University of Michigan, USA enabled the first practical holograms that recorded 3D objects by introducing an *off-axis* reference wave. The results of the 3D holograms were so stunning that people began to see the potential of holography for 3D video [6, 7]. In 1967, Lohmann and Paris generated holograms on a digital computer [8, 9]. In 1980, Iaroslavskii and Merzlyakov formulated the theory of Computer Generated Holograms [10], which generates artificial holograms by numerical methods. Later these computer generated holograms are reconstructed optically [11].

Digital hologram reconstructions were carried out by Goodman and Lawrence first in 1967 [12] by enlarging parts of in-line and Fourier holograms that are recorded on a photographic plate and sampling them, and then numerically reconstructing these digitized holograms [13]. Later Schnars and Juptner [14] created a method for direct recording of holograms on CCDs (charged coupled devices). This technique is called as Digital Holography (DH). Although the terms CGH and DH are used quite interchangeably these days, this thesis will differentiate a Digital Hologram as a hologram obtained by optical means on a CCD, and a Computer Generated Hologram (CGH) is obtained by numerical methods on a computer. Throughout this thesis we will be working only on Computer Generated Holograms.

2.2 Optical Holography

Holography is a lens less imaging process that Gabor called *wavefront reconstruction.* Whenever a suitable coherent reference wave is present simultaneously with the light diffracted or scattered from an object, then information about both amplitude and phase of the diffracted or scattered waves can be recorded in spite of the fact that recording mediums respond only to light intensity. This *interference* of the coherent reference light with the diffracted or scattered light from the object, when recorded on a recording medium is called as a Hologram.

The recording material of such a hologram is assumed to give a linear mapping of the intensity incident during the detection process into amplitude transmitted by or reflected from the material during the reconstruction process. Hence a photographic plate can provide this characteristic by operating in the linear portion of the t_A vs E curve of the emulsion.

2.2.1 In-axis optical holography

The initial *wavefront reconstruction* process proposed by Gabor is as shown in figure (2.1,2.2).

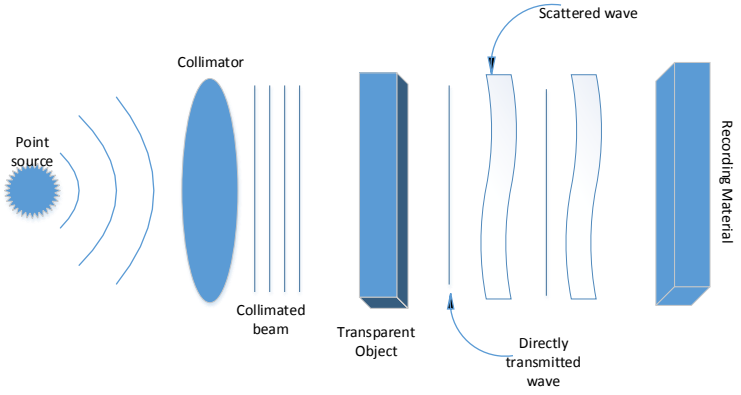

FIGURE 2.1: Gabor hologram generation

This was the first example of an on-axis hologram recording and reconstruction setup. The intensity distribution on the recording material is given as

$$I(x,y) = |A|^2 + |a(x,y)|^2 + A^* a(x,y) + A a^*(x,y), \tag{2.1}$$

where,

$$A(x,y) = |A(x,y)| \exp[-j\psi(x,y)] \tag{2.2}$$

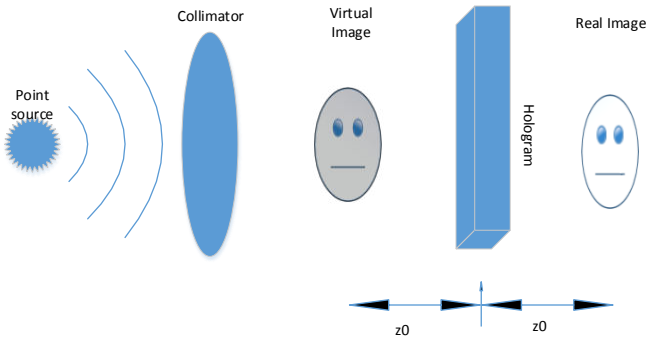

FIGURE 2.2: Gabor hologram reconstruction

is the reference wave and,

$$a(x,y) = |a(x,y)| \exp[-j\phi(x,y)] \tag{2.3}$$

is the diffracted wavefront from the object that needs to be reconstructed. '$*$' denotes the complex conjugate. The recording process needs that the object is a transparent one having a transparency denoted by t_0. Due to this the object provides its own reference wavefront of directly transmitted light A. The interference with the scattered light results in a pattern of intensity that depends on both the amplitude and the phase of the scattered wave $a(x,y)$. The developed recording material will have amplitude transmittance t_A that is proportional to exposure. The slope of this linear region of the t_A vs E curve is given as β and the product of β and the exposure time is denoted as β'. t_b is the transmittance of the emulsion before developing:

$$t_A(x,y) = t_b + \beta'(|a|^2 + A^*a + Aa^*). \tag{2.4}$$

Consider the recording material to be illuminated by a normally incident plane wave with uniform amplitude B, the resulting transmitted field consists of four terms:

$$Bt_A = Bt_b + \beta' B|a(x,y)|^2 + \beta' A^* Ba(x,y) + \beta' ABa^*(x,y) \tag{2.5}$$

The first term is a uniformly attenuated plane wave that passes through the hologram with no scattering. The second term can be dropped only if, $A >> |a(x,y)|$. This condition is satisfied if the object is in majority transparent. The third term is proportional to $a(x,y)$. This defines the *virtual image* of the object and is at distance z_0 from the hologram. The fourth is proportional to $a^*(x,y)$, which defines the *real image* at distance $-z_0$ from the hologram.

There are some serious drawbacks of using this type of a hologram.

- Highly transparent object is needed for this type of hologram. If the object is more opaque than transparent, then $A << |a(x,y)|$. This will result in the second term of equation(2.5) to be large and greatly interfere with the other wave components.
- The virtual image, real image and the attenuated non-diffracted components of the reconstructed wave are in the same line. When the virtual image is brought to focus, it is always accompanied by the real image which is out of focus. The quality is thus reduced by this *twin image* issue. Removal of this twin image has remained a persistent area of research ever since.

2.2.2 Off-axis optical holography

In the early 1960's Leith and Upatnieks introduced the concept of the "offset reference" hologram [6]. The idea was that the reference wave A and the diffracted object wave $a(x,y)$ would not lie on the same optical axis. The reference wave is at angle Φ with respect to the optical axis, while the diffracted object wave lies on the optical axis. The amplitude distribution at the detector due to the reference wave and diffracted wave is given as:

$$U(x,y) = A\exp[-j2\pi\alpha y] + |a(x,y)|\exp[-j\phi(x,y)] \tag{2.6}$$

where

$$\alpha = \frac{\sin\Phi}{\lambda} \tag{2.7}$$

and λ is the wavelength of the incident light. Figure(2.3) shows one possible geometry for the recording of a Leith-Upatnieks hologram.

The intensity distribution across the recording plane is:

$$I(x,y) = |A|^2 + |a(x,y)|^2 + 2|A||a(x,y)\cos[2\pi\alpha y - \phi(x,y)]| \tag{2.8}$$

Hence it can be observed that the amplitude and phase of the object wavefront have been recorded as modulations of the spatial carrier frequency α.

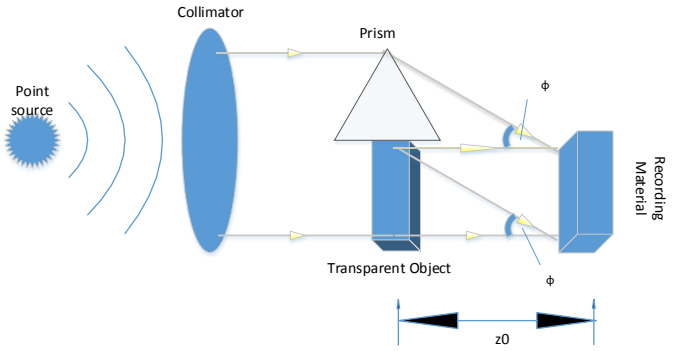

FIGURE 2.3: Off-axis Hologram Generation

For obtaining the reconstruction figure(2.4), the photographic plate is developed and it has transmittance given as:

$$t_A(x,y) = t_b + \beta'[|a(x,y)|^2 + A^* a(x,y)\exp(j2\pi\alpha y) + Aa^*(x,y)\exp(-j2\pi\alpha y)] \quad (2.9)$$

When this film is illuminated by a normally incident uniform plane wave of amplitude B, the transmitted field is given as:

$$U_t = t_b B + B\beta'|a(x,y)|^2 + B\beta' A^* a(x,y)\exp(j2\pi\alpha y) + B\beta' A a^*(x,y)\exp(-j2\pi\alpha y) \quad (2.10)$$

Again it is observed that there are 4 components as with the Gabor hologram. The first term is the attenuated plane wave that passes down the optical axis. The second term is spatially varying hence it will have components that will travel at various angles with respect to the optical axis. But if the bandwidth of $a(x,y)$ is small compared to the carrier frequency α, the energy of this component will be localized close to the optical axis. The third component is the original object wavefront a multiplied by a linear exponential factor. The virtual image is generated at a distance z_0 from the hologram deflected from the optical axis by an angle Φ. The fourth term is similarly the real image that is at an angle of Φ from the optical axis but at a distance $-z_0$ from the hologram.

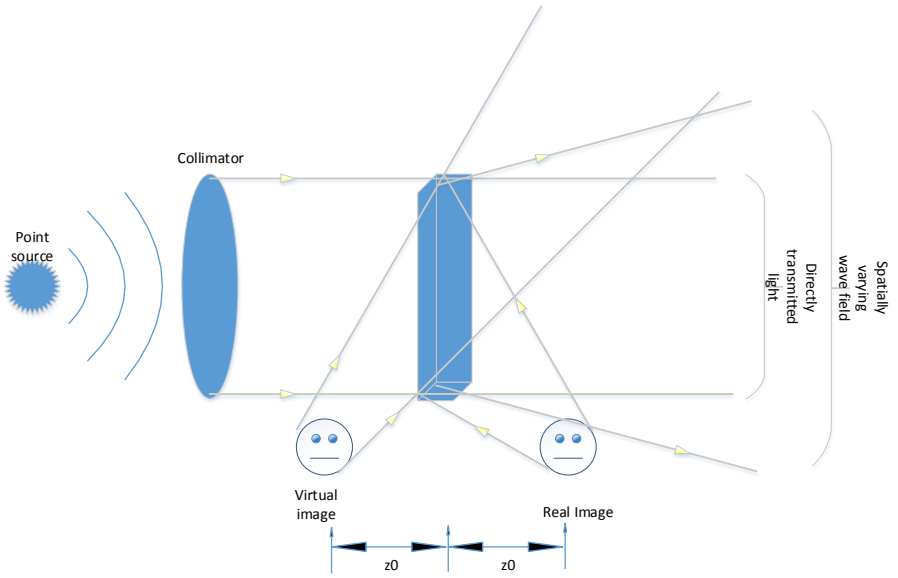

FIGURE 2.4: Off-axis Hologram Reconstruction

The advantage of this process is that the twin-images that are generated are angularly separated from one another and the other wave components. This angular separation allows the spatially filtering of the unwanted wave components by use of lenses and stops. However there is a limitation to the minimum angle Φ that is required between the reference wave and the optical axis. This is given as:

$$\Phi = \sin^{-1} 3F\lambda \tag{2.11}$$

where F is the maximum spatial frequency components of the object in cycles/mm. Later in 1964 Leith and Upatnieks extended their technique to 3-dimensional imagery due to the use of the He-Ne laser which has high spatial and temporal coherence [7].

There are several other configurations of generating holograms, mainly based on the where the hologram is recorded. Like Fresnel holograms, Fraunhofer holograms, Image holograms and Fourier holograms. The reader is advised to read Hariharan's book [15] to have a detailed view at these holograms. Next we try to classify the holograms based on the type of recording material.

2.2.3 Reflection holograms and transmission holograms

For most of the holograms used so far the recording material has been transmissive in nature. Usually these are wavelength tolerant i.e. a reasonable reconstruction can be obtained even if we do not duplicate the reference wave during reconstruction. But white light cannot be used for reconstruction, since it results in *chromatic blur*. There is also the possibility of using holograms that are reflective. Usually these are holograms that are generated by recording the *standing* interference pattern. This is similar to standing waves found in acoustics. This method of generating holograms was first described by Y. Denisyuk in 1962 [16]. The emulsion is placed in between the reference wave and the object. The reference wave is diffracted from the object and creates a standing interference with the reference wave at the emulsion. Such a hologram can be reconstructed using white light because this hologram is highly wavelength selective in nature. However the wavelength during the reconstruction can change due to the shrinking of the emulsion during development, i.e. a hologram that is normally generated by using a red laser will be reconstructed in green color. The figure(2.5) shows the Denisyuk hologram generation and reconstruction.

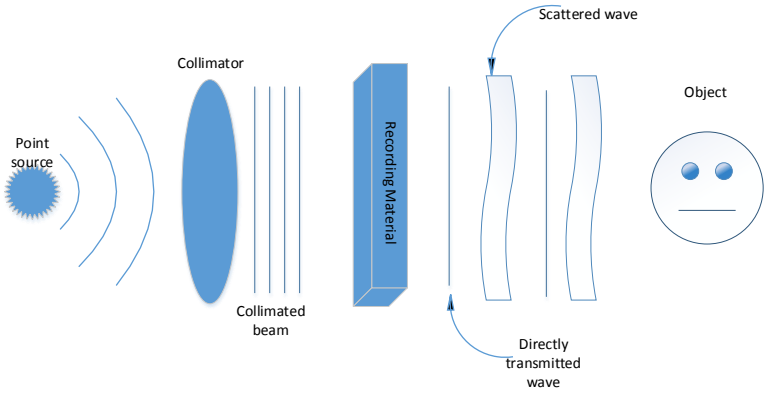

FIGURE 2.5: Denisyuk Hologram

2.2.4 Thick, thin emulsions, plane holograms and volume holograms

Another classification to discuss in classical optical holography is the thickness of the emulsion. This is because reconstructions will be different based on the period of the fringes that are recorded and the thickness of the emulsion. The importance of the third dimension i.e. depth was recognized by Denisyuk and Van Heerden [16]. A hologram could be considered as a thin diffracting structure only if the optical thickness is less than one wavelength. But this is not the case generally. If the finest fringe is larger than the thickness of the hologram then the hologram behaves as a two dimensional diffracting structure. But if the finest fringe is smaller than the thickness of the hologram, then it behaves as a three dimensional diffracting structure. A hologram in general will exhibit both properties of thin and thick diffraction gratings and hence it becomes necessary to view the hologram as a volume grating. This is important because it is related to the formation of random dark and bright spots in the reconstruction called as *speckles*. Speckles are generated when the height variations (fringes recorded) are larger than the wavelength of light. Light is scattered from the surface points of uneven heights and the scattered waves form stationary speckle patterns due to interference among themselves. The mathematics of the field obtained by such a volume grating is beyond the scope of this thesis, since optical holography is only discussed here for the matter of completeness. The reader is encouraged to read the works of Goodman [17], Hariharan [15] for a detailed understanding of optical holography.

2.3 Numerical Holography

2.3.1 Digital Holography

Holograms for digital holography have the similar setup as optical hologram generation, but instead of the film, the interference pattern is captured using a CCD (charged coupled device) [18]. A digital hologram is generated when the interference pattern is recorded on the surface of a CCD. The resulting hologram is electronically recorded and stored, however using these CCDs results in several disadvantages as compared to conventional films. Conventional holographic films offer full-parallax and excellent resolution which is in the order of thousands of lines/mm. However such a resolution is not yet possible for electro-holographic recording [1, 18]. Another difculty arises due to pixelated structures. Compared to wavelength of the visible monochromatic light, pixels are not small enough to yield sufcient viewing angles. The relationship between the *period* (Λ) of a grating (spacing between interference patterns), and the angle of

diffraction (θ) is given by the *grating equation*.

$$\sin\theta = \frac{\lambda}{\Lambda} \tag{2.12}$$

where λ is the wavelength of the incident light.

One of the advantages of digital recordings is the sensitivity of CCD cameras is typically $10e^{-4}J/m^2$ to $10e^{-3}J/m^2$, which is better than the sensitivity of photographic emulsions used for classical holography [18]. The spectral range reaches approximately from 400nm to 1000nm. Also photographic films used in conventional holography need an intensity ratio between the reference wave and object wave to be 5:1 to 10:1 in order to avoid the non-linear effects in the recording medium. But the ideal case is to have a intensity ratio of 1:1 according to interference theory. This is possible with digital holography [18].

The major advantage of using digital holograms is the ability to use numerical reconstruction techniques to reconstruct from these holograms which offers many improvements like suppression of unwanted orders, removal of artifacts and usage of liquid crystal devices (LCDs) and Spatial light modulators (SLMs) for modern holographic display systems becomes possible due to digital hologram recording.

A Spatial light modulator (SLM), depending on the media is classified as:

- Phase only: Modulate only phase of incoming wavefront, amplitude equals unity
- Amplitude only: Modulate only amplitude of incoming wavefront, phase is constant
- Complex: Modulate both phase and amplitude of incoming wavefront

2.3.1.1 Phase-shift Digital Holography

Phase-shift interferometric (PSI) holography [19] originated from object and pattern recognition, and from the need to not rely on chemical processing and mechanical focusing of recording materials. This is an important form of digital hologram generation techniques since several compression methods exploit this type of holograms 3.1.1. A typical setup of generating a PSI hologram is as shown in the figure (2.6).

A two beam interferometer is used where a laser beam is divided into two paths. The first path contains the object beam while the second contains the reference beam. The reference wavefront is obtained from a piezoelectric transducer mirror, which has the ability to phase shift the reference beam. The interference pattern of the object and reference wavefront are taken four times by the CCD camera, each time with a different

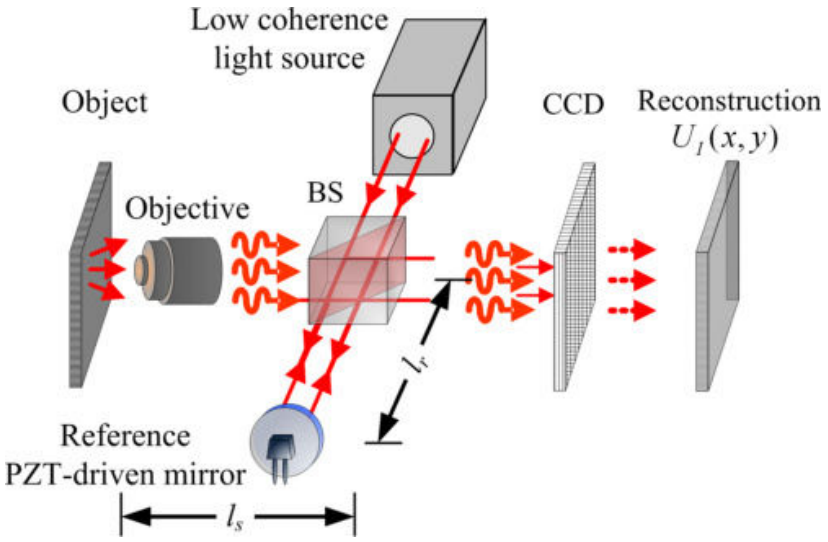

FIGURE 2.6: Phase-shift interferometry hologram generation and reconstruction (image from wikipedia)

phase. The four interference patterns will vary successively by $\pi/2$. Hence the four intensities that are captured are denoted as $I_0, I_{\pi/2}, I_\pi, I_{3\pi/2}$.

The phase of the real image is then given as:

$$\phi_{real} = \frac{I_{3\pi/2} - I_{\pi/2}}{I_0 - I_\pi} \tag{2.13}$$

The advantage of this technique is the possibility to isolate the real image from the other contributions. Hence the quality of the reconstructions is superior to other available techniques. The disadvantage is that several captures are needed for the same object/scene, and the phase-shifts must be accurate.

2.3.2 Computer Generated Holograms

A Computer Generated Hologram (CGH) can generated from a synthetic object (3D model) and the role of the diffractive optical element (DOE) can be realized mathematically. To form a CGH means to calculate a complex transmittance.

A DOE used to store this disturbance is usually an electro-optical device like a SLM. Based on the type of the SLM, we can either store the amplitude, the phase or both. Diffractive Optical Elements are simply another tool to construct optical systems. They are smaller, lighter and can do certain things (like diffraction) that normal refractive optical elements cannot. In laser optics these devices are used extensively in the field of

beam shaping where they reduce the amount of wasted light [20]. We are interested in the numerical representation of DOEs.

The advantage of using numerical algorithms to represent DOEs, is that the images computed will be aberration free and the possibility of using radiations for which no physical lenses exist. Analytical solutions do not exist for many designs of DOEs so an alternative method is required. Iterative projection algorithms are successfully being used as a a substitute of lenses to recombine, numerically rather than optically [21]. The traditional method for designing a DOE is using the Iterative Fourier Transform Method(IFTA)[22][23][24].

The iterative algorithms in essence provide solution to the *Phase retrieval problem*. When we record a diffraction pattern, we record the intensity that is scattered. The phase information is missing. The general approach for phase retrieval was first presented by Gerchberg and Saxton [25]. Now it has evolved into a large bunch of related iterative algorithms with a broad spectrum of applications, including generation of phase holograms. The Gerchberg-Saxton (GS) algorithm, utilizing the fact that the wavefield is reversible, projects the wavefield back and forth between object plane and image plane repeatedly and applies certain constraints in each iteration. Chang, Xia and Jiang [26] used the GS algorithm to generate a CGH by modulating an image on tilted planes.

To generate complex holograms (amplitude and phase information together), the *Point Light Method* [27] [28] is widely used. Here the virtual objects are considered to be groups of independent point light sources. We define the *i-th* point light coordinate as (x_i, y_i, z_i) and the coordinates of the hologram as $(x_h, y_h, 0)$. The complex amplitude distribution on the hologram due to the *i-th* point light source is,

$$u_i(x_h, y_h, 0) = \frac{a_i}{r_i} \exp(-j(kr_i + \phi_i)) \tag{2.14}$$

where, a_i is the amplitude of the point light, r_i is the propagation distance from (x_i, y_i, z_i) to $(x_h, y_h, 0)$, k is the wavenumber, and ϕ_i is the initial phase of the point light. If there are N number of point light sources the complex amplitude distribution at the hologram will be

$$u(x_h, y_h, 0) = \sum_{i=0}^{N} u_i(x_h, y_h, 0) \tag{2.15}$$

2.3.3 Holographic Display Technologies

Today, liquid crystal devices are widely used for holographic reconstructions. Liquid crystal SLMs (Spatial Light Modulators) provide higher pixel density by having smaller pixel periods. In addition they allow for improved optical efficiency and faster operation

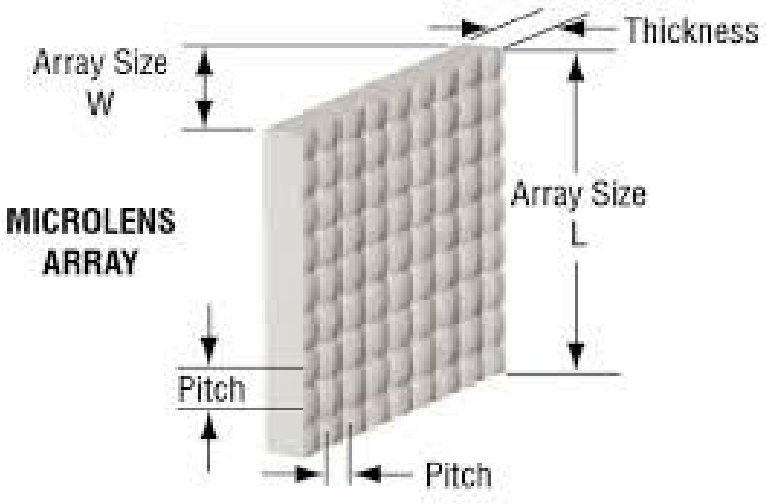

FIGURE 2.7: A Microlens array for Integral Imaging (*image from Wikipedia*)

[29]. Michalkiewicz et al. [30] discuss the improvements in liquid crystal on silicon (LCoS) SLMs. Frauel et al. [31] review holographic reconstructions by SLMs and the problems associated with 3D imaging applications. In [32], T.Ito et al. produced electro-holographic reconstructions that are illuminated by a LED. They managed to reconstruct a color hologram by use of a simple system with a set of red, green and blue LEDs as reference light.

All existing optical and semi-optical based contemporary reconstruction solutions of holograms are based on two technologies namely, Integral Imaging and Electro-holographic displays.

2.3.3.1 Integral Imaging based displays

Integral imaging is an *auto-stereo* method i.e. stereo imagery that is visible without the use of special glasses. It was first invented by Lippmann in 1908 [33]. As defined by Roberts and Smith in [34], an integral image consists of a tremendous number closely packed distinct micro-images, that are viewed with the help of an array of spherical convex lenses. Each micro-image is generated by one lens. This type of lens array is known as *integral* lens array. K.Choi et al. showed in [35, 36] that an integral image can accurately reproduce the wavefront that originated from the photographed or computer generated subject, like a hologram, without the need for lasers to perform the reconstruction . The term Integral comes from the integration of all the micro images into a complete three dimensional image through the lens array [37]. A micro-lens array is as shown in the figure(2.7).

Integral imaging systems consist of two stages. First a pick-up system to obtain elemental images of a 3D object or scene and a display stage which integrates the elemental images for reconstruction. Usually these parts are physical optical setups. The numerical feasibility of the integral imaging setup comes from the fact that the two stages can be separated. The pick-up stage will have a CCD array or digital camera that will capture the elemental images that are imaged by means of the micro-lens array. In the display setup, the reconstruction is observed on an LCD panel observed through a micro-lens array. In [38] methods are discussed for proper alignments and adjustments between the pick-up stage and display stage. Usually this work uses ray-optics as a basis and hence it is not an ideal reference for holographic data. For holographic data we need to look at the data from a wavefront point of view. That means we need to be able to create the elemental images based on the numerical wavefront propagation methods as discussed in section(2.4).

In [36], Onural et. al. do exactly this, by performing diffraction calculations using wave propagation methods based on the Fresnel kernel. Their results have shown that it is very much possible to create a holographic display system based on current generation integral imaging autosteroscopic 3D displays. The lenslet array is easily simulated on a LCoS SLM and by using either lasers or LEDs, a reconstruction based on integral imaging is possible.

2.3.3.2 Electro-holographic displays

After the discover of the liquid crustal (LC) in 1888 by Austrian botanist Friedrich Reinitzer [39], there has been its immense utilization in display technologies. Holograms are reconstructed easily these days using these display systems using these technologies. Here are some of the display systems that have been developed.

Holo-Video This was the first practical electro-holographic display developed by the Spatial Imaging Group at MIT Media Lab in 1989. This display made use of Acousto-Optical Modulators (AO-SLM) [40, 41]. This display could reconstruct volumes of $150mm \times 75mm \times 150mm$ ($W \times H \times D$) and 30 degrees of viewing angle at 2.5 fps.

QinetiQ This display system is the so called Active Titling System developed in 2003 [42]. It uses an EASLM (Electrically addressed Spatial Light Modulator) [43], and the non-pixelated structure of an OASLM (Optically Addressed Spatial Light Modulator) [44]. The EASLM acts as the image engine, to display the reconstruction. The OASLM

is used to store several de-magnified images of the EASLM. OASLMs uses intensity patterns to modulate light, whereas EASLMs use electrical signals to do so. The advantage of this display system is the possibility to display images or patterns with significantly large pixel counts than it was previously possible. Pixel densities of the order of 10^9 are possible with this setup.

Holografika These products are essentially not holographic systems. They are holographic diffusers. The pixels of a holographic scene emit light in different directions. These directed beams have different intensity and color values. These light beams hit the screen at various angles. The holographic screen then makes an optical transformation to generate a continuous 3D view with vertical parallax. The light beams emanating from the scene are under software control, as if they were emitted from the points of a 3D object at fixed spatial locations. They have presented 50 megapixel, 10 megapixel and 7.4 megapixel systems [45].

SeeReal This product line is especially interesting for us, since it use some concepts that are in line with our technique of representing holographic data. SeeReal devices make use of the concept of generating *sub-holograms* to make holographic data compact. We will be looking at this technology in detail in the following chapter.

2.4 Light wave propagation from holograms using Scalar diffraction theory

In this thesis, we use propagating optical waves to perform numerical reconstructions from holograms. There are many texts that are available that explain in detail the concepts of scalar diffraction theory. Most notable is the text on Fourier Optics by Goodman [17]. We provide a brief overview of the various developments in Scalar Diffraction Theory, as they will be used extensively in our work.

A hologram is in essence a diffraction grating and diffraction is phenomena in the realm of physical optics. There are two generally accepted definitions of diffraction:

- Any deviation of light rays from rectilinear (straight line) that cannot be interpreted as reflection or refraction
- Deviation caused by confinement of the lateral extent of the wave (obstruction of a wavefront) and its effects are most pronounced when the size of the confinement is comparable to the wavelength of light.

2.4.1 Fresnel-Kirchhoff theorem and Rayleigh-Sommerfeld theorem

Though we will not go into the details of the derivations of the diffraction equations, we would like to see the various mathematical preliminaries that form the basis of diffraction theory. Scalar optical diffraction theory deals with diffraction field relation between a planer surface and a point in space.

We begin with the Helmholtz equation which gives the basic relation that an optical wave must follow when propagating through free space.

$$(\nabla^2 + k^2)U_c = 0 \tag{2.16}$$

where ∇ is the Laplacian operator U_c is the phasor of a monochromatic wave and k is the angular wave number given as

$$k = \frac{2\pi\nu}{c} \tag{2.17}$$

where ν is the frequency of the wave.

Fresnel came up with several simplifications of the Helmholtz equation by the clever use of the Green's theorem [46]. The equation of interest for the field of holography is the Fresnel-Kirchhoff diffraction integral. It is the field obtained by the point source illumination of a plane screen with an infinitely small aperture. Figure(2.8). The field at P_0 denoted as $U_c(P_0)$, due to a point source at P_2 is given as,

$$U_c(P_0) = \frac{A}{i\lambda}\iint_{\Sigma}\frac{\exp(ik(r_{21}+r_{01}))}{r_{21}r_{01}}\left(\frac{\cos(\bar{n},\bar{r_{01}}) - \cos(\bar{n},\bar{r_{21}})}{2}\right)ds \tag{2.18}$$

where Σ is the area around the aperture, $\bar{n}$ is the vector perpendicular to Σ, and $\bar{r_{01}}$ and $\bar{r_{21}}$ are the distance vectors as shown in figure(2.8), In this equation, P_1 can be considered as the secondary source. But this equation considers 2 fundamental assumptions:

- The field and its first order derivative are equal and non-zero before the aperture (at Σ).
- The field and its first order derivative are zero after the aperture.

As shown in [47], Kirchhoffs theory of diffraction being inconsistent i.e. only working under the above mentioned assumptions and being false in certain very significant respects, is still quite successful in large variety of real world problems. This has been a reason of contention among several scientists for several years.

The inconsistencies of the Kirchhoff theory were removed by Sommerfeld and the formulation of the Rayleigh-Sommerfeld solution.

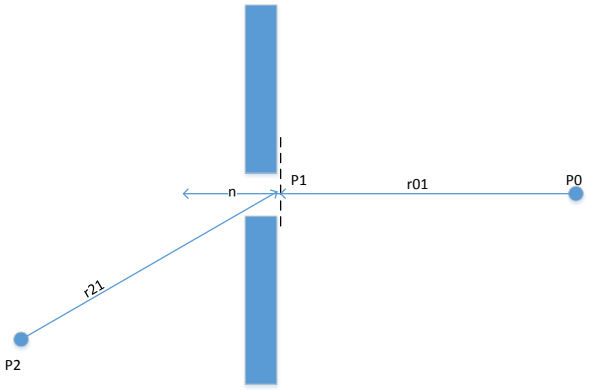

FIGURE 2.8: Fresnel-Kirchhoff Integral

The two solutions of Rayleigh-Sommerfeld and the Fresnel-Kirchhoff integral can be summerised in terms of an obliquity factor ψ. Equation(2.18) can be generalized as:

$$U_c(P_0) = \frac{A}{i\lambda}\iint_{\Sigma} U_c(P_1)\frac{\exp(ik(r_{21}+r_{01}))}{r_{21}r_{01}}\psi ds \tag{2.19}$$

where,

$$\begin{aligned}\psi &= \frac{1}{2}\cos(\bar{n},\bar{r}_{01}) - \cos(\bar{n},\bar{r}_{21}) \text{ Fresnel-Kirchhoff theory}\\ &= \cos(\bar{n},\bar{r}_{01}) \text{ First Rayleigh-Sommerfeld solution}\\ &= -\cos(\bar{n},\bar{r}_{21}) \text{ Second Rayleigh-Sommerfeld solution}\end{aligned} \tag{2.20}$$

2.4.2 Fresnel and Fraunhofer diffractions

Rather than observing the field from a point passing through an aperture as in the case of Rayleigh-Sommerfeld and the Fresnel-Kirchhoff integral, it is more beneficial to consider the field from a plane. Holograms are 2D planes consisting of several points (apertures), and we are interested in the propogations of wavefields originating from this plane. This simplifies the mathematical manipulations as compared to Rayleigh-Sommerfeld and the Fresnel-Kirchhoff integral by propogating a wave between 2 planes

and not considering each point on the hologram individually. This are referred to as Fresnel and Fraunhofer diffraction approximations. Figure(2.9) shows the coordinate system for optical wave propagation. In this figure $p_1 = (x_1, y_1)$ is in the source plane and $p_2 = (x_2, y_2)$ is in the observer plane. We need to evaluate the field $U(x_2, y_2)$ in the observer plane due to a field $U(x_1, y_1)$ in the source plane. In the sense of geometrical optics this in the paraxial approximation case, where the ray makes a small angle with respect to the optical axis. In terms of diffraction, it would mean a near field propagation or Δz (distance of propagation) is small. It is given as:

$$U(x_2, y_2) = \frac{\exp(ik\Delta z)}{i\lambda\Delta z} \int_{-\infty}^{\infty}\int_{-\infty}^{\infty} U(x_1, y_1) e^{\frac{ik}{2\Delta z}[(x_1-x_2)^2+(y_1-y_2)^2]} dx_1 dy_1 \tag{2.21}$$

This equation is called as the Fresnel Diffraction equation.

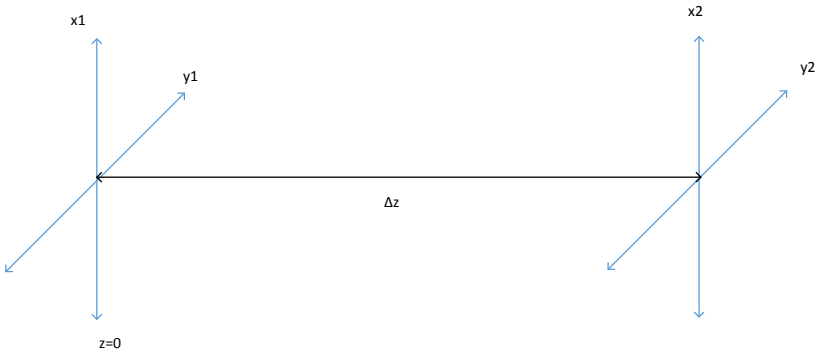

FIGURE 2.9: Diffraction between two planes

When we assume the propagation distance Δz to be very far, then we can approximate the quadratic phase factor in equation(2.21) as being flat. Specifically we must have $\Delta z > \frac{2D^2}{\lambda}$, where D is the maximum spatial extent of the source plane field. This gives us the Fraunhofer approximation.

$$U(x_2, y_2) = \frac{\exp(ik\Delta z) e^{\frac{ik}{2\Delta z}(x_2^2+y_2^2)}}{i\lambda\Delta z} \int_{-\infty}^{\infty}\int_{-\infty}^{\infty} U(x_1, y_1) e^{\frac{-ik}{\Delta z}(x_1x_2+y_1y_2)} dx_1 dy_1 \tag{2.22}$$

Diffractive optical elements (DOEs) like Spatial Light Modulators (SLMs) are used to perform these diffractions in the field of Computer Generated Holograms (CGHs)

- A Fourier DOE and Fourier lens to perform Fraunhofer diffraction, or
- A Fresnel DOE to perform free space propagation of light or Fresnel diffraction.

2.4.3 Angular Spectrum Diffraction

The Fresnel approximation and Fraunhofer approximation can be further explained using the theory of angular spectrum of plane waves (ASPW). In this case the wave disturbance U, has to be Fourier transformed and it gives the associated amplitudes for the plane waves travelling in all possible directions in space. ASPW provides exact solution for the Helmholtz equation.

Consider the propagation of light from the plane $z = 0$ as in figure(2.8) to a parallel plane at nonzero distance $\Delta z = D$. The light field $U(x, y, 0)$ incident on the first plane can be mapped to the new field at plane $\Delta z = D$ by the angular spectrum equation. Let $A(f_x, f_y; 0)$ be the spectrum of the field at $z = 0$ and $A(f_x, f_y; D)$ be the spectrum of the field on the second plane. The equation for the angular spectrum propagation of a plane wave between two planes is given as:

$$U(x, y, D) = \iint_{-\infty}^{\infty} A(f_x, f_y; 0).\exp[j2\pi\frac{D}{\lambda}\sqrt{1 - ((\lambda f_x)^2 + (\lambda f_y)^2)}].\exp[j2\pi(x.f_x + y.f_y)]df_x df_y \tag{2.23}$$

The term $\exp[j2\pi\frac{D}{\lambda}\sqrt{1 - ((\lambda f_x)^2 + (\lambda f_y)^2)}]$ is the transfer function of the wave propagation equation and is valid only when

$$\sqrt{f_x^2 + f_y^2} < \frac{1}{\lambda} \tag{2.24}$$

When $\sqrt{f_x^2 + f_y^2} > \frac{1}{\lambda}$ the transfer function is real and corresponds to evanescent waves.

All the wave propagation algorithms in this thesis follow Equation(2.23). The simplicity of the equation along with the ability to work in the Fourier domain make it a perfect choice for all our algorithms. As will be seen later in the following chapters, we normally work in the Fourier domain for all our pruning and compression needs.

Another important reason for using the Angular Spectrum algorithm is the ability to perform the angular spectrum rotation algorithm [48][49]. In our work we extensively use the angular spectrum rotation algorithm to obtain reconstructions at various angles based on the position of the viewer. In Appendix A we describe the angular spectrum rotation algorithm.

2.5 Conclusion

In this chapter we have been presented with an introduction to the basic concepts of holography. We have discussed about the historical context in which holography was discovered and how it has captured the imaginations to many scientists and scholars. We have discussed optical holography and techniques used by Gabor, Leith-Upatnieks and Denisyuk to generate and reconstruct their holograms. We have talked about the advent of numerical holography and how it has managed to improve upon optical holography. We have also discussed about some conventional holographic display technologies starting with integral imaging. We have then discussed Computer Generated Holograms and briefly described the Gerchberg-Saxton (GS) algorithm and point-source methods of generating CGHs. Later we have seen the basics of Scalar Diffraction theory in a historical context and enumerated the important equations that we will use in this thesis work.

With this background we can now move towards the state of the art in the compact representation of holographic data. The following chapter will focus on how holographic data is stored and compressed for transmission and reconstruction.

Chapter 3

State of the art in compact representation of holographic data

3.1 Compression of digital holograms

3.1.1 Introduction and need to compress holograms

The realism that can be obtained by the reconstruction of holographic images is unparalleled. But it is obtained at the cost of larger amount of spaces required to store these holograms. A traditional point-source hologram of size $10mm^3$ will take about hundreds megabytes of storage. The size requirement is due to the storage of each object point that is spaced in micrometers or nanometers. Larger holograms will need gigabytes. Today the storage of holograms is not a big issue. But the transmission of holograms is indeed a problem. Existing network technologies haven't tackled the technical challenges, among which compression issues hold an important place. The reason for this is that the amount of data for encoding holographic content (and more generally massively multi-view data) is considerable since targeted parallax quality should allow solving the convergence / accommodation mismatch.

In the field of compression of digital holograms much attention has been been given to Phase-shifted digital holograms (2.3.1.1), mainly because of their practical applications in object recognition, imaging and video sequencing of physical objects [50–58]. Due to the numerous different ways to generate computer holograms and digital holograms, we cannot limit ourselves to one type of hologram. Hence we need better generalized

techniques of compactly representing holographic information so that it becomes efficient to store and transmit over existing networks.

In the following sections we will discuss about the lossy and lossless methods used in hologram compression (3.1.2), compression of digital holographic sequences (3.1.3) and compression of digital holograms using wavelets (3.1.4).

3.1.2 Lossy and Lossless methods of hologram compression

The recording of digital holographic data is usually done by recording the complex field. Hence the underlying data is usually a set of complex numbers having a *real* and *imaginary* part. Digital holographic data can be usually stored in 3 different formats.

- Magnitude of the complex field only
- Phase of the complex field only
- Two data sets of real and imaginary parts of the complex data field

Lossless compression techniques are used normally when the data must be faithfully decompressed, eg. in text compression. If we use lossless methods of compression in digital holography, then we can be sure to get 3D reconstruction of the object identical to the original object except for some rounding and pixilation errors [51]. In [51] T.J.Naughton et al. performed lossless compression of holograms using Lempel-Ziv, Lempel-Ziv-Welch, Huffmann and Burrows-Wheeler transforms. They deduce that the optimal compression is achieved when the digital hologram is stored in an intermediate stage having separate data streams for real and imaginary components. In their tests they were able to obtain a compression ratio of 1.9 to 3.20 for the Lempel-Ziv, Lempel-Ziv-Welch and Huffmann and a compression ratio of 4.66 for the Burrows-Wheeler transform. While coding the holograms directly without any separation between real and imaginary parts, the compression ratios obtained were between 1 and 1.9.

Lossy compression techniques involve techniques based on subsampling, quantization and discrete Fourier transformation. The method proposed by T.J.Naughton et al. [51] involves the usage of downsampling of the hologram by half. This resulted in poorer reconstruction quality but a larger compression ratios of 18. The other drawback is the change in the reconstruction distance that varies as a function of the amount of downsampling done. In their example quantization proves to be very effective. The use of simple objects always favors quantization. It was shown that with 4-bit quantization (each for real and imaginary part), compression ratios of ≈ 16 can be achieved.

Later in [58], Y.Xing et al. did a study on the effectiveness of quantization on holographic data. They conclude that 4-bits of quantization is enough for obtaining a satisfactory result that causes small enough degradation so that the reconstruction of the quantized hologram was not visibly different from the original hologram reconstruction.

3.1.3 Compression of digital hologram sequences

There has always been interest to not restrict holography to the imaging domain. Sequences of holograms are created to emulate the sense the motion. But the bigger question of compression still looms over. T.J.Naughton et al. suggest that for 6-bit quantization having a compression ratio of ≈ 11, holographic video frames of 640×640 pixels could be streamed over 100Mbit/sec connection at 20 frames per second and 1024×1024 at 8 frames per second.

Several researchers performed compression with regular conventional video codecs. In 2009 E.Darakis and T.Naughton [59], used MPEG-4 to compress such sequences. The result is a compression ratio of about 20 and normalized root mean square error (NRMS) of 0.7. The NRMS is calculated on the object plane complex wavefronts i.e the reconstruction complex wavefront. They observe that MPEG-4 coding due to its lossy nature performed a low-pass filtering on the hologram and this resulted in the dimming of brightness of the reconstructions. For truly immersive 3D content this would mean lesser diffraction angles and hence poorer reconstructions.

Later in 2010 [52], E.Darakis et al. performed similar experimentation with H264 and Dirac codecs. Both codecs perform equally well and compression ratios of $4 - 7.5$ at NRMS of ≈ 0.3 was achieved. In this work they implemented an experimental threshold estimation model called as the *the staircase algorithm*, to determine the highest compression ratio that was not perceptible to human observers. They observed that even for small compression ratios of ≈ 1.5 the NRMS error was quite high ≈ 0.15, hence showing that it is difficult to evaluate the visual quality from numerical results.

In 2013 Y.Xing et al. [56] performed similar experimentation with HEVC and AVC and compared the results. They created a sequence of holograms based on vector lifting scheme (VLS) which will be discussed briefly in the next subsection(3.1.4). They fed the shifted distance information which is output from the VLS scheme to the H264 AVC and HEVC encoder after converting to YUV 4:2:0 format. They compared the HEVC encoding using various transform unit (TU) sizes for the original hologram and the VLS transformed hologram. The VLS HEVC intra encoded stream performed slightly better to plain HEVC Intra encoding for the same TU size. For Inter encoding the VLS transformed hologram performed slightly inferior to plain HEVC inter encoding. For

the comparison between HEVC and AVC, HEVC as expected outperformed AVC in all their tests.

In another study by Arrifano et al. in the paper [60], they explain a lossy but efficient method of encoding and decoding holograms having large sizes. They consider complex holograms having 2K resolutions having 128 bits of data per pixel (64 bit for real part and 64 bits for imaginary part) having an effective bandwidth of 15.5Gbits/second. They make use of multiple description coding (MDC) techniques to transmit in real-time holographic video on multiple channels. The encoding using MDC is done on the amplitude and phase separately and are quantized at 13 bits and 16 bits respectively. The reconstruction quality (PSNR) is shown to be a varying largely with the bit error rate (BER) of transmission. In an ideal situation (0% BER), PSNR of $\approx$ 46dB is possible with this method.

3.1.4 Compression of digital holograms using wavelets

Shortt et al. [61], applied 1D-DWT wavelet analysis at different resolution levels to the compression of complex-valued digital holograms. They used 53 discrete mother wavelets having resolutions of 1,3,10 and 20. Based on the resolution level the wavelet coefficients are quantized. Borrows-Wheeler transform is performed on these quantized coefficients and the compression ratio is measured. They presented their results for 7 wavelet functions (out of 53) and found out that resolution level 3 performed best with the lowest NRMS error and highest compression ratio for a fixed number of bits of quantization. It was interesting to note that no one wavelet function performed better than the other for their set of holograms.

JPEG2000 based compression of holograms was performed by E.Darakis and J.J.Soraghan in [62]. The compression ratios range from 20 to 27 at acceptable subjective quality.

In 2011 L.T.Bang et al. [63] used Haar wavelet transform to divide a digital hologram into sub-bands and then they used the Wave Bandlets transform to determine the general fringe direction of the geometric flow. This geometric flow indicates the direction in which pixel values have regular variations. Hence the approximation of the pixel values on each fringe becomes possible with minimal information loss. Compression ratios of about $30 - 35$ are shown with this method with NRMS error on the hologram of 0.3.

D.Blinder et al. [64], used wavelet coding for off-axis holograms. They show the importance of directionality and orientation for high frequency components in the hologram. Standard decomposition schemes are not very suitable for this data. They made use of direction adaptive wavelets with a strong condition of using separable transforms.

Separable transforms allow for each dimension of a multi-dimensional data to be transformed one at a time. Results showed significantly improved Bjontegaard delta PSNR of over 4.5 dB on average within a bit-rate range of 0.125 to 2 bpp when combining the direction-adaptive discrete wavelet transform with non-standard decomposition schemes for off-axis holographic recordings; up to 7.5% reduction of file size in the lossless case. The compression efficiency improved due the usage of the directional separable wavelets along with the JPEG2000 algorithm, compared with regular wavelets like Haar.

Y.Xing et al. [55–57] used a vector lifting scheme (VLS) specifically for exploiting the redundancies in the various shifted distance information in phase shifting digital interferometry hologram setup. They propose a separable (SEP) and non-separable (NS) vector lifting scheme (VLS) and show that the non-separable (NS-VLS) one is more suited for the data that they were working on. Both methods were superior to conventional coding schemes. A gain of about 2 dB and 0.15 in terms of PSNR and SSIM, respectively, has been achieved compared to quantizing the amplitude, real and imaginary data, and shifted distance information. The limitation of the work was the use of only 2D (image) data as input holograms. The use of 3D data scenes or immersive environments encoded in holograms will result in larger disparities between the shifted distance information of the PSI holograms and the amount of correlation between the shifted distance information can significantly decrease. Later they used HEVC to encode the separable VLS decomposition to obtain further improvement in performance.

Two other wavelet based schemes are present that use the diffraction and propagation property of light as a basis namely Onural wavelets [65, 66] and Fresnelets [67]. In the next chapter we will look at Fresnelets in detail.

3.1.5 Conclusion of the state of the art in hologram compact representation

In this section we have seen several conventional methods of compression (lossy and lossless) being applied to holograms. We have also observed the usage of conventional video codecs to sequences of holograms. The simplicity of the underlying scenes forms the basis of whether a good compression can be possible or not. To fully conclude that conventional compression methods are enough for all 3D scenes and all immersive scenarios, a more comprehensive set of holograms should be tested. No paper till date has been able to provide comprehensive study on the compression efficiency and the quality possible for true 3D immersive environments. This is mainly due to the fact that it is still very difficult to generate holograms that encapsulate (record) a complete real world 3D scene.

There are certain compression schemes that are specific to phase shifting digital holograms [55–57]. However we would like that the type of the hologram should not be a deciding factor on the compression, since this type of a restriction will put a strong constraint on the encoding process of holograms.

We have also seen the usage of wavelets in the compact representation of holograms. However it must be noted that most conventional wavelets are good only for piecewise smooth signals. Holograms are quite untypical data to encode, and hence the tools classically designed for data compression may not be straight forwardly applicable. The reason for this is that information that is localized in the 3D encoded scene is spread out in the entire hologram, under the form of very rapidly oscillating patterns. Hence wavelets, which take profit of local regularities, are not really suited to hologram coding in their classical form. Some new techniques need be developed to handle this type of information. Holography being a light phenomenon has a strong dependence on the diffraction properties of light. We would like to use certain wavelets that can benefit from this diffraction property.

In the next section we discuss such a scheme that will allow us to prune specific portions of the hologram based on the position of the observer.

3.2 View-dependent representation of holograms

3.2.1 Introduction

In all the methods discussed so far in section (3.1.2), the assumption is that the volume of reconstruction is quite small. The object sizes range from few *millimeters* to few *centimeters*. In a true immersive 3D setup, the volume of reconstruction will be in the range of m^3. This would mean large holograms which have 10^9 pixels and beyond. For this large amount of holographic data we propose an alternative strategy than the one of trying to encode and transmit the whole hologram, but transmitting only the information that is needed at the decoder for a specific set of observers. The need is there for an intermediate stage where irrelevent information from the hologram is first *pruned* and then the remaining information can be quantized, coded and transmitted. In this section we will elaborate on the assumptions for pruning out portions of the hologram.

We make 2 major assumptions here:

- The volume to be reconstructed or the object size is relatively large compared to the view-point of an observer

- There are a limited number of observers

Under these assumptions, our aim is to obtain the portions of the hologram that result in a diffraction at the position of the observer.
The first assumption is to take care of truly immersive 3D technologies and the second assumption allows us to introduce some degradation in order to obtain compression.

The resultant hologram thus obtained by pruning should be lossless in nature i.e. the reconstruction obtained at the observer position is identical to the reconstruction obtained from a complete hologram. This resultant hologram obtained is called as a *subhologram*. This concept of sub-hologram is not new and has been used before. The following section discusses this approach.

3.2.2 SeeReal Approach

A holographic display system based on the construction of sub-holograms has been proposed by SeeReal technologies. The principle is to reconstruct only part of the wavefront originating from the object that actually is incident on the eye pupils of the observer [68]. It happens to be only a vertical parallax system. A wavefront is reconstructed in a small region called 'virtual viewing window' . The size of this virtual viewing window is related to the size of the eye pupil. The size of this window determines the pixel period needed on the display.

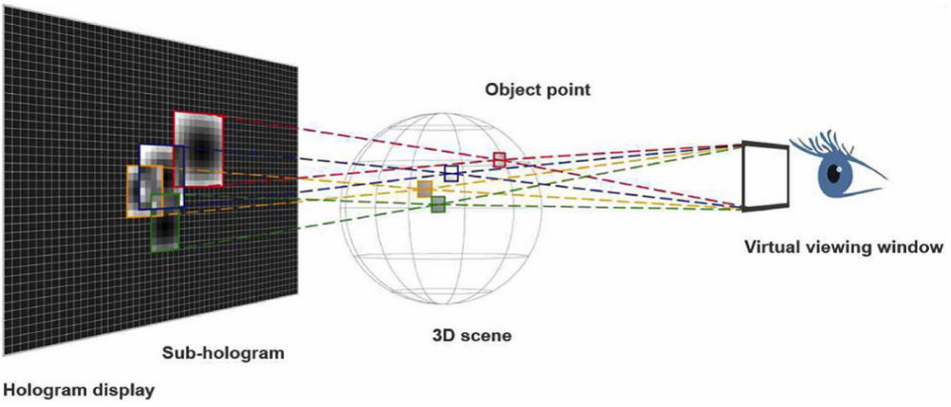

FIGURE 3.1: SeeReal approach to generate subholograms

Closely related to the concept of the observer window is the subhologram which is a limited region related to the object point and eye pupil as shown in figure(3.1). The biggest advantage of such a setup is the ability to reconstruct a large volume limited only by the size of the display used. The reconstruction is located in the frustum ranging from the observer window to the borders of the display and beyond. The movement

of the observer pupils is tracked. The problem that arises is that at the edges of the hologram the amount of light entering the pupils may not be enough. A method to change the orientation of the light source so as to allow maximum light entering the pupils is also proposed.

In 2007 a monochrome porotype using a 20-inch monitor was demonstrated. This special configuration allows using displays with a relatively large pixel size. In the 20-inch prototype, a state-of-the-art high resolution desktop LCD panel was used with separation of about $70\mu m \times 210\mu m$ between adjacent pixels. Since the pixel size of the used SLM (the LCD panel) is large, the diffraction angle is about 0.5 degree, and the viewing window is also very small. However, a clear large reconstruction can be displayed on the space with a wide depth range of about 4 meters, because of the large SLM with a light steering technique (movement of the light source). An eye tracking system using two CCD cameras is also integrated to this prototype. According to the tracked eye position, the light path is adjusted to match the viewing window to the eye position in real time. The correct hologram which will generate the correct image and parallax from the observed position is computed and written to the SLM in real-time.

This method of generating subholograms although being good in theory has its limitations. As can be seen from the figure(3.1), every object point is encoded in the form of a subhologram. As the observer changes position, the subholograms are updated rapidly on the LCD panel. This type of setup is very easy to construct when the objects are simple and have limited number of object points. The problem arises when the 3D scene contains large number of object points. The construction of subholograms for every point becomes difficult.

3.2.3 Requirements for a view-based representation of holograms

In this section we propose the requirements of a basic framework of a view-based system which mitigates the problems of the SeeReal approach. We will enumerate the assumptions and put forward some requirements for such a view-based system.

- The system will take as input a hologram and the output shall be subholograms generated based on the position of the observer.
- The system should take into account short lateral movements of the observer. That would mean the same subhologram can be reused for a small threshold of change in position of the observer.
- The reconstruction system should be depth independent. That is the generated subhologram will be able to reconstruct the object at all the depths for a particular

observer position. This removes the necessity of having a separate subhologram for every object point at every depth. This will result in a large reduction of computations.

- Also the view dependent system should construct lossless subholorgams by extracting the information from the hologram based on the position of the observer.

3.3 Wavelets used for hologram representation

In this section we will try to give a broad understanding of the type of wavelets that can be used with the view dependent representation system whose requirements we formulated in section (3.2.3) .

The basic criteria that a wavelet should fulfill is that it should be able to approximate the hologram reasonably well (wavelet transform) i.e. capture the frequency information at each pixel location. Holograms are not smooth functions that can be approximated easily. Also, to capture the large frequency variations in a hologram, it is natural to expect a wavelet which is well localized in space and frequency.

So far the wavelet transforms for holograms are divided into two broad categories. The first category is the set of wavelets that fulfill the admissibility criteria (mathematically) and are in line with the principles of wavelet multi resolution analysis. The important thing about these wavelet is the time (space) - frequency analysis that can be possible. Wavelets like the Haar wavelet, Meyer wavelet, Coifflet, Daub-4 etc. fall under this category. Direct application of filter banks used for image compression may thus be applied to hologram when using this first category of wavelets [61].

However a second category of wavelets is to be considered. In order to be suitable for representing or approximating holograms for view based systems, wavelets have to be adapted, often by relaxing some requirements. This is necessary when designing wavelet-like functions by observing the close relation between the optical diffraction phenomenon and wave propagation to the scaling of wavelets, i.e. the scale parameter s denotes the distance (depth) of the propagation. This was first proposed by Onural in [65]. Though this theory is interesting in the sense that if we are ready to give up the multi-resolution analysis framework and focus on the space - depth analysis rather than time - frequency analysis, there are certain mathematical questions that remain unanswered [69]. Its has been shown by Onural in [66], that the chirp function (chirplet), performs a transform which is reversible, but yet it is not a mathematically admissible wavelet. Such wavelets are part of the second category of wavelets.

Other wavelets belonging to this second category have been proposed such as, Fresnelets [67] try to compensate the effect of wavefront propagation by bringing the Fresnel transform of the original signal into the wavelet analysis. This implies adapting some conditions on multiresolution analysis denition, but above all releasing properties of space and frequency localization.

On the other hand, if one wants to keep good space and frequency localization, this may be at the expense of computational properties. This is the case for Gabor wavelets, which in particular do not form a partition of unity. The acceptability of the loose conditions of Fresnelets and Gabor wavelets will be discussed in the next chapter.

For a view-based representation system we require a wavelet function that can perform multi-resolution analysis of the hologram based on the viewpoint decomposition of the observer positions, i.e. the configurable parameters of the wavelet (*scaling, dilation etc.*) that correspond to each decomposition should represent a unique position or set of positions of the observer.

3.4 Conclusion

In this chapter we looked at the existing methods used for hologram compression. We noted that conventional compression techniques are not the best way forward for compressing holographic data and do not allow for an efficient compact representation system. We looked at quantization, and concluded that it needs to be used in conjunction with an intermediate pruning stage.

The pruning of hologram coefficients can be achieved by using a view-based reconstruction setup which tracks the head position of an observer. We gave the assumptions under which such a setup can be realized, namely

- The volume to be reconstructed or the object size is relatively large compared to the view-point of an observer
- There are a limited number of observers

In terms of pruning of the hologram we concluded that the subhologram after pruning should be able to reconstruct a lossless reconstruction at the position of the observer

We looked at various wavelet based compression techniques and concluded that conventional wavelets are good for piecewise smooth signals and not suitable for holographic data. We also concluded that the wavelet

- should be localized in space and frequency
- should perform space-frequency analysis and not space-depth analysis
- should be mathematically admissible

In the next chapter we will look at 2 leading wavelets that are used in holography namely, Fresnelets and Gabor wavelets and compare them on the basis of the above conditions.

Chapter 4

Fresnelets and Gabor wavelets for hologram representation

4.1 Introduction

As explained in the previous chapter, there have been several attempts to compress holographic videos. The straightforward approaches such as applying block based video coding methods or pixel-based wavelets haven't come up with satisfactory results since they clearly don't take into account the special frequency characteristics of holograms; indeed, holograms are diffraction patterns that can have local frequencies of the order of magnitude of the coherent light wavelength used for their reconstruction.

Wavelets have been used for extracting the frequency information from the raw hologram, however, the special nature of the hologram requires designing dedicated wavelets. These considerations have lead to Fresnelets [67], wavelets obtained by Fresnel transform of B-Spline wavelets. As discussed later in the chapter, Fresnelets do not show good localization in frequency which may be crucial for coefficient selection.

In this chapter we analyze the limitations of Fresnelets regarding both compression and adaptive reconstruction and show why Gabor wavelets may appear to be the ideal candidate for adaptive reconstruction (4.5) and we will suggest improvements towards the use of Gabor-like wavelets for efficient viewpoint-based scalability.

4.2 Importance of localization for a view-dependent system

Although wavelets are a powerful tool for data compression, their special capability of local analysis of the signals make them especially suited to partial and adaptive reconstruction. This feature is classically used to degrade some data in space (or time) and frequency according to the final user requirements or rendering parameters. When it comes to holography, wavelets can efficiently help exploit a particular type of adaptivity, namely the adaptivity in point of view.

Holograms can be seen as a superimposition of patterns associated to specific directions of light emission. This property is widely exploited by stereograms, which isolate the various directions of diffraction. A partial reconstruction of a hologram can be made according to these pattern, as in [70], where they are denoted as *sub-holograms*.

Such degradation is all the more important for digital holography that it can be exploited not only at the stage of transmission, but also on the display side, with resolutions that would not allow to handle a full hologram. We thus see that in special cases, when only a restricted number of users are allowed to view the hologram, a good compression scheme may not be the one that provides the best absolute compression ratio, but the one that allows efficiently degrading the signal so as to transmit only the data relevant for identified observers.

Indeed, due to the grating equation (4.1),

$$\sin\theta = \frac{m\lambda}{\Lambda}, \tag{4.1}$$

where θ is the angle of diffraction, λ the wavelength, Λ is the localized period of the hologram and m an arbitrary integer, light emission in the direction θ will be produced only by hologram contents with wavelength λ. Thus, considering a specific observer position (see Figure 4.1), there is only a sub-set of the hologram data that contributes to the light-field reaching this observer. This sub-set (that we will call "sub-hologram") may be obtained by selecting the appropriate frequencies associated with the angles of the viewing lines from the hologram to the observer. The frequency to be selected depends on the spatial localization in the hologram. Thus a wavelet decomposition of the hologram data by a wavelet that has *good* localization in space and frequency, will be the natural way to extract space and frequency localized information from hologram data. Extracting the sub-hologram information for a given observer view-point is an adaptation carried out by pruning across the wavelet coefficients.

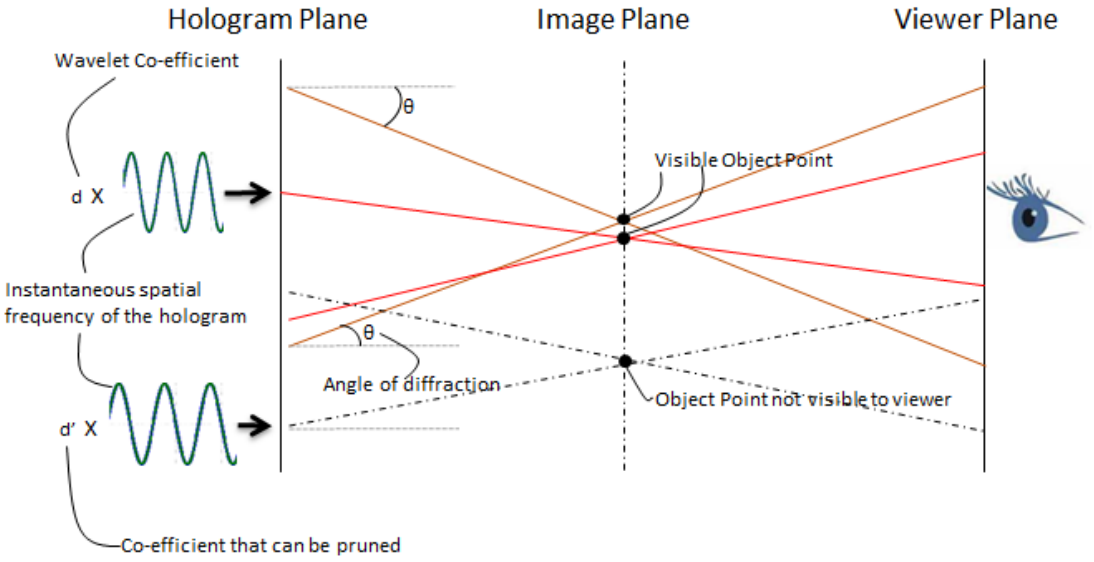

FIGURE 4.1: View-dependent compression of holograms

We see that a coefficient will become relevant for a given propagation angle if it is related to the proper frequency according to this relation, i.e. the spectrum of these wavelets have to be concentrated around this value. On the other hand, wavelets have also to have good localization in space, since this directional diffraction is considered locally, figure(4.1).

In the next sections we will discuss which wavelet bases provide this "good" localization which is best suited for this kind of representation technique.

4.3 Fresnelets and their shortcomings

In this section we will introduce Fresnelets [67] as one of the wavelets used for compact representation of holograms. We will show that these wavelets are not well localized in space and frequency and hence cannot form a good basis for compactly representing holograms for view dependent systems. We will provide our argument from two different perspectives. First we will theoretically observe Fresnelets, and using the uncertainty relation show that space frequency localization is not possible. Second, we will try to obtain the best possible function that can be Fresnel transformed to form a basis, and check whether such a basis can be well localized in space and frequency.

Digital holography being a lensless process (diffraction phenomenon), will tend to spread out the sharp features like edges over the entire hologram plane. This spreading out of information is exploited in the formation of the Fresnelet bases. Fresnelets are formed

by taking the Fresnel transform of appropriate B-Splines (usually of a finite order) to simulate the propagation phenomenon (spreading out) in the hologram reconstruction process and use it as a wavelet basis.[67]

From the uncertainty relation of Fresnel transforms [67] , the bound on the time-bandwidth product given as the product of the square of the variances for complex functions

$$\sigma_g^2 \sigma_{\tilde{g}}^2 \leq \frac{\tau^4}{16\pi^2} \tag{4.2}$$

where σ_g^2 is the variance of the signal $g(x)$ and $\sigma_{\tilde{g}}^2$ is the variance of the Fresnel transformed signal $\tilde{g}(x)$. In order to make this inequality an equality (i.e. to obtain the best possible space frequency localization) we need to have [67]

$$g(x) = a e^{i\omega_o x} e^{-b(x-x_o)} e^{-i\pi(x/\tau^2)} \tag{4.3}$$

where $\tau = \sqrt{\lambda d}$ and d is the distance of propagation. Taking the Fresnel transform of this family of functions, we obtain the product of a chirp function of the form $e^{\alpha x^2}$ by a Gaussian function, which may be interpreted as its envelop. As shown in [67], as parameter τ (which is directly proportional to the distance of propagation) increases, the spatial spreading of this envelop increases further. Since the chirp function frequency varies monotonically as we move away from the origin, more relevant frequency will then be taken into account. Since the function in equation (4.3) is the best possible case with respect to uncertainty relation, we see that this frequency spreading will occur for any arbitrary function.

If we were to use the wavelet coefficients that are generated after a Fresnel transform, the frequency information captured by them would be indistinguishable. Hence localization capability of such wavelets is not very strong. It is then useless for view-dependent hologram representation.

The spatial spreading of the wavelet basis (due to Fresnel transform of the B-Splines) is another feature which is not well suited for view-based hologram representation techniques, figure (4.2). It is imperative that there be a good localization in the spatial domain to capture the local features of the hologram. In [67] it is shown that as the scale becomes finer, the Fresnelet bases tend to spread out (instead of becoming smaller) in the spatial domain. This eventually will lead to smaller number of bases functions to represent the hologram. Later extraction of the features of the hologram based on these fewer bases will result in poorer reconstruction for view-based representation systems, according to the requirements mentioned in Section (4.2). Figure (4.3) shows the time (spatial) domain spreading of the function for the finest scale.

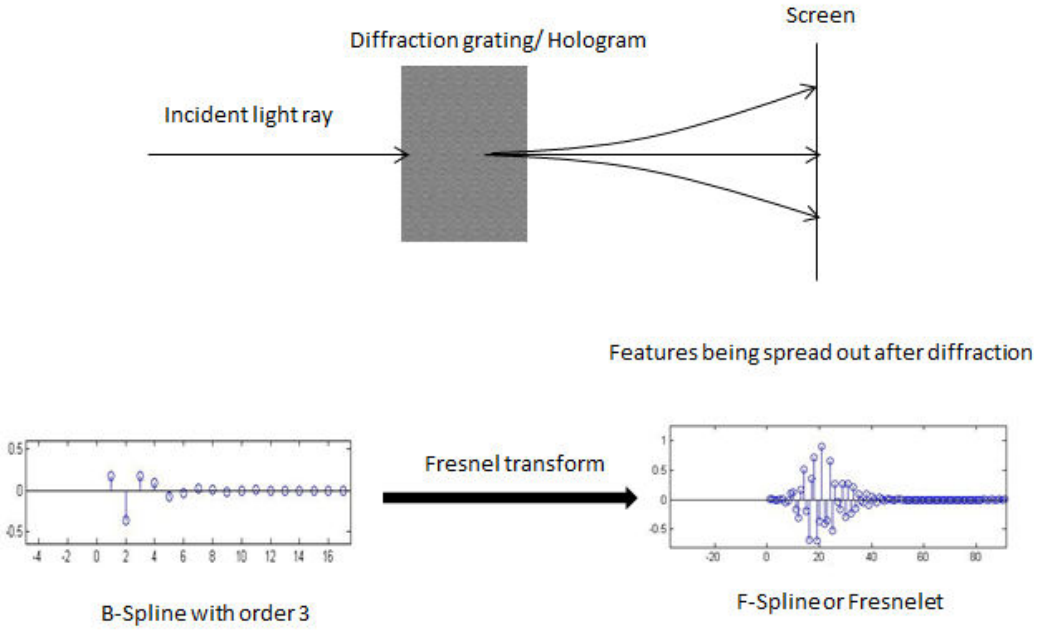

FIGURE 4.2: B-Splines and diffraction

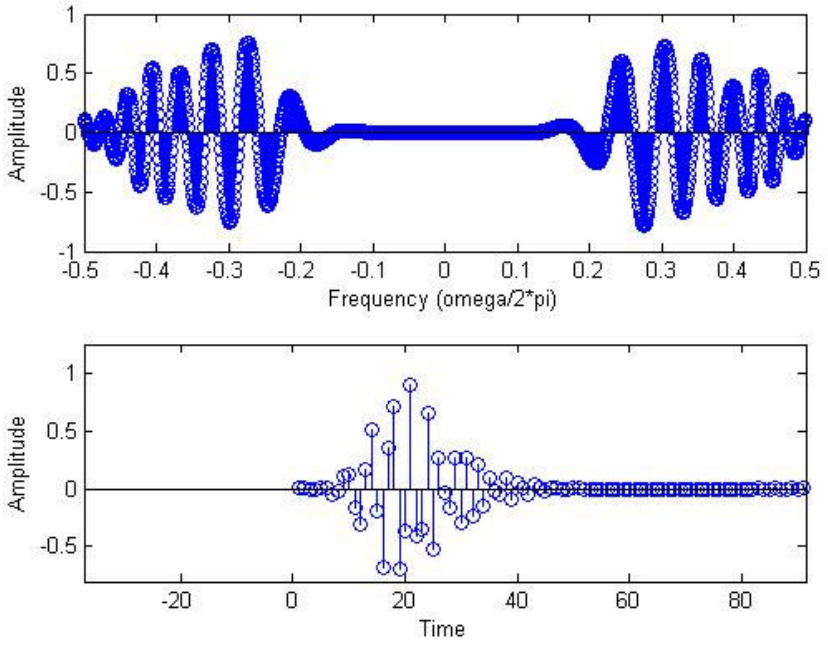

FIGURE 4.3: Fresnelet Basis showing the Frequency (top) and Time domain representations for the real part for the finest scale. Notice the spreading of the base in the time (spatial) domain

Although theoretically proved that Fresnelets can't have good localization in time and frequency, one may argue that in practice, they can be chosen close enough to functions that do have this property. This is countered by the following arguments:

It has been shown in [71], that B-Splines asymptotically converge to Gabor functions as the degree tends to ∞. Gabor functions are Gaussian functions which are modulated with a sinusoidal carrier. That means B-splines tend to converge to the form $e^{i2\pi mbx}g(x-na)$ as the order of the B-spline goes to ∞.

If we make the assumption that the limit Gabor basis is a Riesz basis, then we can invoke the Bailen-Low [72] theorem and deduce that this limit basis is not well-localized in time and frequency; the approximating series of B-Spline functions will then not behave better, not matter how close they approach the limit:

$$(\int_{\mathbb{R}} \mid xg(x) \mid^2 dx)(\int_{\mathbb{R}} \mid \gamma\hat{g}(\gamma) \mid^2 d\gamma) = \infty \tag{4.4}$$

The equation(4.4) states that there is no well-localized window function (or Gabor atom) g either in time or frequency for an exact Gabor frame (Riesz Basis).

It has been proved in [67] that the Fresnelet also forms a Riesz basis. Fresnelets which are Fresnel transforms of these B-Splines, will in fact spread the frequency further, and hence it can be said that Fresnelets cannot fulfill Bailen-Low theorem (4.4). Hence there cannot be a good localization in space and frequency. Figure (4.3) shows the spreading out of the frequency information in a Fresnelet with degree 3. Such a large spread in the spatial and frequency domains of the Fresnelets is not well suited for application in view-dependent hologram compression.

Finally, among other properties, we can note that Fresnelets can bring about the suppression of the unwanted orders. In [67] it is shown that the systematic modulation of the hologram, using the experiment parameters k_x and k_y which are the frequencies around which the real and virtual images are localized in the frequency domain, causes a shift of these images, such that the virtual image is localized at $(0, 0)$ and the unwanted orders at (k_x, k_y) and $(2k_x, 2k_y)$. The lower frequency information is located in the coarser sub-bands. Hence the coarser resolutions of the Fresnelet decomposition tend to suppress the zero order and real image.

For further encoding of wavelet coefficients, [53] proposes a uniform sub-band quantization of the Fresnelet coefficients followed by the lossless Burrows-Wheeler transform. Another method proposed in the same work is the Set Partitioning in Hierarchal trees (SPIHT) coding algorithm on the Fresnelet coefficients.

4.4 Gabor wavelets

Gabor wavelets are finding increasing use in the field of many computer vision applications and modelling of biological vision [73–75]. Gabor wavelets provide for scaling and rotation along with translation, and hence they are very well suited for measuring the local spatial frequencies of holograms. The uncertainty bound plays an important role in time-frequency localization. It is known that the Gaussian function ideally provides the best uncertainty bound. Gabor functions are in essence Gaussian functions which are modulated with a sinusoidal function.

The main objective of a wavelet transform, is to obtain the best approximation of the hologram in the hologram plane. As reminded in [74] by T.S.Lee, in line with the theory of the uncertainty product, Gabor showed that there is a lower bound to the product of time and frequency which signifies the trade-off between time resolution and frequency resolution [76]. He discovered that the Gaussian modulated complex exponentials provide the best trade-off [76].

Let $g(x, y)$ represent the mother wavelet, then a set of Gabor functions $g_{s,\theta}(x, y)$ can be generated by rotating (using parameter θ) and scaling (using parameter s) $g(x, y)$ to form an almost complete non-orthonormal basis set

$$g_{s,\theta}(x, y) = c^{-2s} g(x', y') \tag{4.5}$$

where $x' = c^{-s}(xcos\theta + ysin\theta), y' = c^{-s}(-xsin\theta + ycos\theta)$ and c is selected based on the frequency centering of the Gaussian function and the scaling parameter s.

The basic Gabor function is represented by using 2 operators:

- The modulation operator $E_b \mid (E_b g)(x) := e^{i2\pi bx}, b > 0$
- The translation operator $T_a \mid (T_a g)(x) := g(x - a), a > 0$

$$\{E_b T_a g\} = e^{i2\pi bx} g(x - a) \tag{4.6}$$

Hence the overall Gabor wavelet is composed of 4 tweak-able parameters for modulation, translation, scaling and rotation and the wavelet is denoted as $g_{s,\theta,a,b}(x)$. Usually the selection of a, b form an important role in the selection of the wavelet. The frame bounds A, B are dependant on these values. The famous result of Gabor frames states that $\{E_b T_a g\}$ can be a frame for $L_2\mathbb{R}$ only if $ab \leq 1$. If $ab = 1$ then it forms a Riesz basis. Hence we need select a and b such that $ab < 1$, so that the above mentioned Bailen-Low theorem does not affect us.

It is also known that the Gabor wavelet transform is not reversible. In other words we know that at 0 frequency we will get an non-zero output [77]. The parameters of the Gabor wavelet can be selected in such a way, that this limitation can be overcome. If the modulation frequency is selected to be large, then the output at 0 frequency tends to 0. Hence we select the modulation parameter $b = 1$, which is the frequency 2π.

We consider the wavelet equation provided in [74] for our reconstruction process.

$$\psi(x) = \frac{1}{\sqrt[4]{\pi}}\sqrt{\frac{2\pi}{\gamma}}exp[-\frac{(2\pi/\gamma)^2x^2}{2} + j2\pi x] \tag{4.7}$$

Here it is observed that $a \approx 0.55$ and $b = 1$ when $\gamma = \pi\sqrt{2/ln2}$. The other features of this wavelet equation are that it is centered at $x = 0$ at frequency $\omega = 2\pi$. Then the function $\psi_{s,a}(x - k)$, which is the scaled and translated version of this wavelet will be centered at $x = k$ and $\omega = \frac{2\pi}{s}$, with a full width of half maximum of $\Delta x = 2s$.

Another way of circumventing the Balian-Low condition was proposed by Daubechies et al. [78]. They prove that if one is ready to give up the Gabor structure as described in equations(4.5,4.6), it is possible to obtain a well localized orthonormal basis: if $g \in L_2\mathbb{R}$ is chosen such that $\hat{g}$ is real valued and $\{E_bT_{a/2}g\}$ is a frame with bounds $A = B = 2$, then the collection of functions $\{\psi_{l,k}\}_{l\geq 0,k\in\mathbb{Z}}$ constitutes an orthonormal basis for $L_2\mathbb{R}$. These bases are called Wilson bases. The trick is to alternately use Sine and Cosine functions for odd and even coefficients instead of the complex exponentials. This is sufficient to circumvent the Bailen-Low condition and obtain well localized Gabor wavelets in space and frequency.

But since we intend to use the 2D Gabor wavelet transform, which has been shown to provide better results than 1D Gabor wavelets by J.Zhong and L.Weng in [79], the use of complex exponentials in the calculation of coefficients becomes necessary. According to T.S.Lee, the 2D Gabor function achieves the best space frequency localization only in its complex form. This is because of the presence of an even-symmetric cosine component and an odd-symmetric sine component in quadrature projection [74].

Figure 4.4 shows a well localized Gabor wavelet centered at the frequency 2π.

Once we have the Gabor wavelet transformed coefficients, these can be used for view-based pruning techniques like the one explained in Section (4.2). Also it can be observed that the Gabor wavelet bases are well localized in the spatial domain as compared to Fresnelets as seen in figure(4.4). Hence the approximation of a local area in the hologram using these wavelet bases will result in better extraction of features for reconstruction based on view-dependent representation.

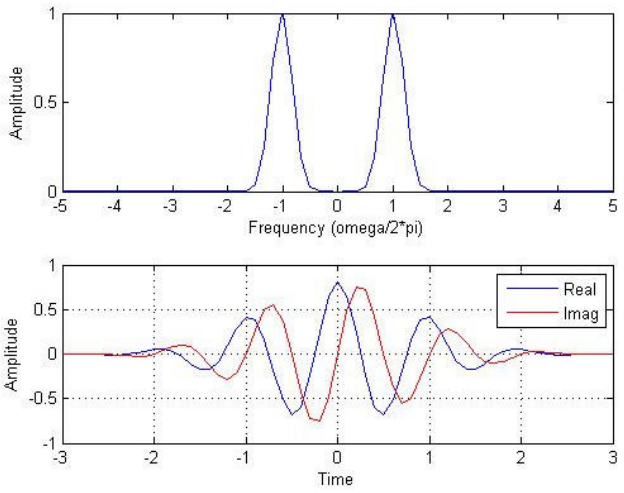

FIGURE 4.4: Gabor wavelet basis showing the Frequency (top) and Time domain representations

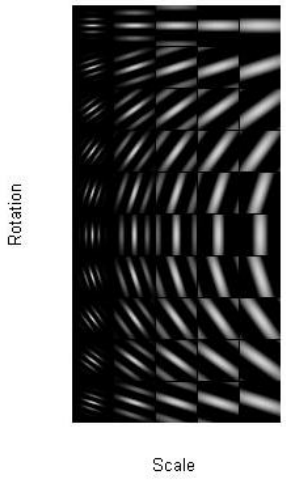

FIGURE 4.5: 2D Gabor wavelets for 5 different scales and 10 different rotations

Holograms have the inherent problem of generating unwanted orders of diffraction as seen in section(2.2). 2D Gabor wavelets on the other hand provide natural suppression of the unwanted orders [74] under some assumption as detailed earlier ($ab < 1$).

The Gabor wavelet used for our experiment is the one given in [74].

Figure 4.5 gives the ψ functions for 5 s values at intervals between 2π and $\frac{\pi}{4}$ radians and rotation values at intervals of 18 degrees.

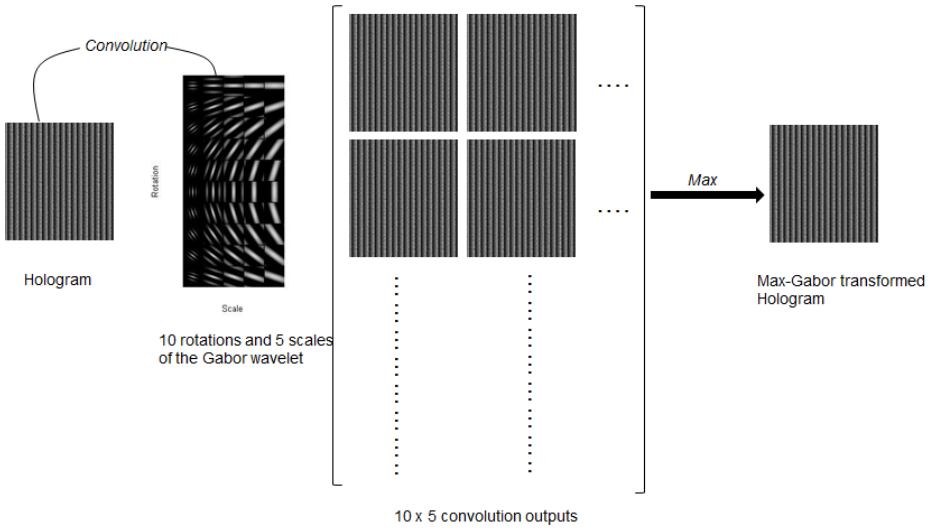

FIGURE 4.6: Max-Gabor Transform

$$\psi(\frac{x-a}{s},\frac{x-b}{s},\theta) = \frac{1}{\sqrt[4]{\pi}}\sqrt{\frac{2\pi}{\gamma}}\exp\{-\frac{(2\pi/\gamma)^2[(x-a)^2+(y-b)^2]}{2s^2}\} \exp\{j2\pi\frac{(x-a)\cos\theta+(y-b)\sin\theta}{s}\} \tag{4.8}$$

s represents the scaling of the wavelet function, θ represents the rotation and a and b represent the translation of the wavelet function. γ is selected to be $\pi\sqrt{2/ln2}$.

The Gabor wavelet transform used here is also called as the *Max-Gabor* transform [80]. The wavelet coefficients are obtained by performing the convolution operations between the hologram and Gabor wavelets at specific scale s and rotation θ values at each localized part of the hologram described by the translation parameters a and b, where a is translation parameter in the *x-direction* and b is the translation parameter in the *y-direction*. s and θ values are based on the various discrete diffraction planes where we need to reconstruct the hologram. For each set of (s,θ) a sub-hologram is obtained that contains the specific frequency information that can cause the necessary diffraction at the plane that is defined by the grating equation (4.1). To obtain the peak of the 2D Gabor wavelet transform, the maximum magnitude of the wavelet coefficients at every a and b position in every sub-hologram is calculated. This is shown in figure(4.6). This is called as the *ridge* of the Max-Gabor wavelet transform. It has been shown that the wavelet co-efficient constructed in this manner is equal to the object wave at the hologram plane multiplied by a constant [74]. This method also has shown that there is natural suppression of the zero-order and real images without the need of any spatial filtering[74].

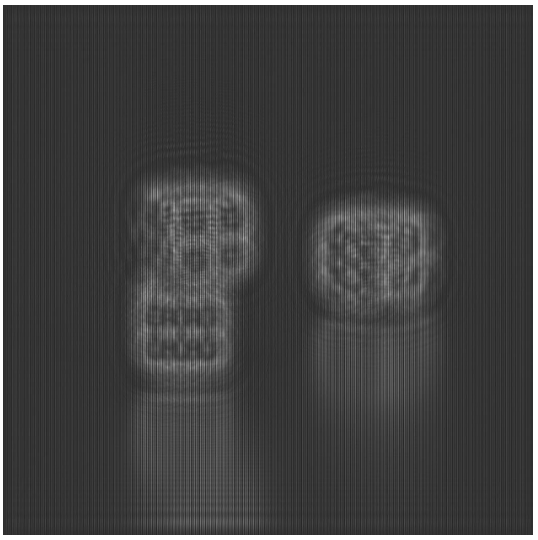

FIGURE 4.7: Hologram of an image of some dice

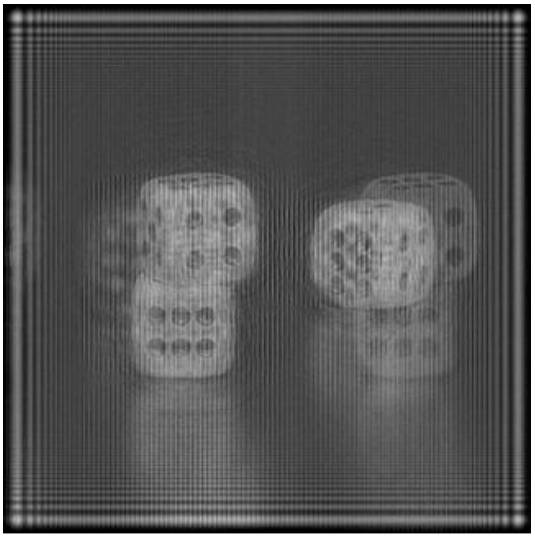

FIGURE 4.8: Fresnelet transformed reconstruction of the hologram. Note the unwanted order are visible in the reconstruction

4.5 Experiments

Using the two wavelets we have discussed so far (Fresnelets and Gabor wavelets), we obtained the reconstruction of a hologram. The hologram is of a simple image (2D) of some dice. Hence it has only one view that can be reconstructed. The hologram was generated numerically in off-axis configuration with a separation of 10 degrees between reference wave and object wave Figure (4.7). For Gabor wavelets we used the Angular Spectrum method see Appendix(A) to perform the reconstruction. For Fresnelets as

FIGURE 4.9: Reconstruction of a Gabor transformed hologram using Angular Spectrum method. Notice that the unwanted orders are suppressed

usual it is the Fresnel transform, since the Fresnelet transform shall inherently perform the Fresnel propagation as explained in 4.3.

Gabor wavelets show a suppression of the unwanted orders if the wavelet coefficients are calculated at the ridge of the transform. cf. Figure (4.9). The output of a Fresnelet transformed image in Figure (4.8) shows unwanted orders being generated.

The code for both the transforms is written in Matlab©, and the results are generated on a PC with a Xeon©E5-1620 CPU running at 3.6 Ghz with 8 GB of RAM. The hologram in Figure (4.7) is of 1024x1024 size. The Fresnelets code in its unoptimised form performs the transform in 25 seconds while the unoptimised 2D Gabor Wavelet transform code, takes about 4 minutes for completion. This is evident from the fact that each rotation angle and scale of the Gabor wavelet produces one transformed image. Later the maximum of the Gabor coefficients is found, to obtain the values at the *ridge* of the transform.

4.6 Conclusion

In this chapter view-based compression techniques have been discussed and the importance of having good localization for the wavelet has been emphasized. Two wavelet bases (Fresnelets and Gabor wavelets) have been compared on the basis of space - frequency localization. It has been experimentally verified that Gabor wavelets are able to suppress the unwanted orders created in the reconstruction process without the need for spatial filtering. The good localization properties of the Gabor wavelet bases in

space and frequency domain, make them an easy choice for view-based representation techniques for digital hologram reconstruction. However, it is at the cost of heavy computational complexity at encoding stage, and this has to be studied further to possibly exploit the parallel character of analysis and provide efficient GPU implementations.

The max Gabor transform is inherently not a reversible transform, but can be made reversible by making the Gabor wavelet admissible based on certain assumptions as shown in section(4.4). The max-Gabor transform is capable of extracting the localized frequency information from the hologram, but it may not be well suited for holograms that contain multiple views of truly immersive environments. This is because the pruning is carried out only to contain the dominant frequencies throughout the hologram by selecting only the *max* of the coefficient values. In truly immersive or multi-view scenes, this would mean loss of information for several views.

In the next chapter we will discuss a modification of the Gabor wavelet that is more suitable to a view-based reconstruction system.

Chapter 5

Morlet wavelets for view-dependent representation systems

5.1 Introduction

In the previous chapter we have seen that the '*good*' localization properties of the Gabor wavelet make it a potential candidate for representing holograms in a view dependent compression system. But again there are several problems that arise with Gabor wavelets such as failure of the admissibility condition and unequal number of the sinusoids for various frequencies [74, 81]. Admissibility is a condition needed for obtaining the original signal back from the wavelet transformed coefficients [82] and the Parseval formula is applicable. Another problem pertaining to the view-dependent system is that there are unequal number of oscillations of the sinusoids within the Gaussian window function for different frequencies, which causes a non-uniform weighing of the coefficients across all frequencies. This causes an inefficient pruning of coefficients for our view-dependent system.

An interesting fact about the Gabor wavelet is that it has nothing to do with Denis Gabor the scientist. It is in fact modified Morlet wavelet, both of which don't satisfy the admissibility criteria [83]. We fulfilled the admissibility condition in the previous chapter by making sure certain conditions are met, see section(4.4). But there was still the issue of unequal oscillations for the various frequencies. In this chapter, we present a better method by eliminating the DC term from Gabor function to form the Gabor kernel which is the basis for our modified Morlet wavelet [84]. This will ensure the admissibility condition is met. Also we will make sure that there are equal number

of oscillations of the sinusoid within the Gaussian window function by discretizing the family of wavelets appropriately in order to have the same physical properties of a Morlet wavelet.

Using the same transform method of convolution as in the last chapter, we will provide an example of a simple object and obtain the reconstructions at various angles, using the tilted angular spectrum propagation method. We shall also provide results based on a dot-product approach in which we calculate the angle of diffraction at every point on the hologram. Such an approach will require a separate wavelet for each point that can capture the local frequency information specific for an arbitrary observer position. The dot-product approach is also called as the *perfect reconstruction* approach.

The following sections discuss the design and implementation of a view-based compression system based on the Morlet wavelets. Section 5.2 mathematically explains the coefficient selection process for the dot-product based approach. Section 5.3 provides the basic theory of the Gabor basis function and gives the continuous form of the 2D Morlet wavelet. Section 5.4 describes the discretization of the Morlet wavelet, with respect to the application of view-based compression systems. In Section 5.5 we describe how the observer space in a view dependent system can be discretized. In Section 5.6 we show the results for the cube hologram using the discrete Morlet wavelets that we designed in the previous section.

5.2 Selection of coefficients for a view-based compression setup

The convolution approach that is detailed in chapter 4 is not a perfect reconstruction solution. It is frequency selection operation that is best suited for obtaining near perfect reconstructions under the assumption that the observer is positioned far away from the hologram. In order to obtain a perfect reconstruction we need to perform the dot-product approach which is described as follows.

Here we provide the mathematical understanding of a view-based reconstruction system for obtaining the coefficients that cause diffraction to an arbitrary point in space. We consider the hologram in a 1D case first and then the 2D case. We firstly obtain the general equations for obtaining the coefficients and the corresponding sub-hologram. We then comment on the efficiency (speed of computation and memory requirements) of such a setup.

5.2.1 Dot product approach in the 2D observer space

As we are aiming at perfect reconstruction, we will dismiss the assumption that the observer is far from the hologram, and that the viewing direction corresponds to a unique angle of diffraction for any pixel of the hologram. Thus the viewing direction for a given observer will vary as a function of the considered position in the hologram. This will lead to extracting the wavelet representation of the hologram using a dot product operation, rather than an convolution operation. Let us consider the 2D space in $\mathbb{R}^2$ containing a 1D hologram denoted by H with n pixels of complex values indexed by k.

$$H = \{H_1, H_2, H_3, \ldots, H_n\} \tag{5.1}$$

Let $X : \mathbb{N} \to \mathbb{R}^2$ be a function that maps any index $k \in \mathbb{N}$ to the 2D position of pixel of value H_k in $\mathbb{R}^2$. Thus the pixel of value H_k in H has 2D position $X(k)$.

Consider an arbitrary view-point V in 2D space $\mathbb{R}^2$.

Let $\alpha : \mathbb{R}^2 \to \mathbb{R}^n$ be a function that maps V to the vector of polar coordinates

$$\alpha(V) = \theta^V = \{\theta_1, \theta_2, \theta_3, ..., \theta_n\} \tag{5.2}$$

which are the angles subtended by the point V to every point $X(k)$ on the hologram as shown in figure(5.1).

From these angles we can compute the set of frequencies in H that contribute to the diffracted light field received by V from the hologram. In order to extract these frequencies from the hologram, we build a set of wavelet basis functions that can capture these frequencies.

Let f be a function that gives the localized spatial frequency from an angle θ following the grating equation.

$f : \mathbb{R} \to \mathbb{R}$

$$f(\theta) = \frac{\sin(\theta)}{\lambda} \tag{5.3}$$

We define the set of frequencies

$$f^V = \{f_1, f_2, ..., f_n\} \tag{5.4}$$

where,

$$f_k = f(\theta_k) \tag{5.5}$$

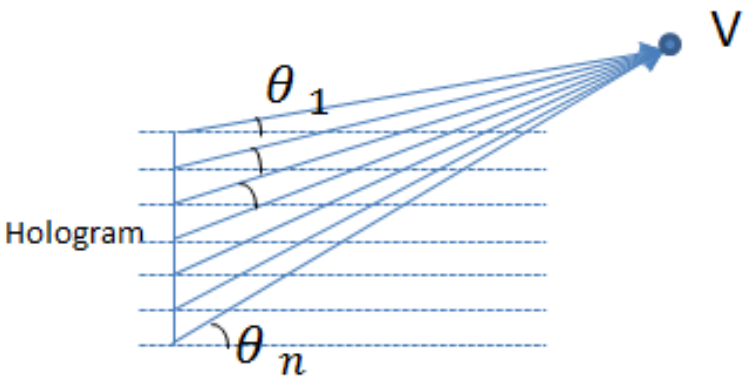

FIGURE 5.1: Diffraction at point V from the hologram H

At point $X(k)$ only the frequency f_k will generate a light field at V, due to the grating equation (5.3). We want to obtain this localized frequency information at each location $X(k)$.

Consider a basis function ψ which is a wavelet basis function having a central frequency f. For each k in H, we can obtain a ψ function by translating it to be centered at k and by scaling it to have a frequency f_k, giving function ψ_{k,f_k}. We define ψ^V as:

$$\psi^V = \{\psi_{1,f_1}, \psi_{2,f_2}, \psi_{3,f_3}, ..., \psi_{n,f_n}\} \tag{5.6}$$

To obtain each of the wavelet weights (contributions) to the diffracted wavefield at V, we perform a dot product of H with each wavelet providing a set C^V of wavelet coefficients. These coefficients will generate the same light field at the observer position V as the original hologram H.

$$C^V = \{C_1, C_2, \ldots, C_n\} \tag{5.7a}$$

where,

$$C_k =< H, \psi_{k,f_k} >= \sum_{i=1}^{n} H(i)\psi^*_{k,f_k}(i) \tag{5.7b}$$

The subhologram that can generate a diffracted light field at the point V is defined as H^V. The set ψ^V represents a family of wavelet functions that are spatially centered at each *k-th* position on the hologram and have a frequency f_k corresponding to the localized spatial frequency at $X(k)$, in order to obtain a diffraction at V.

If this family of wavelets ψ^V is orthogonal, then the sub-hologram H^V can be obtained from the coefficients C_k as

$$H^V = \sum_k C_k \psi_{k,f_k} \tag{5.8}$$

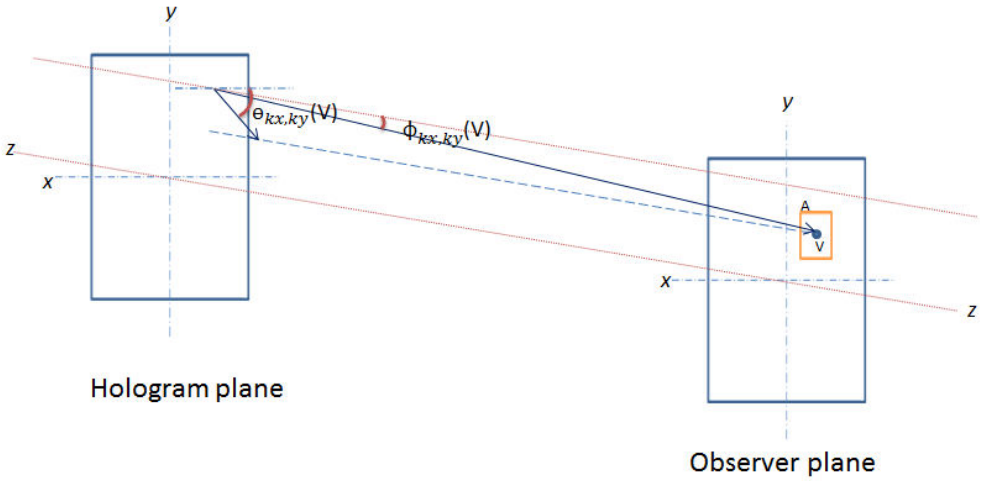

FIGURE 5.2: Case of 2D hologram and observer in 3D space

5.2.2 Dot product approach in the 3D observer space

In this section we extend the previous section to the case of 3D space and 2D hologram. Consider a reference system in 3D space $\mathbb{R}^3$ that contains the hologram $H \in \mathbb{C}^{2n}$ in the hologram plane indexed by k_x and k_y with $m \times n$ discrete points and a point $V \in \mathbb{R}^3$, which is the position of the viewer in the observer plane as shown in the figure(5.2).

Let $X : \mathbb{N}^2 \to \mathbb{R}^3$ be a function that maps any couple (k_x, k_y) in the hologram to the 3D position of the pixel $X(k_x, k_y)$ in $\mathbb{R}^3$.

Let $\alpha : \mathbb{R}^3 \to \mathbb{R}^{mn}$ be a function that maps the observer 3D position V to the spherical coordinates $\alpha(V) = (\theta^V, \phi^V)$ for all pixel positions $X(k_x, k_y)_{k_x=1\ldots m\, k_y=1\ldots n}$ on the hologram.

As shown in figure(5.2) the set of spherical coordinates associated with the observer point V

$$\phi^V = \{\phi_{1,1}, \phi_{1,2}, \ldots \phi_{m,n}\} \tag{5.9a}$$

$$\theta^V = \{\theta_{1,1}, \theta_{1,2}, \ldots \theta_{m,n}\} \tag{5.9b}$$

The localized frequency of the wavelet for one pixel point on the hologram H is given as

$$f_{k_x,k_y} = \frac{\sin(\phi_{k_x,k_y})}{\lambda} \tag{5.10}$$

The frequencies of the family of wavelets corresponding to equation(5.10) for all the points in the hologram relevent for generating a wavefront at V are defined in the set

$$f^V = \{f_{1,1}, f_{1,2}, \dots f_{m,n}\} \tag{5.11}$$

In the 2D scenario the orientation of the wavelet needs to be considered. The discrete rotation parameter for one point $X(k_x, k_y)$should be equal to θ_{k_x,k_y} for selecting hologram contents that will generate a wavefront at V.

The wavelet functions, that we choose are sinusoids at different *scales* (frequencies), and *rotations* (orientations), which are a having a compact support, i.e they are modulated with a time/space limited function. The shifts of these modulating functions provide the *translation* of the wavelet functions.

If we perform the dot product of set of modulated (windowed) sine wave functions with the hologram, then the result is a another hologram that has the same frequency content as the modulated sine waves at each localized (k_x, k_y) positions on the hologram. One of these modulated sine waves is called as the *kernel* function, denoted by ψ_{k_x,k_y} and forms the basis of the transform operation. Let ψ^V be a family of wavelet functions related to a fixed 3D point V

$$\psi^V = \{\psi_{k_x,k_y}\}_{k_x=1\dots m\ k_y=1\dots n} \tag{5.12}$$

The dot product of each element of ψ^V with H is given as

$$C_{k_x,k_y} =< H, \psi_{k_x,k_y} > \tag{5.13}$$

where C_{k_x,k_y} is the wavelet coefficient associated with the pixel (k_x, k_y) of the hologram.

We define C^V as the set of wavelet coefficients that are associted with the point V.

$$C^V = \{C_{k_x,k_y}\}_{k_x=1\dots m\ k_y=1\dots n} \tag{5.14}$$

These are the coefficients selected from the wavelet decomposition of the hologram to get the wavefront diffracted at V by the hologram.

In the case that ψ^V are orthogonal wavelet functions, we can obtain H^V from C^V, with H^V being the sub-hologram specifically associated with observer point V.

$$H^V = \sum_{k_x,k_y} C_{k_x,k_y}\psi_{k_x,k_y} \tag{5.15}$$

5.2.3 Comment on the complexity and memory requirements of the calculation

For the 1D case, the sub-hologram H^V is obtained from the minimum number of coefficients that are needed to cause a diffraction at V. This calculation requires $L \times n$ complex multiplications and $L \times n$ complex additions, where L is the number of discrete points in ψ_{k,f_k}. Apart from being computationally intensive, this approach will also need enough memory to store the vectors ψ^V for every discrete point in the hologram $L \times n$ values. If there are N such observer points, then the memory needed will be $L \times n \times N$. Also the computation will require $L \times n \times N$ complex multiplications and $L \times n \times N$ complex additions. These are the results for the 1D case. For the 2D case (which is the requisite use case), the complexity for a $n \times m$ hologram with $N \times M$ observer positions will be $L^2 \times n \times m \times N \times M$ complex multiplications and $L^2 \times n \times m \times N \times M$ complex additions, with a memory requirement of $L^2 \times n \times m \times N \times M$ complex values.

5.3 The Gabor Basis Function and the Morlet Wavelet

In order to understand the construction of the Morlet wavelet [84] we need to clearly differentiate the Gabor function and the Gabor kernel. A Gabor function or Gabor atom is a non-zero mean function which was introduced by Dennis Gabor in 1946 who was suggesting the idea of using a granular system to produce sound [85]. These Gabor functions form a basis for a family of wavelets called as the Gabor wavelets. A Gabor kernel is a zero-mean function, and hence will satisfy the admissibility condition for wavelets, thus being suited for multi-resolution analysis [86].

We begin by refreshing the concepts of the Gabor basis function. Gabor basis functions have the limitation of not being inherently admissible. As per section 3.3, we have emphasized that for a wavelet function to be used in a view-based representation and reconstruction system for holograms, the wavelet needs to satisfy the admissibility criterion. In this section we shall design a Morlet wavelet [84] beginning with the Gabor function in the 1D form and forming the corresponding Gabor kernel, and then moving to the 2D form.

A Gabor function is formed by combining a sinusoid and a gaussian. Figure(5.3) shows this for the 1D form. The Gabor function which is chosen is taken in the complex form because the best theoretical space-frequency localization is obtained in this form [74]. We define the Gabor basis in the one dimensional continuous form as

$$g_{\beta,f_c}(x) = K.w(\beta x)S(2\pi f_c x) \tag{5.16}$$

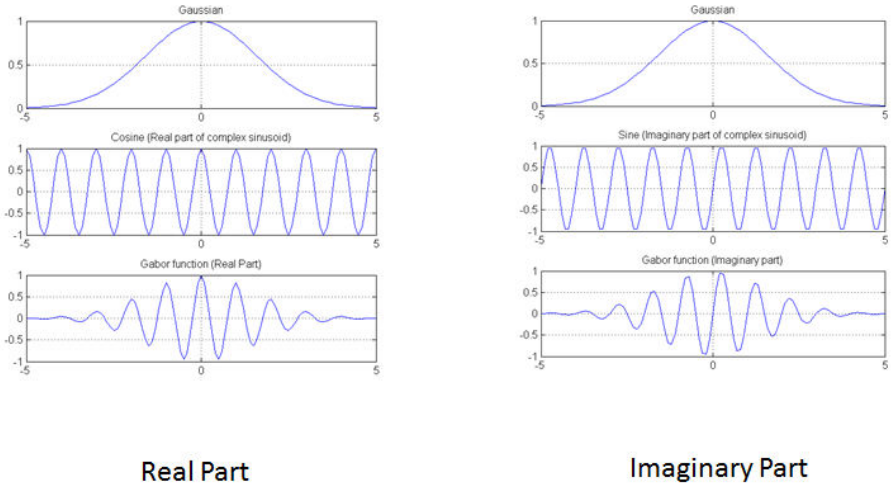

FIGURE 5.3: Gabor function formed by combining a Gaussian and a complex sinusoid

where,

$$w(x) = \exp(-x^2) \tag{5.17}$$

and

$$S(x) = \exp(jx) \tag{5.18}$$

where $w(.)$ represents the gaussian window function and $S(.)$ represents the sinusoid function having frequency f_c, K is the norm of the basis function and β is a function of the parameter of the Gaussian function σ (standard deviation). β is given as,

$$\beta^2 = \frac{1}{2\sigma^2} \tag{5.19}$$

The full width at half maximum (FWHM) or 3dB width of the Gaussian is given as

$$W_{s_c} = 2\sqrt{2\ln(2)}\sigma \tag{5.20}$$

Taking the Fourier transform of equation(5.16), we get the spectrum G of the Gabor basis function,

$$G_{\beta,f_c}(f) = K.\int_{-\infty}^{\infty} w(\beta x).\exp(j2\pi f_c x).\exp(-j2\pi f x)dx \tag{5.21}$$

We choose,

$$f_c = \frac{1}{\sqrt{2}}\pi\beta \tag{5.22}$$

From the above choice we would like to have an inverse variation of the standard deviation σ with respect to f_c. This allows for better space localization of the wavelet at

higher frequencies and better frequency localization at lower frequencies. Hence,

$$\beta = \frac{\sqrt{2} f_c}{\pi} \tag{5.23}$$

The Fourier transform of the Gabor basis function (5.16) is given as

$$G_{\beta,f_c}(f) = K. \int_{-\infty}^{\infty} \exp(-j2\pi(f - f_c)x).w(\beta x).dx \tag{5.24}$$

$$G_{\beta,f_c}(f) = \frac{K}{\beta} W(\frac{f - f_c}{\beta}) \tag{5.25}$$

$G_{\beta,f_c}(f)$ is centered at f_c, i.e the peak is at this frequency and $W(.)$ is the Fourier transform of $w(.)$,

$$W(f) = \exp(-\pi^2 f^2) \tag{5.26}$$

The half magnitude bandwidth (HMB) is given as

$$W_{f_c} = \beta = \frac{1}{\sqrt{2}\sigma} \tag{5.27}$$

Equation (5.23) gives an important relation between the parameter β related to the Gaussian function, and the frequency of the sinusoid f_c. Later the parameter β can be tuned for centering the Gabor function on different frequencies. As it can be observed from equation(5.20) and equation(5.27), the product of the FWHM and HMB is always a constant and it is independent of the parameter σ. This shows the good localization property of the Gabor basis function in space and frequency domains as discussed in [87].

5.3.1 Elimination of the DC term

To enforce the admissibility condition we introduce a term to eliminate the DC response of the filter. The Gaussian low pass filter is chosen as an intuitive choice to eliminate the DC term. After the low pass filtering operation we need the shape of the Gabor basis function to be retained so as to maintain the physical characteristics of the Morlet wavelet. In the following, we detail the successive steps of this computation. We rewrite equation(5.16) for simplicity

$$g(x) = K.w(\beta x).S(2\pi f_c x) \tag{5.28}$$

The Fourier transform is given as,

$$G(f) = \frac{K}{\beta} W(\frac{f - f_c}{\beta}) \tag{5.29}$$

We need to eliminate the magnitude at $f = 0$ [77]. Hence we subtract the output of a low pass Gaussian filter in order to obtain the Gabor kernel. The low pass filtered output and its Fourier transform is given as:

$$h(x) = K.w(\beta x).S(2\pi f_c x) - K.w(\beta x).c.w(\beta x) \tag{5.30}$$

The term $c.w(\beta x)$ is the DC term in the equation. the Fourier transform of which is given as, at $f = 0$

$$G(0) = \frac{c}{\beta} W(\frac{0 - f_c}{\beta}) \tag{5.31}$$

But $G(0) = 1$, which would mean that $c = \beta$.

Therefore equation(5.30) is written as

$$h(x) = K.w(\beta x)[S(2\pi f_c x) - W(\frac{-f_c}{\beta}] \tag{5.32}$$

The Fourier transform of the gaussian function is given as

$$W(f_c) = W(-f_c) = \exp(-\pi^2 f_c^2) \tag{5.33}$$

hence the DC term in 1D form is

$$W(\frac{f_c}{\beta}) = \exp(-\frac{\pi^2 f_c^2}{\beta^2}) \tag{5.34}$$

Equation(5.35) defines the Morlet mother wavelet in 1D form

$$g(x) = K. \exp(-\beta^2 x^2)(\exp(2\pi j f_c x) - \exp(-\frac{\pi^2}{\beta^2} f_c^2)) \tag{5.35}$$

5.3.2 The 2D Morlet wavelet

The discussion in the continuous domain for the Gabor function can be extended in the 2D domain as follows. In the continuous 2D form, we consider the basic Gabor function equation with the parameter of the Gaussian function in the x and y directions to be β.

$$g(x, y) = K. \exp(-\beta^2(x^2 + y^2))(\exp(2\pi j(u_0 x + v_0 y)) - \exp(-\frac{\pi^2}{\beta^2}(u_0^2 + v_0^2))) \tag{5.36}$$

Where u_0 and v_0 are the spatial frequencies in x and y directions respectively in cycles/unit length. We consider a continuous variation in the rotation of the sinusoid within the Gaussian window in the 2D plane. This is denoted by the parameter θ. The

variation of θ in essence signifies the variation of the spatial frequencies in x and y directions of the Gabor function. Representing the spatial frequencies u_0 and v_0 into polar form

$$u_0 = f_c \cos\theta, v_0 = f_c \sin\theta \tag{5.37}$$

where, $f_c^2 = u_0^2 + v_0^2$. K is a multiplier, which is the L2-norm of the basis, and the term $\exp(-\frac{\pi^2}{\beta^2}(u_0^2 + v_0^2))$ is introduced to eliminate the DC response of the Gabor function.

From equation(5.23) we get

$$u_0^2 + v_0^2 = f_c^2 = \pi^2\beta^2 \tag{5.38}$$

Substituting equation(5.38) in the DC term of equation(5.36) we get

$$\exp(-\frac{\pi^2}{\beta^2}(u_0^2 + v_0^2)) = \exp(-\frac{\pi^2}{\beta^2}\pi^2\beta^2) = exp(-\pi^4) \approx 0 \tag{5.39}$$

Hence this term can be neglected.

The general equation of the Gabor function in 2D continuous form becomes after substituting equation(5.39) in equation(5.36) and incorporating the parameter θ

$$\psi(x,y) = g(x,y) = K.\exp(-\beta^2(x^2+y^2))exp(2\pi^2\beta j(x\cos\theta + y\sin\theta)) \tag{5.40}$$

Equation(5.40) is the Morlet mother wavelet in 2D form, which will be denoted as $\psi(x,y)$ from now on. It can be used as a basis for the application in view-based representation of holograms.

5.3.3 Scaling of the Morlet wavelet

In order to build a family of Morlet wavelets we introduce the *scale* parameter in its continuous form in 1D and then extend to 2D form. The Morlet mother wavelet function in one dimensional form from equation(5.35), where $\beta = \frac{\sqrt{2}f_c}{\pi}$ is given as follows:

$$\psi(x) = K.\exp(-\frac{2f_c^2x^2}{\pi^2}).\exp(j2\pi f_c x) \tag{5.41}$$

The Fourier transform is given according to equation(5.25) and centered at f_c

$$\hat{\psi}(f) = \frac{K\pi^4}{2f_c^2}\exp(-\frac{\pi^4(f-f_c)^2}{2f_c^2}) \tag{5.42}$$

We can consider equation(5.41) like a mother wavelet centered at f_c. The suitable translation and dilation of this equation will give us a family of functions that will span the frequency plane. The parameter s controls the spatial and frequency resolution of

the basis decomposition. The scaled frequencies based on parameter s will be given as:

$$f = \frac{f_c}{s} \tag{5.43}$$

The Full Width at Half Maximum (W_s) and Half Magnitude Bandwidth (W_f) will be scaled as:

$$W_s = W_{s_c}.s\frac{\pi}{2f_c} \tag{5.44}$$

$$W_f = \frac{W_{f_c}}{s} \tag{5.45}$$

where $s > 0$. On utilization of the parameter s and a parameter b which is a shift variable in the spatial domain, the Gabor basis function forms a family of functions given as:

$$\psi_{s,b}(x) = K.\exp(-\frac{2f_c^2x^2}{\pi^2}\frac{(x-b)^2}{s^2}).\exp(j2\pi f_c\frac{x}{s}) \tag{5.46}$$

Each $\psi_{s,b}(x)$ contains the local frequency information at $x = b$.

From equation(5.40) we can give the 2D form of the basis function centered at $f_c = \sqrt{u_c^2 + v_c^2}$, with the parameters s and θ

$$\psi_{s,\theta}(x,y) = K.\exp(-\frac{f_c^2}{s^2\pi^2}((x-a)^2 + (y-b)^2))\exp(2\pi^2\frac{f_c}{s\pi}j(x\cos\theta + y\sin\theta)) \tag{5.47}$$

The variation of s and θ allows for the spanning of the spatial frequencies along the x and y directions. For example, 3 rotations and 3 scales of the 2D basis function shall provide for 9 different combinations of spatial frequencies.

It can be noted the scaling parameter s, scales both the sinusoid as well as the Gaussian function.

5.4 Discretization of the Morlet Wavelet

In this section we explain the discretization of the Morlet wavelet for the application of view-based representation of holograms where we will aim to achieve equal number of oscillations for every scaled and translated Morlet wavelet. The analysis so far is limited to the continuous domain. The theory so far presented is very close to the theory of Continuous Wavelet transforms (CWT). The Morlet wavelet does not have a unique spanning function. Instead the spanning of the frequency domain is done at discrete frequencies as it will be explained in this section. To begin with the discretization, we need to identify the degrees of freedom that the Morlet wavelet provides. It gives us 4

degrees of freedom (5.47), namely a, b, s and θ, and these need to be discretized for the application of view based representation of holograms.

We begin by the discretization of x and y. As seen in equation(5.30), the Gabor kernel is composed of a sinusoid enveloped by a Gaussian. We begin by considering a suitable length of the Gaussian given by L. The length L is selected based on the tapering of the Gaussian function where the values can be considered to be close to 0. We then ensure that there are N_0 oscillations of the sinusoid with frequency f_0 within this Gaussian. N_0 needs to be at least 1, implying that there will be at least one oscillation of the sinusoid. The length of the Gabor kernel hence becomes:

$$L = \frac{N_0}{f_0} \tag{5.48}$$

This ensures that there are equal number of oscillations within the Gaussian irrespective of the frequency. We need to have equal oscillations for an even weighing of the coefficients for better pruning in our view-based representation system. For the discretization of the function we use the Nyquist criterion. The sampling frequency f_s is selected to be twice the frequency of the sinusoid. This gives us the actual discrete length of the analog window function L_w that is needed for the numerical representation of the Morlet wavelet (5.47).

$$L_w = L.f_s \tag{5.49a}$$

$$= \frac{N_0}{f_0}.2f_0 \tag{5.49b}$$

$$= 2N_0 \tag{5.49c}$$

The discrete sampling parameters in the 2D case are m with a length of $M = L_w$ for the x direction and the y direction as n with length $N = L_w$, since we consider isotropic envelope Gaussian functions. Usually the L_w and N_0 parameters are fixed as shown in figure(5.4) where $L_w = 20$ and $N_0 = 1$. This ensures that for every frequency the shape of the wavelet is constant. Only the changes are in the length L for each wavelet. Hence we do not observe any change of size or shape after discretization. This will ensure us an even weighing of the wavelet coefficients for all the frequencies.

Now we discretize the scale (s) as (s_l) and the rotation parameter (θ) as (Θr).

$$s_l = \frac{f_c}{f_0} \tag{5.50}$$

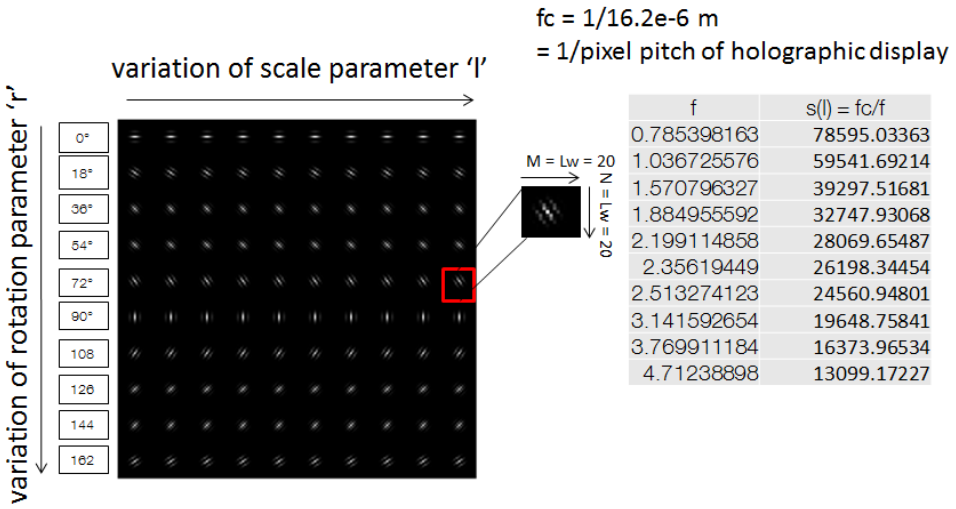

FIGURE 5.4: Morlet wavelet discretization

The complete discrete equation in 2D form is given as in equation(5.51).

$$\begin{aligned}\psi_{l,r}[m,n] &= \exp\left(-\frac{f_c^2}{s_l^2\pi^2}(m^2+n^2)\right)\\ .\exp&\left(2\pi^2\frac{f_c}{s_l\pi}j(m\cos(\Theta r)+n\sin(\Theta r))\right),\end{aligned} \tag{5.51}$$

The square brackets represent discrete parameters, where $-\frac{M}{2} \leq m < \frac{M}{2}$ and $-\frac{N}{2} \leq n < \frac{N}{2}$ and M and N represent the lengths of the wavelet functions in the spatial domain and are integers, $l > 0$ and integer, and $\Theta = \frac{\pi}{K}$ and $-K \leq r \leq K$ and K is the total number of discrete rotations with $K > 0$ and is integer. This is a wavelet function that is centered at f_c and scaled by a discrete parameter l and rotated by the discrete parameter r.

The dot-product approach can be performed as per the explanation given in section 5.2.2 and for the convolution approach we perform the convolution of this wavelet function (in its scaled, rotated and translated form), and the hologram H results in a set of wavelet coefficients that approximate the hologram for a particular frequency and direction. The figure(5.4) shows the discrete form of the Morlet wavelet. The figure shows the family of Morlet wavelets obtained by the variation of the discrete rotation parameter r and the discrete scale parameter l.

The convolution of the hologram and the wavelet function is denoted as

$$H_{l,r} = H \circledast \psi_{l,r} \tag{5.52}$$

For both the approaches (convolution and dot-product) we ensure that the operation is performed on the exact physical size L on the hologram. In our implementations we have resampled portions of the hologram that undergo convolution or dot-product operations based on the frequency of the wavelet that is used. The resampling in fact automatically performs a low pass filtering operation to remove all frequencies higher than $\frac{f_s}{2}$.

This results in the set of various frequencies selected from the hologram based on the l and r parameters, each corresponding to a viewing direction.

Now we will determine which wavelet coefficients should be transmitted based on the observer position.

5.5 Discretization of the observer space

Assuming that the viewer is far compared to the size of the hologram, we can consider as a first approximation that all rays coming from the hologram to the observer are parallel. Thus each observer position is associated with a unique viewing direction. All viewing directions are spanned by considering observer positions lying on a plane parallel to the hologram, that we call "observer plane". Each point on the observer plane defines a viewing direction.

Let V denote the position of the viewer in the observer plane in a given coordinate system attached to the hologram. We consider the orientation of V with respect to M, the center of the hologram. We express $X - M$ in spherical coordinates $(\phi(V), \theta(V))$ in a given coordinate system attached to the hologram as shown in the figure(5.5).

Point V will receive light diffracted from the hologram in the direction $\theta(V)$,$\phi(V)$. Due to the grating equation (4.1), light diffraction in the direction of V is produced by hologram contents with orientation $\theta(V)$ and frequency $\frac{\sin(\phi(V))}{\lambda}$, where λ is the wavelength of the incident light.

Thus the discretization of Morlet wavelets defines a discretization of the observer space : for each couple $\{l, r\}$ defining a specific wavelet, there is an associated point V per viewing direction defined by $\theta(V)$, $\phi(V)$ such that:

$$\begin{cases} \theta(V) = \Theta r \\ s_l = \frac{\sin(\phi(V))}{\lambda} \end{cases} \tag{5.53}$$

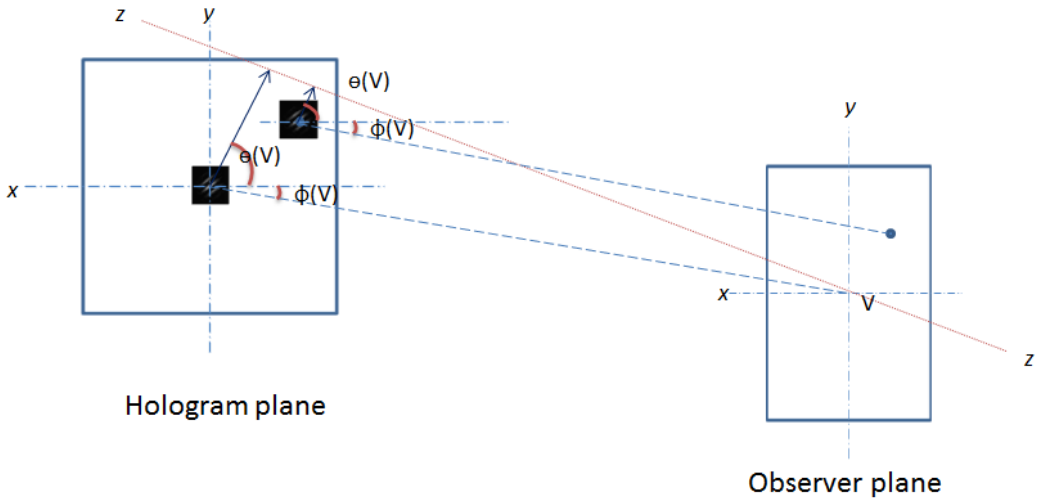

FIGURE 5.5: Discretization of the observer space for convolution operation

This indicates the selection of coefficients for the propagation of the wavefront from the hologram in the general direction of the position of the viewer. Based on the position V of the viewer, we calculate the general couple $(\phi(V), \theta(V))$ from the center of the hologram plane M. We use the same wavelet (l, r) corresponding to $(\phi(V), \theta(V))$, for every point in the hologram plane. This is dot product at every point in the hologram with the same wavelet function i.e convolution of the hologram H with wavelet ψ_l, r.

If the viewer positions are limited, then there will be less $\{l, r\}$ values, while for large number of observer points (caused by fast movement of the observer or more number of viewers), there will be more $\{l, r\}$ values to be transmitted.

5.6 Calculation of scaling frequencies of the Morlet wavelet: an example

In our example we discretize the observer plane based on the dynamics of the scene to be reproduced. The selection of the zones of reconstruction depends on the areas of the scene that are more prominent for the viewer at a particular position. We consider in the following example a simple cube object, and show step-by-step the process for identifying the diffraction angles for various observer positions and in turn discretize the reconstruction plane.

The cube is of 20 cms per side having 11 points each. The front face of the cube is 20 cms from the hologram plane and the rear face is at 40 cms. The figure(5.6) explains the scene. We will try to simulate 4 viewer positions that can see 4 distinct edges

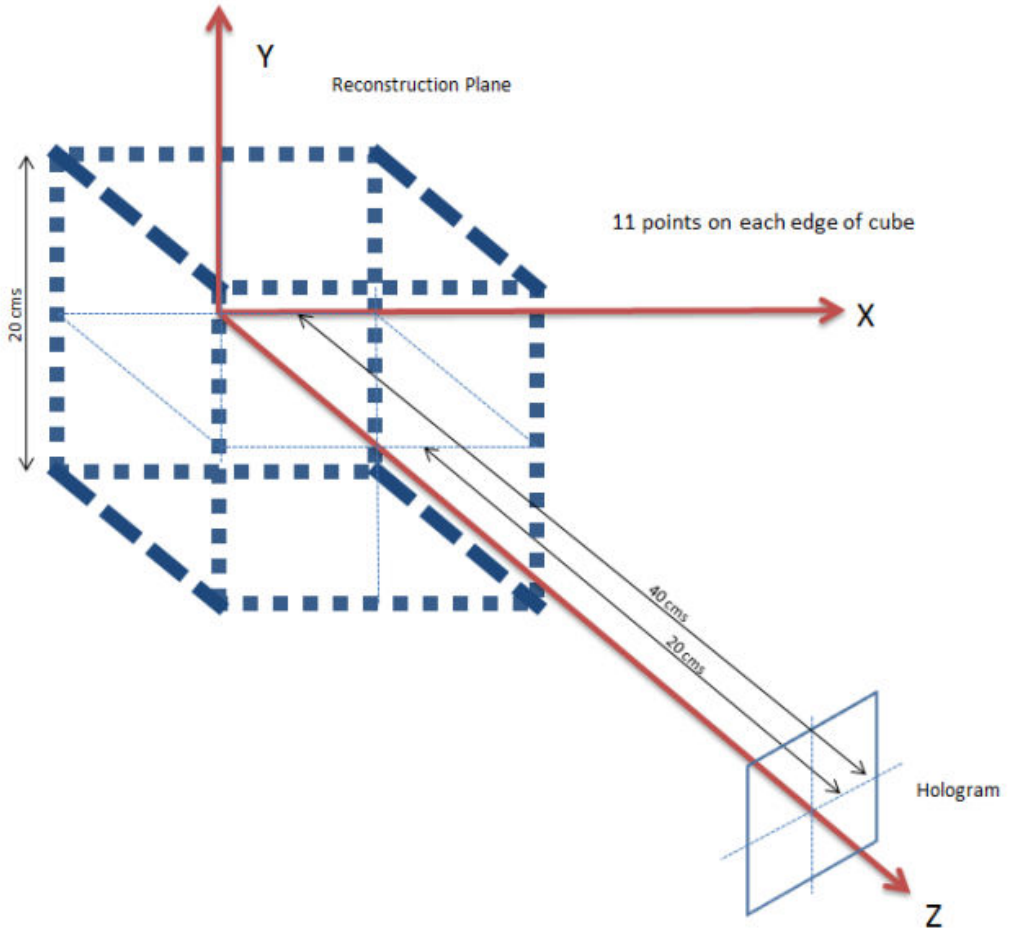

FIGURE 5.6: Cube location and scene dynamics

of the cube, namely the Front face Left Edge (FL), the Front face Top Edge (FT), the Rear face Bottom Edge (RB) and the Rear face Right Edge (RR). Each of these edges will be observed from 4 distinct observer positions $(\phi(V), \theta(V))$ given according to equation(5.53).

For these large angles of diffractions, we consider the wavelength $\lambda = 1732\mu m$ and pixel period $PP = 2mm$ for generating the hologram. These values allow for a maximum diffraction angle of about 60^o. The convolution operation is a dot-product operation on the hologram with only one wavelet per view. Since there are only 4 observer points, 4 Morlet wavelets are sufficient. We need only 2 scale 'l' values and 4 rotation 'r' values to discretize the observer space. Since this is a very simple scene, we selected this approach.

We first begin by calculating the various $(\phi(V), \theta(V))$ values in the observer space. The table(6.1) gives these values.

TABLE 5.1: Angles of reconstruction for Front face Left Edge (FL), the Front face Top Edge (FT), the Rear face Bottom Edge (RB) and the Rear face Right Edge (RR)

Edge	$\theta(V) = \Theta r$(degrees)	$\phi(V)$(degrees)	$s_l = \frac{\sin\phi}{\lambda}$(cycles/unit length)
FL	0	26.57	258.21
FT	90	26.57	258.21
RR	180	14.04	140.03
RB	270	14.04	140.03

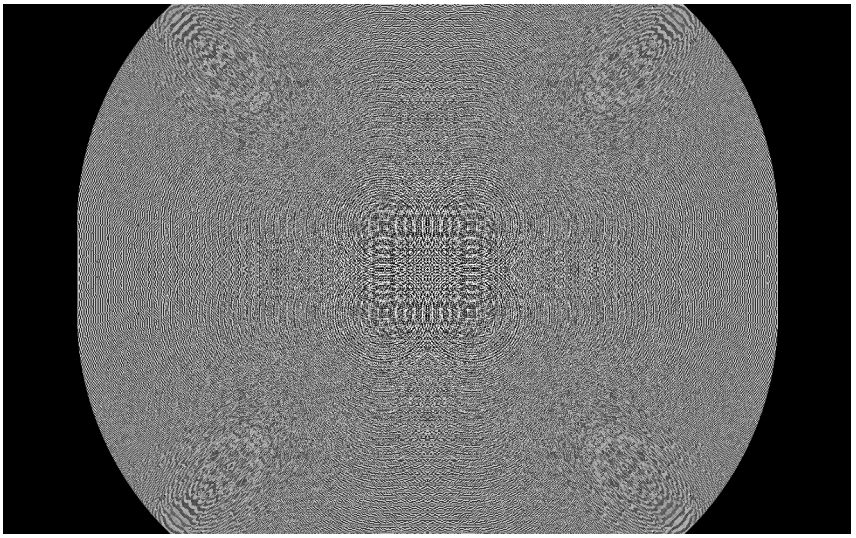

FIGURE 5.7: Cube hologram (1920x1200px)

Numerical reconstruction is done by using the angular spectrum method on tilted planes as shown in Appendix A. We perform the Morlet transform of the hologram using the basis function as described in the last section. The figure(5.7) shows the hologram. The Morlet transform is carried out on a Matlab implementation using CUDA. The time taken for the transform is about 1 second on a Quadro 3000M GPU. We compare the reconstructions of the Morlet transformed hologram and that of the original (non-transformed) hologram. Figures(5.8,5.9,5.10,5.11,5.12).

Let us now attempt to reconstruct the FT edge with a Morlet transformed sub-hologram of the RB edge. The figure(5.12) shows the results. Notice how the output loses the sharpness. In this example we have used the Morlet wavelet to reconstruct the cube at different angles of observer positions. We have used convolution method to obtain the wavelet coefficients. It is observed that the reconstruction seems acceptable, but as the complexity of the scene increases this method of transform may not be suitable. The reconstruction obtained using the convolution method is not a *perfect* reconstruction, since we have considered an approximation by considering the same angles of diffraction for

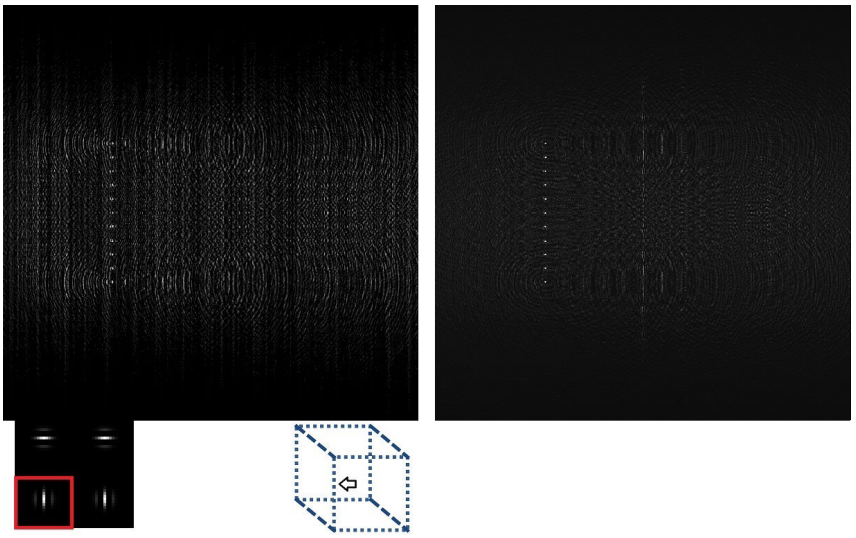

FIGURE 5.8: (Left)Reconstruction of Morlet transformed hologram for FL edge.(Right)Numerical reconstruction of the FL edge

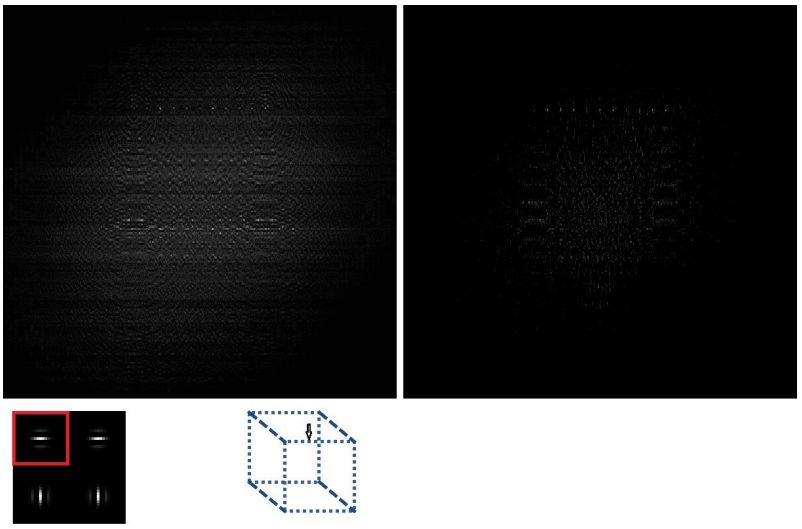

FIGURE 5.9: (Left)Reconstruction of Morlet transformed hologram for FT edge.(Right)Numerical reconstruction of the FT edge

any point on the hologram instead of varying angles (individual localized dot-products). We have also shown that if we use the wrong general direction (i.e the incorrect wavelet for the transform that does not correspond to V), we will obtain a highly degraded output visually.

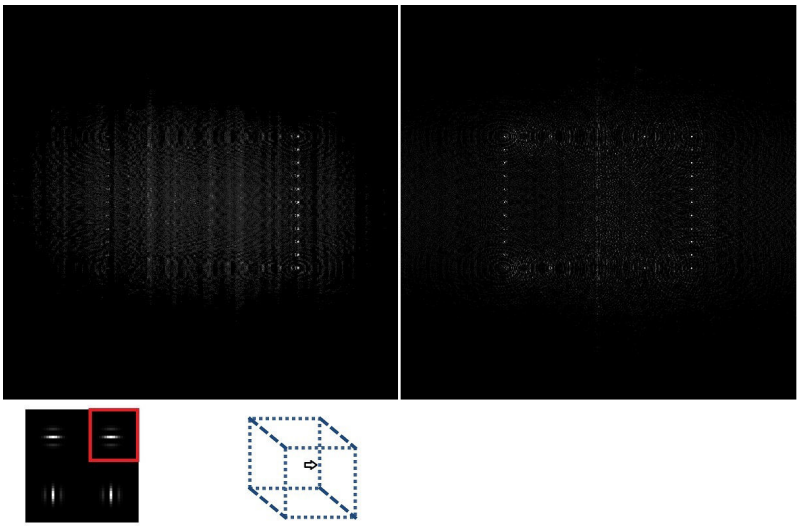

FIGURE 5.10: (Left)Reconstruction of Morlet transformed hologram for RR edge.(Right)Numerical reconstruction of the RR edge

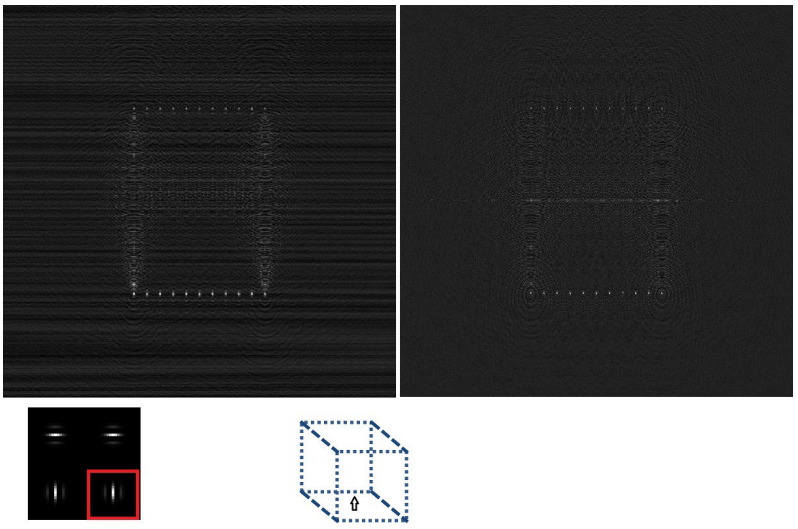

FIGURE 5.11: (Left)Reconstruction of Morlet transformed hologram for RB edge.(Right)Numerical reconstruction of the RB edge

5.7 Results

In this section we generate some results for a hologram having the following specifications:

- Pixel pitch = 8.1 μm
- Wavelength = 11.08 μm
- Dimensions = 2048x2048 pixels

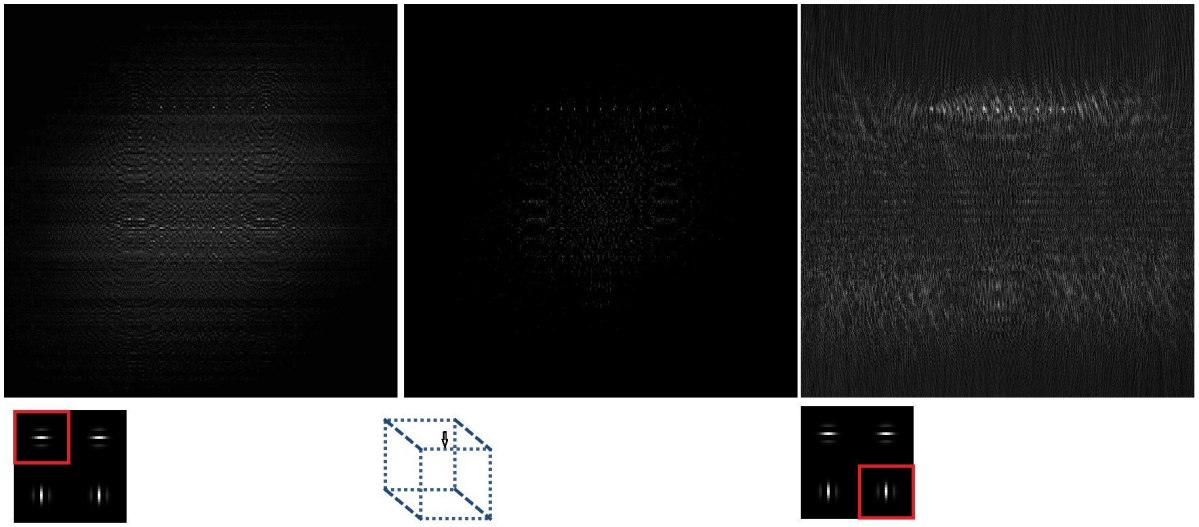

FIGURE 5.12: (Left)Reconstruction of Morlet transformed hologram for FT edge.(Center)Numerical reconstruction of the FT edge. (Right)Reconstruction of Morlet transformed hologram using the sub-hologram for the RB edge

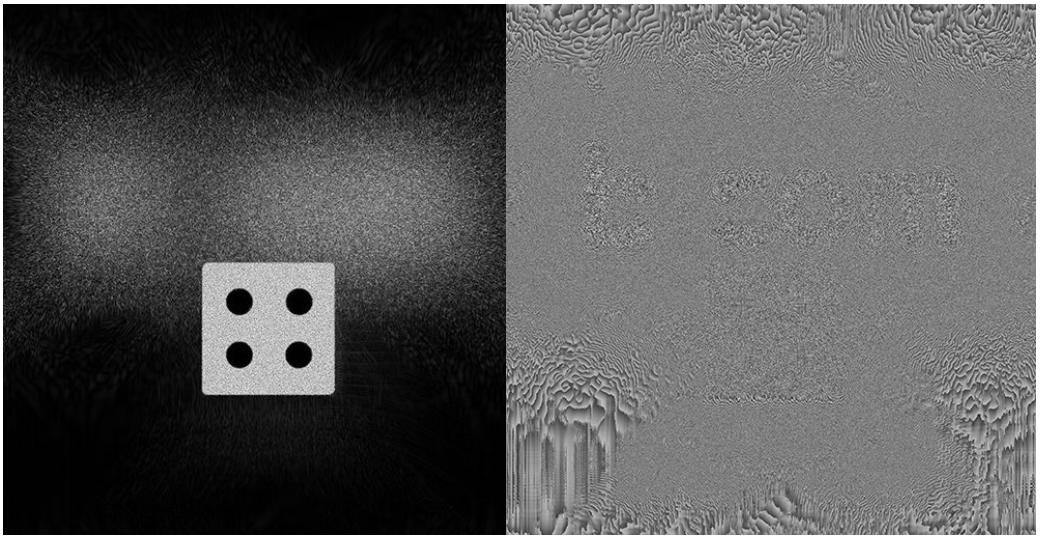

FIGURE 5.13: Amplitude of the logo_dice hologram

FIGURE 5.14: Phase of the logo_dice hologram

The scene contains a dice which is present at the plane of the hologram and a logo of $b<>com$ at $0.0025m$ from the dice behind the hologram plane. This is a relatively small sized object. Hence we simulate the observer to be at maximum 0.0025m in front of the hologram. It is observed that at this distance, only about 25% of the coefficients are needed for reconstructing the hologram by simulating an eye aperture of $0.001m$.

The logo_dice hologram is illustrated in figure(5.13,5.14).

In this experiment we compare Morlet wavelets based representation with respect to the golden reference i.e the dot product result or perfect reconstruction as explained in section(5.2.2). Results are obtained for a use case having 25% of coeffcients for viewing angles of 0^o and 15^o, for size of the hologram of 2048x2048, and at quantization values of 5 and 8 bits. Linear quantization is performed on the coefficients. Table(5.2) presents the RD results. C.r represents the compression ratio between the transformed hologram and the uncompressed original hologram, bpp (bits per pixel) are obtained after entropy coding of the transformed coefficients and dB is the PSNR between the golden reference or perfect reconstruction as explained in section(5.2.2). The reconstructions obtained are themselves quantized at 8-bits before calculating the rate distortion. It can be observed that a quantization of 5 bits is sufficient to get good approximation of coefficients. The Gaussian window (Morlet wavelet) provides a stable PSNR of $32db - 35db$ for different viewing angles. The effective bitrate for a 30 frame per second video sequence will be 69 Mbits/sec for quantization of 8-bits and 27.5 Mbits/sec for quantion of 5-bits.

TABLE 5.2: Morlet wavelet transformed reconstructions at 5-bit and 8-bit quantization

Q=8 (Morlet)	c.r	bpp	dB
0^0	7.2356	1.1056	33.61
15^0	7.2184	1.1083	35.46
-15^0	7.2401	1.1050	35.16
Q=5 (Morlet)	c.r	bpp	dB
0^0	17.9037	0.4468	32.88
15^0	17.8791	0.4474	35.62
-15^0	17.9402	0.4459	35.37

5.8 Conclusion

In this chapter we have used a modified Morlet wavelet for obtaining the localized space and frequency information from the hologram. Beginning with the Gabor function, we have overcome the problem of inherent non-admissibility by eliminating the DC term to obtain the Gabor kernel and then discretized it in order to maintain the physical properties of the Morlet wavelet. The design, discretization and implementation of these modified Morlet wavelets for the view-dependent compression system is explained in detail.

We have used the same method of the transform as used in the previous chapter i.e convolution. These Morlet transformed coefficients are shown to be used in conjunction with a view-based compression systems. Due to a limited number of view-points and the utilization of GPU processing for the convolution operation, the speed of the transform

is satisfactory if used for scenes with minimal details. The convolution method does not create an accurate reconstruction at the observer space. We showed that the Morlet wavelets selected can produce a reasonable reconstruction from the sub-holograms, and the usage of a Morlet wavelet which does not correspond to a particular view results in a poorer quality output.

In the next chapter we will perform the Morlet wavelet transform using the dot product approach. Shannon wavelets will be considered as a candidate for efficient computation and we will evaluate it with respect to Morlet wavelets in terms of computational efficiency and quality.

Chapter 6

View dependent representation of holograms with Shannon wavelets

6.1 Introduction

The purpose of an efficient hologram representation system is the effective pruning of the hologram with the ability to be able to reconstruct accurately the views at the observer positions. With the wavelets seen so far (Gabor wavelet Chapter 4 and Morlet wavelet Chapter 5), for an accurate reconstruction the complexity of generating the hologram representation (sub-hologram) is too large to be able to be completed in real time. In such a case where the sub-hologram needs to be generated *offline*, we would need to store large numbers of sub-holograms corresponding to all possible observer positions. Based on the real-time position of the observer the corresponding sub-hologram is selected and transmitted. The problem with this approach is the large memory requirement to store all the sub-holograms. An alternative approach is to generate the view-dependent sub-holograms on *on-the-fly*. This requires a real-time scheme of sub-hologram generation. In both the cases of Gabor wavelet and Morlet wavelet we have used the convolution approach. This is at the cost of not obtaining perfect reconstructions at the position of the observer as shown in chapter 5.

Under restrictive assumptions, we need to get a sub-hologram on the fly (without pre-computation) by making the pruning in the frequency domain. The assumptions are :

- There is only one observer
- The large scene setting, large hologram resolution, viewing distance etc., lead to a small cropping window in the observer plane

With the restriction of having a large or *immersive* scene, it is not possible to use the convolution operation of a single wavelet function to obtain the accurate coefficients of the hologram that can generate a field at an arbitrary point in the observer space. This is because convolution will enable us to gather the coefficients from the hologram that generate a field in the general direction of the observer. When this field is cropped based on the physical property of the observer i.e. pupil size, a lot of information will be lost. In the case of the example shown in section 5.6, the object (cube) is small in size (20 cms). In that case the cropping of the field at the observer would not make much difference, even though it does not contain all the information at the observer point. These reconstructions that have been carried out so far are *imperfect* reconstructions. For a *perfect* reconstruction, we need to be able to capture all the coefficients from the hologram that cause a field at the observer position. In (section 5.2) we have described in detail the selection of coefficients (transform operation) by the dot product approach, and commented on the complexity of using the dot product based approach (section 5.2.3). In this chapter, we are looking for a solution that combines both real-time constraints and perfect reconstruction. For this purpose we propose the use of Shannon wavelets.

In the following sections we will , introduce the Shannon wavelet in discretized form (section 6.2) and provide an optimized Shannon wavelet that will perform the convolution operation for a perfect reconstruction at the observer position (6.3) and comment on the performance. We shall provide results for representing one hologram with Shannon wavelets and compare the results with Morlet wavelets (6.5), and end with some conclusions (6.6).

6.2 Shannon Wavelet Analysis

The hologram is decomposed through a wavelet transform. The chosen wavelet basis needs to be well localized in spatial and frequency domains [87], since the spatial localization allows for the efficient pruning of the coefficients and the frequency localization provides the accurate cones of diffractions for reconstructions at discrete observer positions. Earlier methods have attempted the use of Fresnelets, which are Fresnel transformed B-splines as discussed in chapter 3. The Fresnel transform in essence spreads-out the features of the B-splines and hence the space localization is lost. Hence we focus on wavelet functions such as the Gabor wavelet, which provide the best theoretical space-frequency localization as discussed in chapter 3 and chapter 4. However, testing various window functions in place of the Gaussian window of Gabor wavelets, we found that using cardinal sine provided interesting results, which indicates that for our application

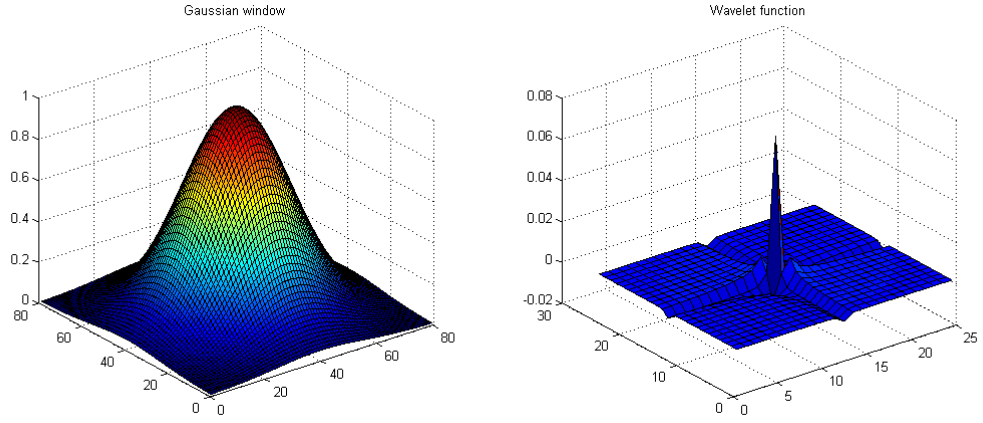

(a) Gaussian window and the Gabor wavelet function

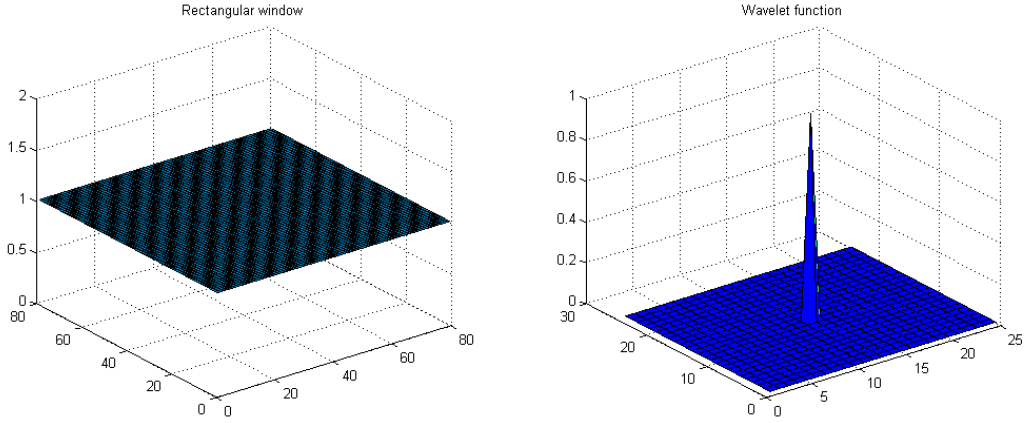

(b) Rectangular window and the Shannon wavelet function

FIGURE 6.1: Window functions

space localization is of utmost importance and the condition of good frequency localization can be relaxed for better reconstruction quality. Moreover, the Fourier transform of the sinc window (which is a Shannon wavelet) is a Heaviside function (rectangular window), which allows fast windowing in frequency domain. Hence we used both Gabor and Shannon wavelets figure(6.1) in our implementation and compared the results.

6.2.1 Shannon wavelet equation in 1D form

The Shannon wavelet centered at frequency F_c and bandwidth F_b is defined by the following equation

$$\psi_{sh} = \sqrt{F_b}(\text{sinc}(F_b x).\exp(2i\pi F_c x)) \tag{6.1}$$

The Fourier transform of the Shannon wavelet is the boxcar function

$$\hat{\psi}_{sh} = \text{rect}(\frac{u - F_c}{F_b}) \tag{6.2}$$

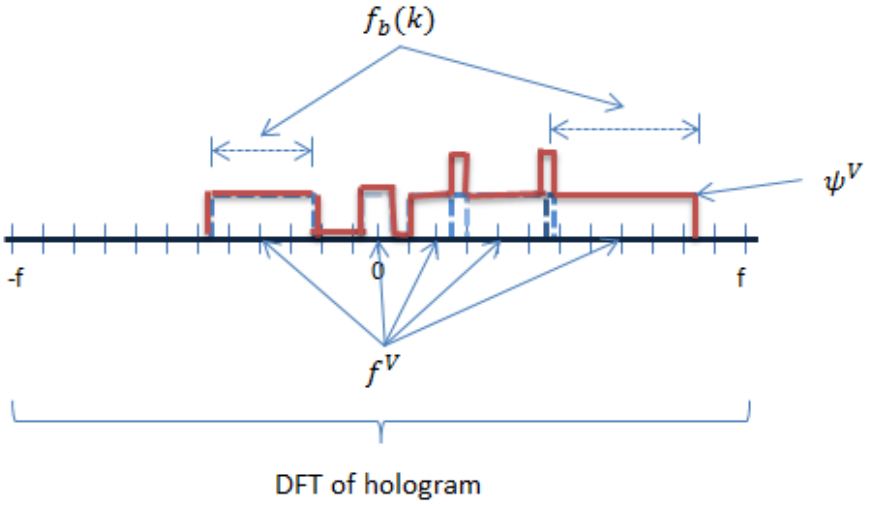

FIGURE 6.2: Frequency domain representation of H_V sub-hologram

Here it is important to derive the relation between f_b and f_c (discrete frequency counterparts of F_b and F_c), which will become evident when we discretize the Shannon wavelet. We perform a N-point DFT of the hologram. Let the pixel pitch of the hologram be denoted by P. The spacing between the DFT points or the pixel pitch in the Fourier domain is given as

$$D_p = \frac{1}{PN} \tag{6.3}$$

The size of the wavelet should be at least enough to cover one period of the sinusoid. The number of discrete points in one wavelet (ψ_{k,f_k}) is given as

$$L = \frac{1}{f_k P} \tag{6.4}$$

We can now easily get the number of discrete points in the DFT as

$$M = \frac{N}{L} \tag{6.5}$$

and the frequency bandwidth to be

$$f_b = M D_p \tag{6.6}$$

From equation(6.4) and (6.6) it can be seen that as f_k increases L decreases, signifying a better space localization, but f_b increases, signifying a poorer frequency localization, and vice-versa. Equation(5.15) can be observed in the frequency domain representation of H^V as shown in the figure(6.2), where each localized dot product in the frequency domain will be a weighted multiplication of varying rectangular functions based on the bandwidth.

The complete discretized form of the family of Shannon wavelets is given as

$$\psi_k[u] = \sqrt{f_b[k]}(\text{sinc}(f_b[k]u).\exp(j2\pi f_c[k]u)) \tag{6.7}$$

6.2.2 Shannon wavelet equation in 2D form

The family of Shannon wavelets in the 2D form that transform the hologram to generate a diffraction at V is given as

$$\psi_{k_x,k_y}[u,v] = f_b[k_x,k_y](\text{sinc}(f_b[k_x,k_y](u+v)).\exp(j2\pi f_c[k_x,k_y](u\cos\theta_{k_x,k_y}+v\sin\theta_{k_x,k_y}))) \tag{6.8}$$

The discretization is done in a similar fashion as the Morlet wavelet, where the number of discrete window points L_w is kept constant for all the wavelet functions and the dot-product operation is performed by resampling the part of the hologram to have the same L_w number of discrete points. This as mentioned earlier allows for natural low-pass filtering operation and all frequencies above $\frac{f_s}{2}$ (where f_s is the sampling frequency) will be automatically filtered out.

6.3 Proposed scheme of calculating sub-holograms

In order to reduce the computational complexity and the memory requirement, we propose a scheme to calculate the sub-holograms in the frequency domain. Using the 1D Shannon wavelet for an observer in 2D space in the frequency domain, we can create a rectangular window to cover all the frequencies in f^V. In essence we will be obtaining a single Shannon wavelet ψ'^V which will have a bandwidth of

$$f'_b = \max(f^V) - \min(f^V) \tag{6.9}$$

and central frequency

$$f'_c = \frac{\max(f^V) + \min(f^V)}{2} \tag{6.10}$$

The definition of the Shannon wavelet is given as

$$\psi'^V[m] = \sqrt{f'_b}(\text{sinc}(f'_b m).\exp(2i\pi f'_c m)) \tag{6.11}$$

The dot-product of this wavelet with hologram H will provide us the coefficients C'_k at pixel positions k on the hologram.

$$C'_k =< H, \psi'^V_k > \tag{6.12}$$

$\psi_k'^V$ is the translated wavelet at each k pixel on the hologram. C'_k are the wavelet coefficients i.e they are the scalar product of the wavelet with the hologram. Thus we define,

$$C'_k = H'^V_k \tag{6.13}$$

C'^V is defined as the set of coefficients obtained by performing the dot-product of equation(6.12) at all the discrete points on the hologram.

$$C'^V = C'_1, C'_2, \ldots, C'_n \tag{6.14}$$

There is subtle difference between the coefficients obtained in equation(5.7a) and equation(6.14). It must be noted here that C'^V is not the set of coefficients that will represent a sub-hologram which generates a *perfect* diffraction or reconstruction at V, but it will represent a super set of coefficients that will represent the sub-hologram which generates a reconstruction at the plane of V.

The dot product operation in equation(6.12) is the convolution operation denoted as

$$H'^V = H \circledast \psi'^V \tag{6.15}$$

The convolution operation in the frequency domain is a multiplication (by using the Fourier property of convolution).

$$\hat{H}'^V = \hat{H}\hat{\psi}'^V \tag{6.16}$$

$$\hat{H}'^V = \hat{H}.\text{rect}(\frac{u - f'_c}{f'_b}) \tag{6.17}$$

The figure (6.4) shows calculation of H'^V in comparison with the calculation of H^V. It can be seen that the H'^V will contain some extra frequencies along with all the relevant frequencies in H^V needed for a reconstruction at an arbitrary point V. Also the coefficient values of the frequencies will not be identical to a dot-product approach. But the observed reconstruction at the observer position V after the Fresnel transform and cropping operations as shown in figure 6.3, will be identical.

$$\text{Fresnel}_{-d2} \circ \text{Crop}_V \circ \text{Fresnel}_{d1}(H^V) = \text{Fresnel}_{-d2} \circ \text{Crop}_V \circ \text{Fresnel}_{d1}(H'^V) \tag{6.18}$$

Considering the generic case as shown in the figure(6.4), we need to cover all the frequencies in f^V that cause a diffraction at V.

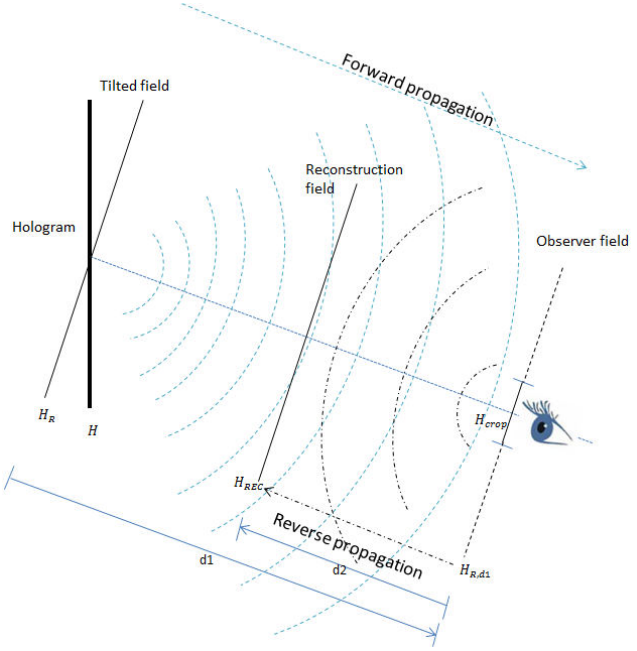

FIGURE 6.3: Illustration of propagation of light field for reconstruction

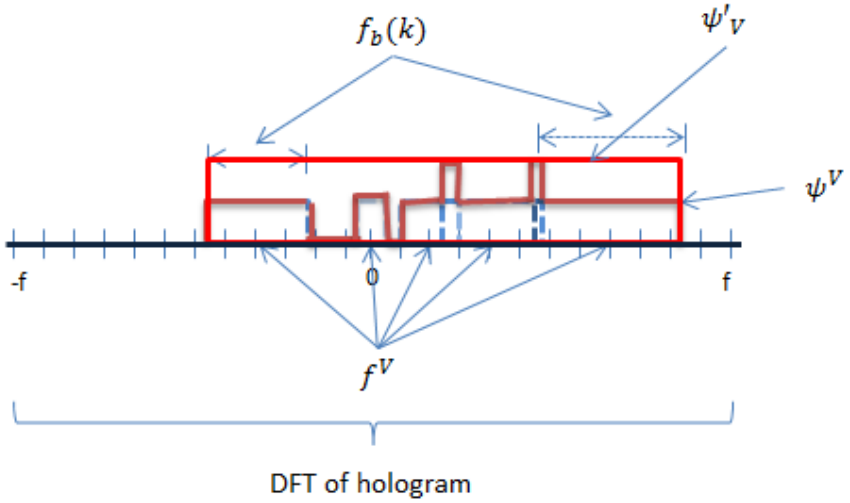

FIGURE 6.4: Frequency domain representation of H'^V sub-hologram

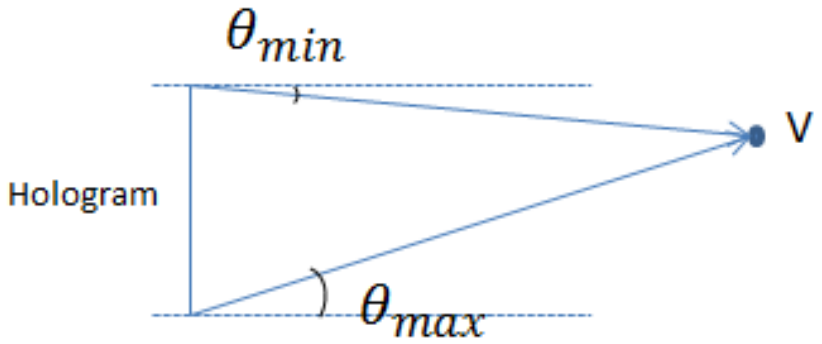

FIGURE 6.5: Max and Min frequencies at V

We can calculate the max(f^V) and min(f^V) as follows. The figure(6.5) shows the maximum and minimum angles. Note that angles are positive in the clockwise direction and negative in the counter-clockwise direction. Using the grating equation we can obtain the maximum and minimum frequencies.

The central frequency F_c, on which the ψ'^V will be centered is given as

$$F_c = \frac{\max(f^V) + \min(f^V)}{2} \tag{6.19}$$

6.3.1 Improvement obtained by the proposed scheme

It is can be observed that using equation(6.16), the maximum number of possible multiplications is now n, (considering that all the frequencies are available at the point V). This approach will not require any extra memory for storage of ψ^V. Hence in terms of memory this method is very efficient and has no overhead compared to the approach in section(5.2).

H'^V will contain all the frequency information that is needed for a diffraction at V, plus some extra frequencies (since we select all the discrete frequencies between f^{max} and f^{min}). Also the values of the coefficients (weights) for these selected frequencies will be different.

Since this approach is completely performed in the frequency domain, it is very useful in the cases of numerical reconstruction techniques since the FFT operation need not be performed if it follows our proposed approach.

6.3.2 Apertures

We can easily consider the point V to be an aperture. It is useful to simulate the observer based on the physical characteristics of the human eye. We can do this by considering the amount of light that is entering the eye via the pupils, which is a natural aperture. The observer position is considered in the form of an aperture also to anticipate the fast motions of the observer. Using the earlier approach this would lead to the calculation of several H^Vs for each discrete point in the aperture, increasing the complexity manifold. With the proposed approach, there will still be only one multiplication operation in the frequency domain just as in the case of a single point, except that we need to calculate the maximum and minimum frequencies that are incident on the aperture. In the next sections we will perform this approach to a 2D hologram plane and an aperture in a 3D space.

For an aperture of area A, having $p \times q$ discrete points, as shown in the figure(5.2),

$$A = \{V_{1,1}, V_{1,2}, \ldots, V_{p,q}\} \tag{6.20}$$

$$H^A = H^{V_{0,0}} + \ldots H^V \ldots + H^{V_{p,q}} \tag{6.21}$$

where H^A is the *sub-hologram* to create a light field around V with area A.

The frequencies incident on the aperture will be

$$F^A = \{f^{V_{1,1}}, f^{V_{1,2}}, \ldots, f^{V_{p,q}}\} \tag{6.22}$$

where $f^{V_{i,j}}$ is defined according to equation(5.11).

The angles of rotation of the wavelets are given as

$$\theta^A = \{\theta^{V_{1,1}}, \theta^{V_{1,2}}, \ldots, \theta^{V_{p,q}}\} \tag{6.23}$$

where $\theta^{V_{i,j}}$ is defined according to equation (5.9).

For a 2D hologram plane, we can split the frequencies in F^A into its constituent frequencies in x and y directions.

$$F_x^A = F^A \cos\theta^A \tag{6.24a}$$

$$F_y^A = F^A \sin\theta^A \tag{6.24b}$$

For the numerical reconstruction of the holograms, a simulation of the eye is performed by considering it as an aperture. In our case we consider this to be a rectangular aperture. The area A around V is the aperture that controls the amount of light entering the eye.

We need to obtain the maximum and minimum diffraction angles from the hologram plane that are incident on the aperture. These angles can be obtained in a similar manner as shown in figure(6.5). The set F^A contains all the spatial frequencies that cause a diffraction on A, hence

$$F' = \{\min(F_x^A) : \max(F_x^A), \min(F_y^A) : \max(F_y^A)\} \tag{6.25}$$

and the central frequency is obtained as

$$F_c' = \{\frac{\max(F_x^A) - \min(F_x^A)}{2}, \frac{\max(F_y^A) - \min(F_y^A)}{2}\} \tag{6.26}$$

When performing the wavelet transform of a hologram, now we can perform the convolution operation , between the hologram and the shifted, rotated and scaled versions of the wavelet function.

Let $\hat{\psi}$ be the Fourier transform of the wavelet function.

The convolution operation in the frequency domain is the multiplication operation between the Fourier transform of the hologram ($\hat{H}$) and the Fourier transform of the wavelet function ($\hat{\psi}'$). Equation(6.21) can be written as

$$\hat{H}^A = \hat{H}.\hat{\psi}' \tag{6.27}$$

Then the multiplication is performed on the discrete frequency given by $F_{C_A} = (F_x, F_y)$, as shown in figure(6.6).

6.4 Framework proposed for the adaptive reconstruction

The flow of the encoding and decoding and reconstruction process is shown in Figure(6.7).

After the wavelet transform and coefficient selection process as explained in section(6.3), we perform uniform quantization and Huffmann entropy coding to the selected coefficients and transmit them over to the decoder side. At the decoder side we perform entropy decoding operation, dequantization and coefficient reconstitution operations.

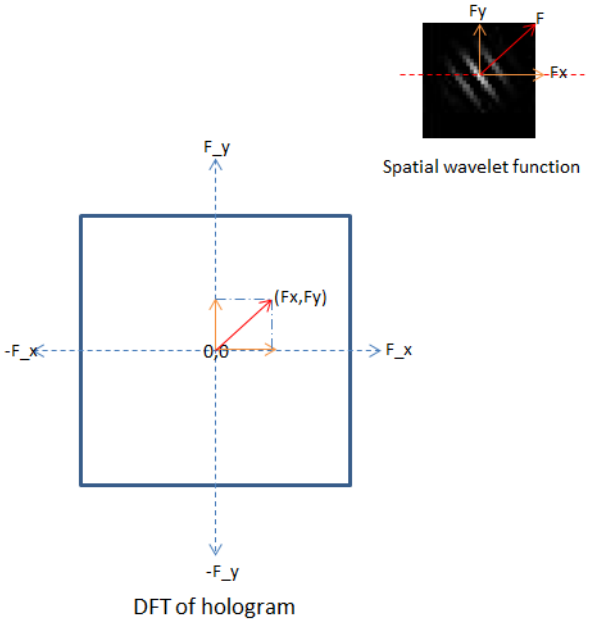

FIGURE 6.6: Frequency selection in DFT output

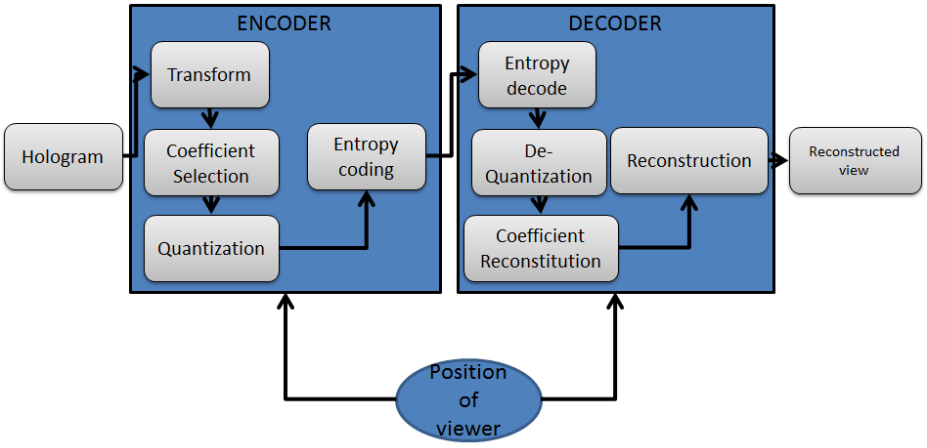

FIGURE 6.7: Flow of encoding and decoding of the hologram

Then these *adaptive* set of coefficients are reconstructed as explained in the next section (6.4.1).

6.4.1 Adaptive Reconstruction

At the decoder side, the transmitted coefficients are used to reconstruct the partial hologram by coefficient reconstitution by identifying the central frequency as in equation(6.19) based on the observer position as explained in figure(6.5). With a real holographic display, this partial hologram is expected to provided valid viewing conditions

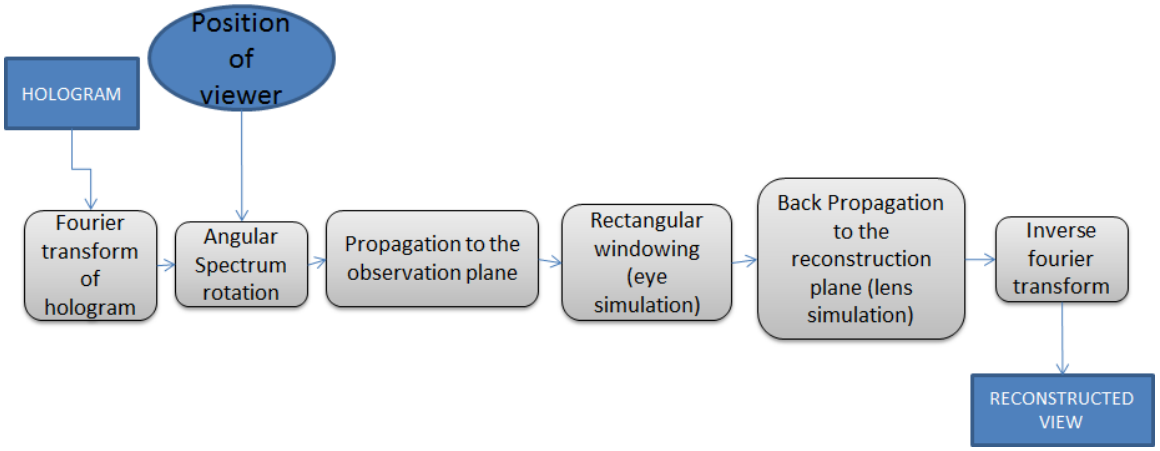

FIGURE 6.8: Adaptive Reconstruction flow

for the observer position. In order to evaluate the quality of the observed view, we simulate the view reconstruction on the observer plane, both from complete and partial holograms. The wave propagation is performed using the Angular Spectrum titled reconstruction and propagation method as proposed by [48, 49] explained in Appendix(A) and illustrated in figure(6.3).

Figure(6.8) shows the reconstruction flow. H denotes the hologram and $\hat{H}$ denotes its Fourier transform. The Fourier frequencies are denoted as (u, v) for the x and y spatial directions respectively. The wave vector is defined as:

$$k = 2\pi \begin{bmatrix} u & v & w \end{bmatrix} \tag{6.28}$$

where,

$$w = (\lambda^{-2} - u^2 - v^2)^{\frac{1}{2}} \tag{6.29}$$

Angular spectrum rotation is used to obtain a cross-section of the field denoted as $\hat{H}_R$, parallel to the observer field Appendix A. The rotations of the frequencies is given as:

$$R = \begin{bmatrix} 1 & 0 & 0 \\ 0 & \cos\theta & -\sin\theta \\ 0 & \sin\theta & \cos\theta \end{bmatrix} \begin{bmatrix} \cos\phi & 0 & \sin\phi \\ 0 & 1 & 0 \\ -\sin\phi & 0 & \cos\phi \end{bmatrix} \tag{6.30}$$

The rotated wave vector is now obtained as

$$\hat{k} = Rk \tag{6.31}$$

where

$$\hat{k} = 2\pi \begin{bmatrix} \hat{u} & \hat{v} & \hat{w} \end{bmatrix} \tag{6.32}$$

with

$$\hat{w} = (\lambda^{-2} - \hat{u}^2 - \hat{v}^2)^{\frac{1}{2}} \tag{6.33}$$

The tilted (cross-section) field is represented as:

$$\hat{H}_R = \hat{H}(\hat{u}, \hat{v}) \tag{6.34}$$

Angular spectrum rotation in essence uses only the frequencies needed for the reconstruction at a particular tilted plane. Then propagation of this cross-sectional field is done using the angular spectrum algorithm as explained in [17]. In Figure(6.3), the observer field is at distance d_1 from the tilted hologram plane. The field at the observer plane is given as:

$$\hat{H}_{R,d_1} = \sum_{\hat{u}} \sum_{\hat{v}} H_R . \exp(i\hat{w}d_1) \tag{6.35}$$

We simulate the observer view-point by an aperture stop and a lens. The spatial filtering operation by the aperture of size L, provides the field obtained in the observer plane by eliminating the rays that do not reach the eye position. The spatially filtered resultant field is given as:

$$\hat{H}_{crop} = \hat{H}_{R,d_1} . \text{rect}\left(\frac{\hat{u}}{L}, \frac{\hat{v}}{L}\right) \tag{6.36}$$

The simulation of the passage of the resulting field through the lens is performed by back-propagating it to the plane of focus (reconstruction plane), as shown on Figure (6.3).

$$\hat{H}_{rec} = \sum_{\hat{u}} \sum_{\hat{v}} H_{crop} . \exp(i\hat{w}(-d_2)) \tag{6.37}$$

The inverse transform of the reconstruction field provides the view observed.

6.5 Results

6.5.1 Reconstruction of *b<>com dice* hologram

In this section we generate some results for the logo_dice hologram used in the previous chapter. We shall provide the description of the scene again for convenience:

- Pixel pitch = 8.1 μm
- Wavelength = 11.08 μm
- Dimensions = 2048x2048 pixels

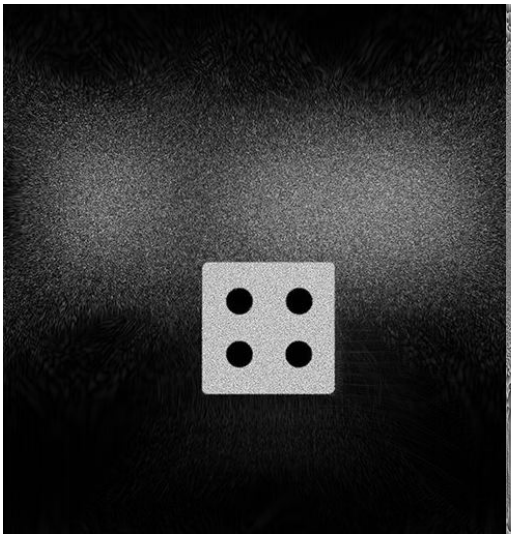

FIGURE 6.9: Amplitude of the logo_dice hologram

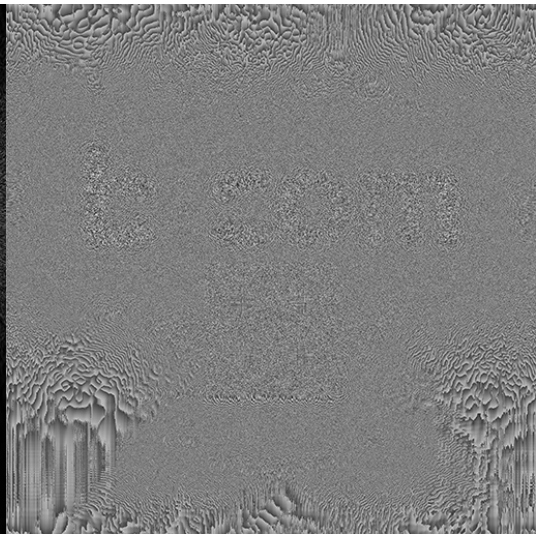

FIGURE 6.10: Phase of the logo_dice hologram

The scene contains a dice which is present at the plane of the hologram and a logo of $b<>com$ at 0.0025m from the dice behind the hologram plane. This is a relatively small sized object. Hence we simulate the observer to be at maximum 0.0025m in front of the hologram. It is observed that at this distance, only about 25% of the coefficients are needed for reconstructing the hologram by simulating an eye aperture of $0.001m$. We perform a comparison between the dot product approach which is our golden reference as detailed in section(5.2.2) and the proposed optimized approach in section(6.3.2)

The logo_dice hologram is illustrated in figure(6.9,6.10).

6.5.1.1 Quality of reconstruction based on the number of coefficients used

Figure(6.11) shows the variation of the quality wrt. different window sizes for a Shannon wavelet function. It must be noted that for this analysis, the eye simulation is done with a square aperture having 25% coefficients. The number of coefficients selected for reconstruction (at hologram plane) $0.4\%, 6.25\%, 12.5\%, 25\%$ respectively. As the number of coefficients increases, the PSNR improves as shown in Figure(6.11).

6.5.1.2 Degradation of quality

These experiments evaluate degradation of quality for the viewer positioned away from the transmitted position (case of delay or uncertainty in position estimation). Figure(6.12) gives the reconstruction quality at observer positions deviated from the transmitted view-point by an angle upto 30 degrees. It shows that quality degrades abruptly.

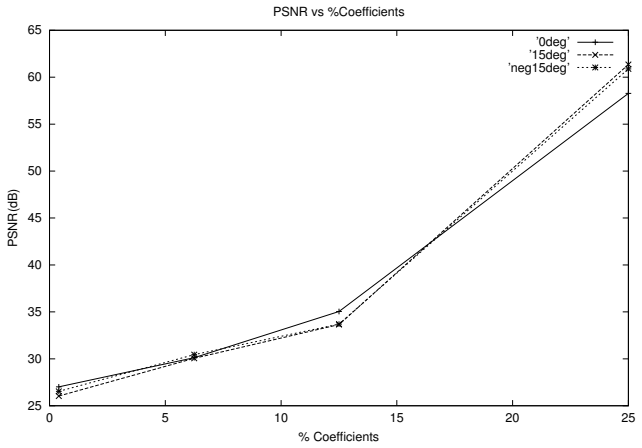

FIGURE 6.11: PSNR vs %Coefficients

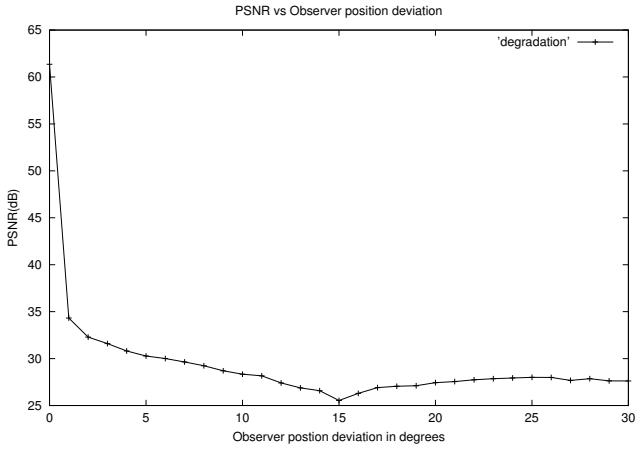

FIGURE 6.12: Degradation of quality

6.5.1.3 Coding of selected coefficients

In this experiment we compare Shannon wavelets and Morlet wavelets with respect to the golden reference i.e. the dot product result or perfect reconstruction as explained in section(5.2.2). In figure(6.13) RD-plots are obtained by using 25% of coefficients for viewing angles of 0^o and 15^o, for size of the hologram of 2048x2048, and at 2 quantization values of 5 and 8 bits. Linear quantization is performed on the coefficients. Table(6.1) presents the RD results. C.r represents the compression ratio between the transformed hologram and the uncompressed original hologram, bpp (bits per pixel) are obtained after entropy coding of the transformed coefficients and dB is the PSNR between the golden reference or perfect reconstruction as explained in section(5.2.2) and the optimized transformed hologram using Shannon wavelet and Morlet wavelet as explained

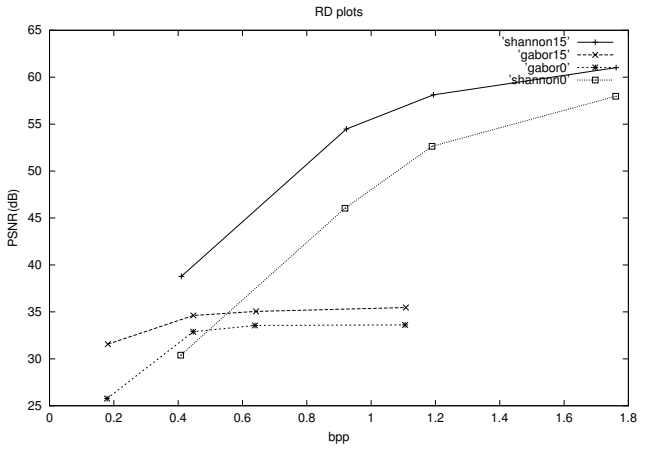

FIGURE 6.13: RD-plots at Q=5,8 bits

in section(6.3.2). The reconstructions obtained are themselves quantized at 8-bits before calculating the rate distortion. It can be observed that a quantization of 5 bits is sufficient to get good approximation of coefficients. The Shannon wavelet produces the best quality output as its Fourier transform closely matches with the spatial filtering window. If the gaussian window (Morlet wavelet) is used then there is a drop in quality, but still the result is visually appealing. The effective bitrate for a 30 frame per second video sequence with the Shannon wavelet is 0.11 Gbits/sec for quantization of 8-bits and 57.5 Mbits/sec for quantization of 5-bits.

TABLE 6.1: RD-plots for Shannon and Morlet wavelet transformed reconstructions at 5-bit and 8-bit quantization

Q=8 (Fast decay Sinc)	c.r	bpp	dB
0^0	4.5441	1.7605	57.97
15^0	4.5403	1.7620	61.02
-15^0	4.5470	1.7594	60.72
Q=5 (Fast decay Sinc)	c.r	bpp	dB
0^0	8.7098	0.9185	46.04
15^0	8.6672	0.9230	54.48
-15^0	8.7337	0.9160	54.07
Q=8 (Morlet)	c.r	bpp	dB
0^0	7.2356	1.1056	33.61
15^0	7.2184	1.1083	35.46
-15^0	7.2401	1.1050	35.16
Q=5 (Morlet)	c.r	bpp	dB
0^0	17.9037	0.4468	32.88
15^0	17.8791	0.4474	35.62
-15^0	17.9402	0.4459	35.37

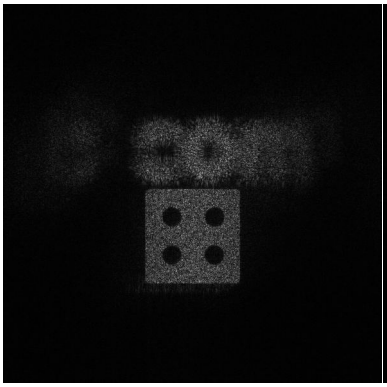

FIGURE 6.14: Perfect Shannon wavelet Dice reconstruction with observer at 0.0025m and at -15° from the reconstruction plane

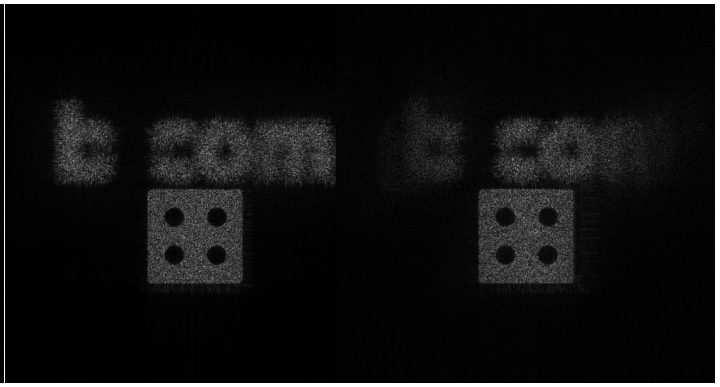

FIGURE 6.15: Perfect Shannon wavelet Dice reconstruction with observer at 0.0025m and at 0° from the reconstruction plane

FIGURE 6.16: Perfect Shannon wavelet Dice reconstruction with observer at 0.0025m and at 15° from the reconstruction plane

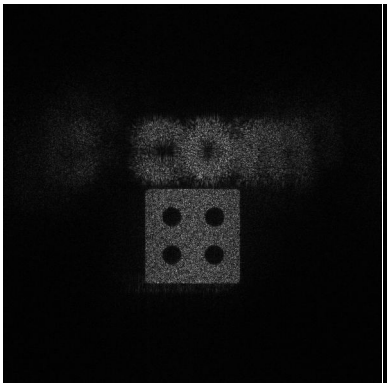

FIGURE 6.17: Shannon wavelet based Dice reconstruction with observer at 0.0025m and at -15° from the reconstruction plane

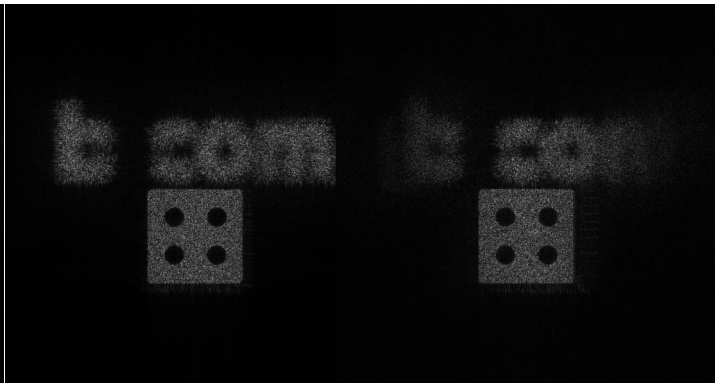

FIGURE 6.18: Shannon wavelet based Dice reconstruction with observer at 0.0025m and at 0° from the reconstruction plane

FIGURE 6.19: Shannon wavelet based Dice reconstruction with observer at 0.0025m and at 15° from the reconstruction plane

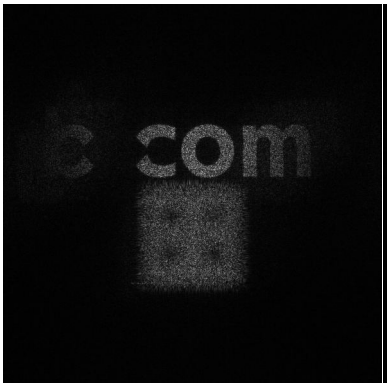

FIGURE 6.20: Perfect Shannon wavelet logo reconstruction with observer at 0.0025m and at -15° from the reconstruction plane

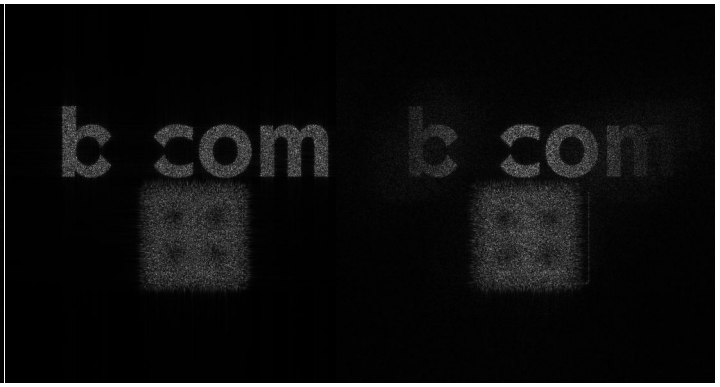

FIGURE 6.21: Perfect Shannon wavelet logo reconstruction with observer at 0.0025m and at 0° from the reconstruction plane

FIGURE 6.22: Perfect Shannon wavelet logo reconstruction with observer at 0.0025m and at 15° from the reconstruction plane

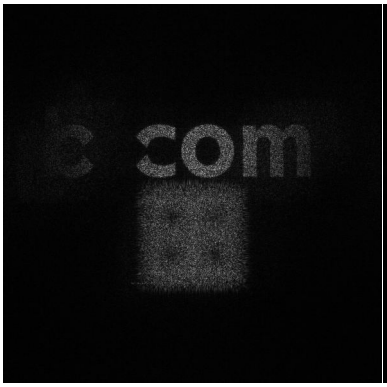

FIGURE 6.23: Shannon wavelet based logo reconstruction with observer at 0.0025m and at -15° from the reconstruction plane

FIGURE 6.24: Shannon wavelet based logo reconstruction with observer at 0.0025m and at 0° from the reconstruction plane

FIGURE 6.25: Shannon wavelet based logo reconstruction with observer at 0.0025m and at 15° from the reconstruction plane

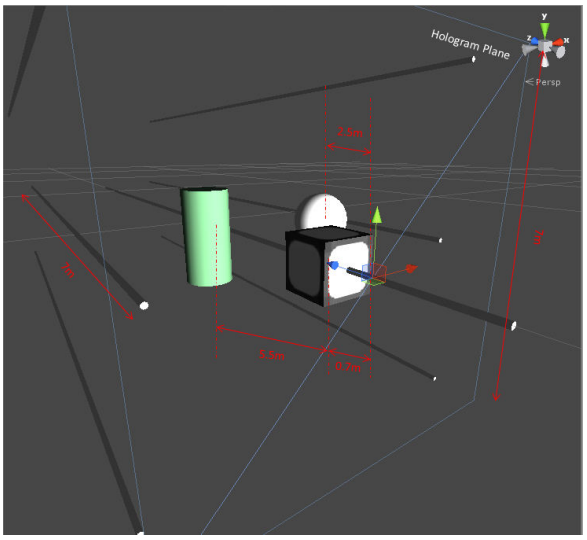

FIGURE 6.26: The 3shapes scene

6.5.2 Reconstructions for 3-Shapes hologram

In this section we show results based on our optimized view based reconstruction system. We will compare the PSNR and MSE of the optimized reconstruction with the results obtained from perfect reconstructions. We will show that the percentage of coefficients needed for reconstruction decreases with the increase of observer distance from the plane of the hologram.

6.5.3 Description of the scene

The figure(6.26) explains the scene. It contains 3 solid shapes at different distances from the hologram plane as shown. The cube or dice is places at 0.7m, the sphere is at 2.5m and the cylinder is at 5.5m from the hologram plane. The hologram is created with a pixel pitch of 0.0034m and with a resolution of 2048×2048.

6.5.3.1 Quality of the reconstruction *wrt* the perfect reconstruction golden reference

The figures(6.27..6.35) compare the reconstructions between the perfect reconstruction (dot product) and the optimized reconstruction method (convolution). The reconstructions are generated at various viewer positions at $2m$,$4m$ and $6m$ from the hologram plane at angles $0°$, $20°$ and $-20°$. The reconstructions are obtained for eye window sizes of 0.01m, 0.02m and 0.03m.

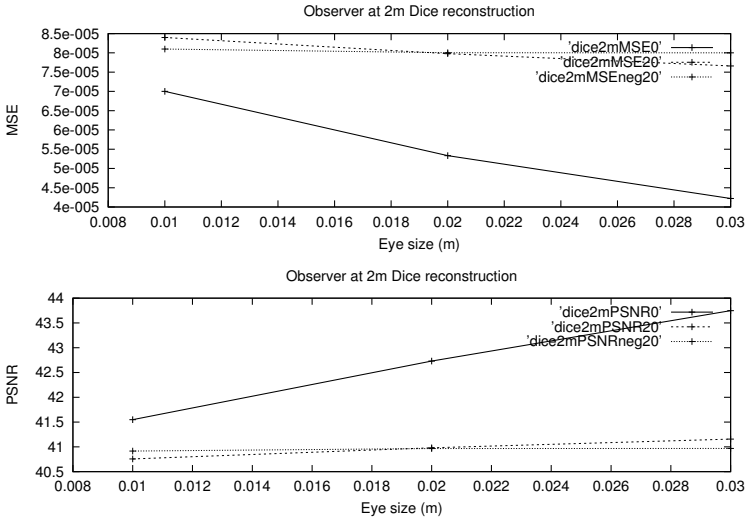

FIGURE 6.27: MSE and PSNR of Dice wrt. perfect reconstruction output with observer at 2m from hologram

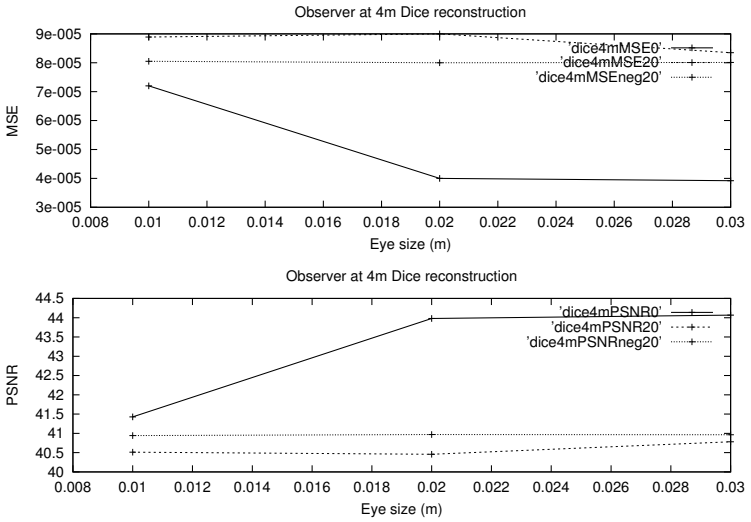

FIGURE 6.28: MSE and PSNR of Dice wrt. perfect reconstruction output with observer at 4m from hologram

It can be observed from the graphs of PSNR and MSE that the quality is close to what is obtained using the perfect reconstruction method. The difference arises mainly due to the fact that the reconstruction is done on a plane at the position of the observer. The spatial filtering operation at the observer window (eye simulation) needs to be done accurately to take into account only the light field incident at the eye. Currently in the numerical implementation we perform a uniform coefficient scaling proportional to the size of the observer window. For better eye simulation, another more accurate algorithm needs to be used to obtain the exact coefficient values for all the incident frequencies.

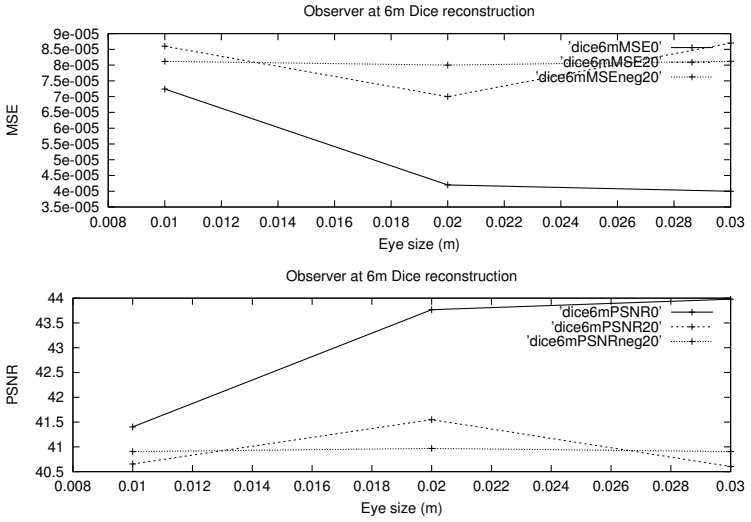

FIGURE 6.29: MSE and PSNR of Dice wrt. perfect reconstruction output with observer at 6m from hologram

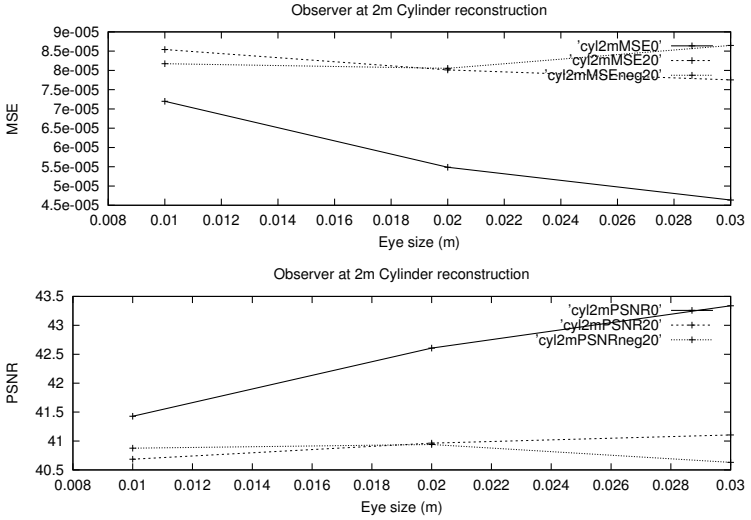

FIGURE 6.30: MSE and PSNR of Cylinder wrt. perfect reconstruction output with observer at 2m from hologram

6.5.3.2 %Coefficients *wrt* change in observer depth

Figure(6.36) shows how well the algorithm is capable of pruning the coefficients based on the position of the observer. We reconstruct the dice at each position of the observer. We observe that as the distance of the observer increases from the plane of the hologram, less number of coefficients are needed.

As the observer approaches the hologram more coefficients are needed for a better reconstruction (better details). This is inline with the fact that as an observer goes closer

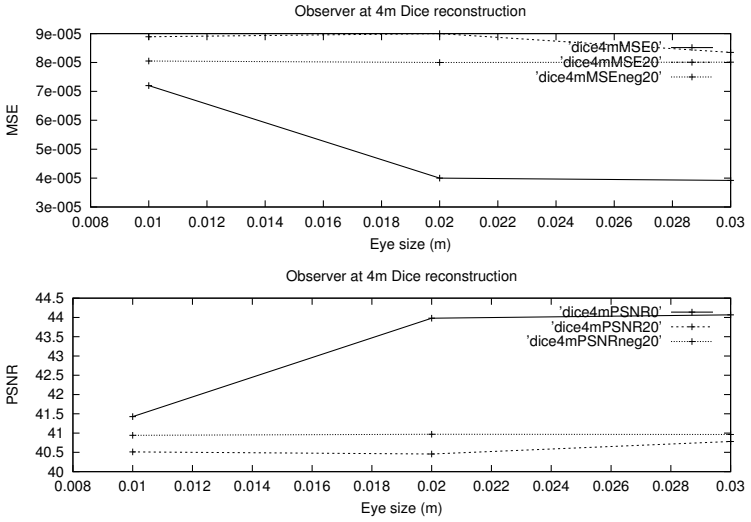

FIGURE 6.31: MSE and PSNR of Cylinder wrt. perfect reconstruction output with observer at 4m from hologram

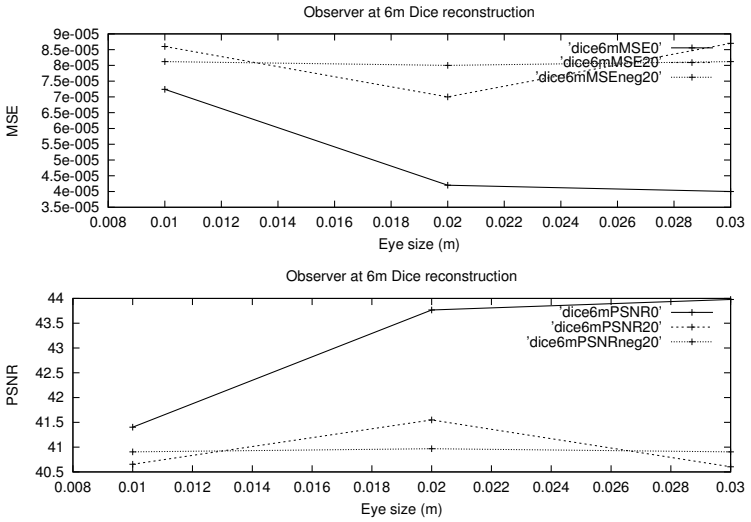

FIGURE 6.32: MSE and PSNR of Sphere wrt. perfect reconstruction output with observer at 6m from hologram

to an object, more frequencies are incident on the eye. As the observer moves further away, less frequencies are incident on the eye of the observer.

6.5.3.3 Screenshots

In order to judge the visual quality of the reconstructions, figures(6.37..6.63) show some reconstructions for observer positions from 2m to 6m for angles $-20°$ to $20°$. All the reconstructions obtained for an eye window size of 0.01m. In AppendixB we will present

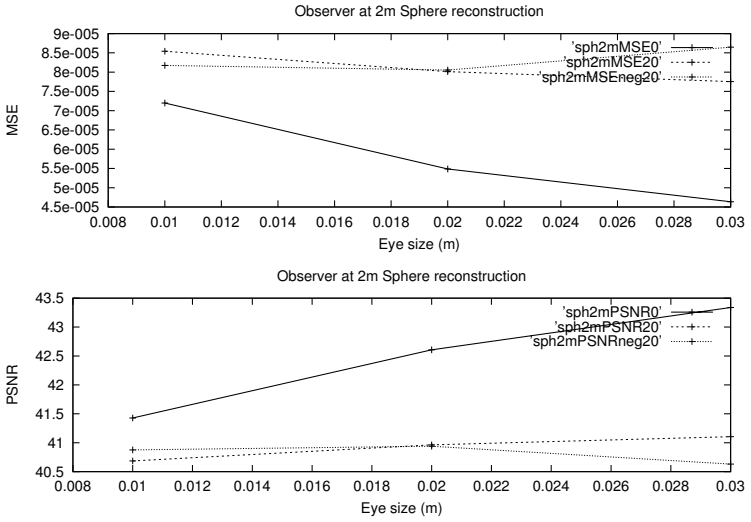

FIGURE 6.33: MSE and PSNR of Sphere wrt. perfect reconstruction output with observer at 2m from hologram

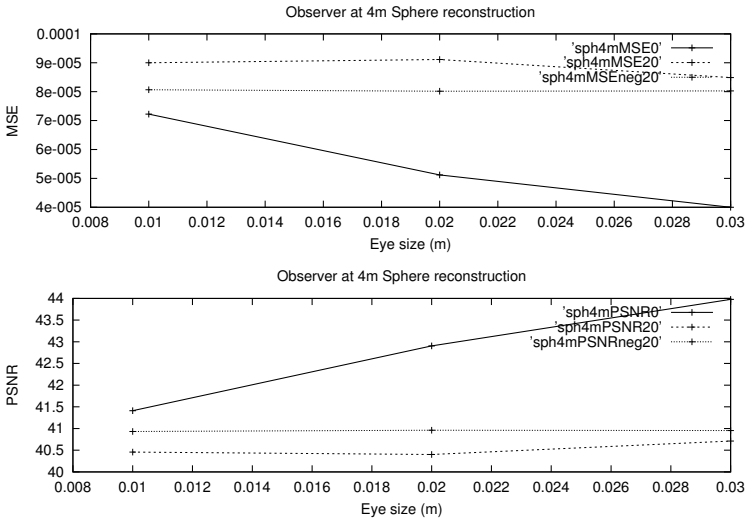

FIGURE 6.34: MSE and PSNR of Sphere wrt. perfect reconstruction output with observer at 4m from hologram

the Interactive interface for view-dependent display systems which was used to generate the following screenshots.

6.6 Conclusion

In this chapter we have presented a framework for wavelet analysis, coefficient selection and view-dependent reconstruction of arbitrarily generated holograms. We have described in detail the *dot-product* approach and *convolution* approach for performing

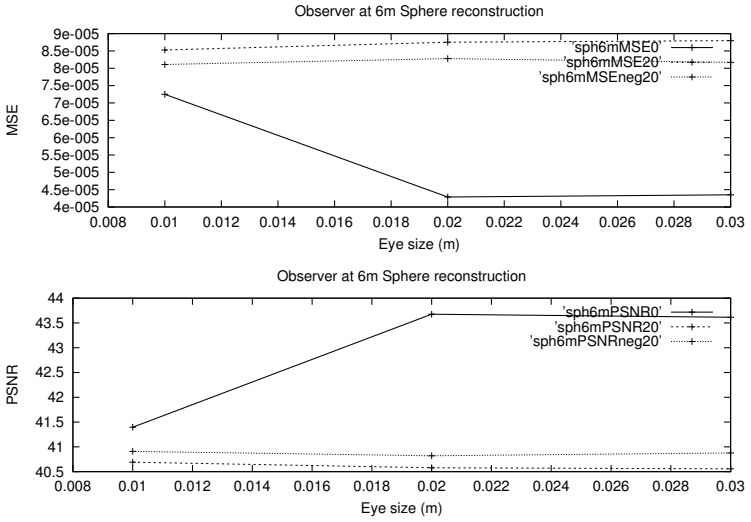

FIGURE 6.35: MSE and PSNR of Sphere wrt. perfect reconstruction output with observer at 6m from hologram

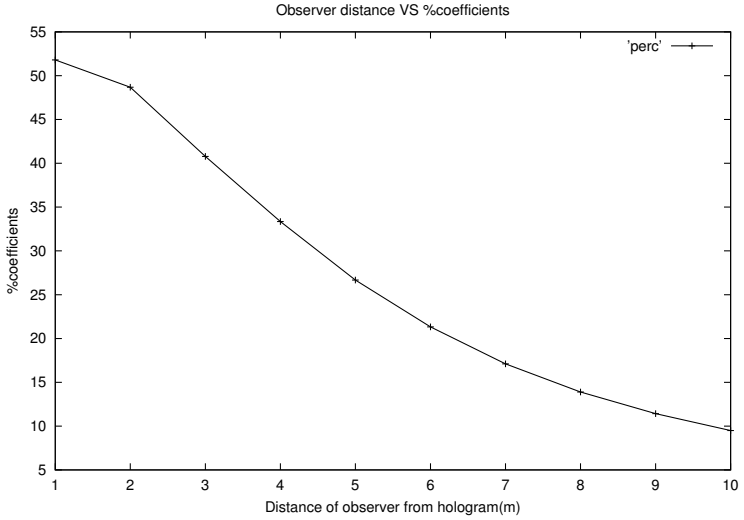

FIGURE 6.36: Observer distance from hologram VS the % coefficients for reconstruction

the transform operation and commented on the complexity. We proposed a Shannon wavelet decomposition into windowed wavelet basis and detailed the process of selecting the relevant wavelet coefficients for reconstructing sub-holograms corresponding to a given user viewpoint, as well as the partial reconstruction itself, including the optical assumptions and settings for simulation of the viewer optical system. We concluded that the Shannon wavelet though not well localized in frequency, forms a good candidate our view-dependent representation and reconstruction setup as we used it to propose a faster convolution based pruning method to obtain accurate reconstructions. We showed numerical results of directional degradation and provided distortion curves in function

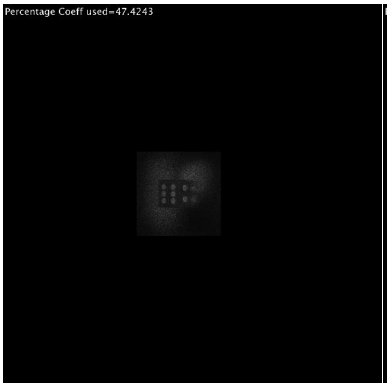

FIGURE 6.37: Dice reconstruction with observer at 2m and at -20° from the reconstruction plane

FIGURE 6.38: Dice reconstruction with observer at 2m and at 0° from the reconstruction plane

FIGURE 6.39: Dice reconstruction with observer at 2m and at 20° from the reconstruction plane

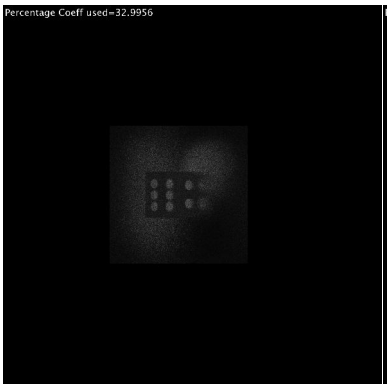

FIGURE 6.40: Dice reconstruction with observer at 4m and at -20° from the reconstruction plane

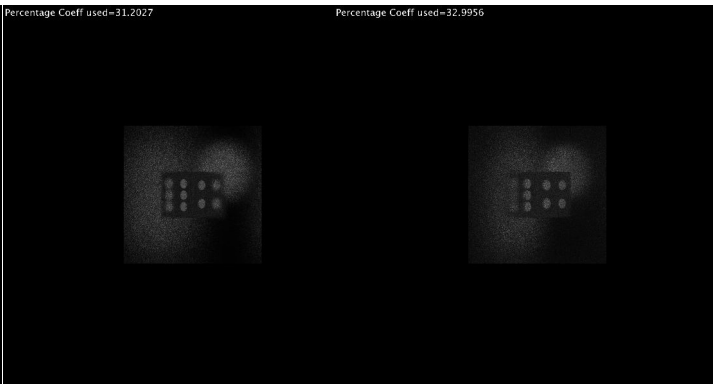

FIGURE 6.41: Dice reconstruction with observer at 4m and at 0° from the reconstruction plane

FIGURE 6.42: Dice reconstruction with observer at 4m and at 20° from the reconstruction plane

FIGURE 6.43: Dice reconstruction with observer at 6m and at -20° from the reconstruction plane

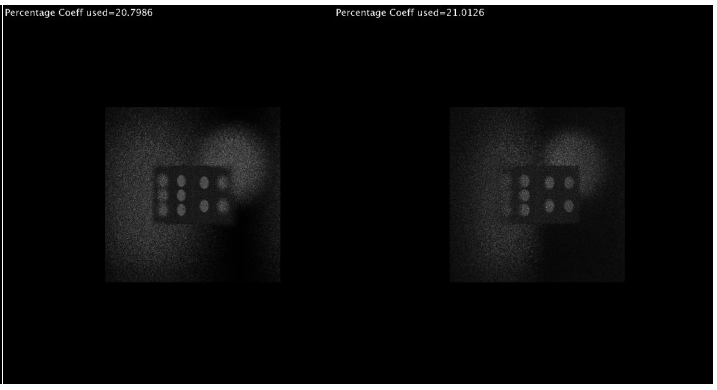

FIGURE 6.44: Dice reconstruction with observer at 6m and at 0° from the reconstruction plane

FIGURE 6.45: Dice reconstruction with observer at 6m and at 20° from the reconstruction plane

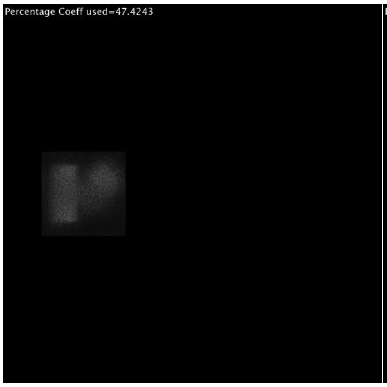

FIGURE 6.46: Cylinder reconstruction with observer at 2m and at -20° from the reconstruction plane

FIGURE 6.47: Cylinder reconstruction with observer at 2m and at 0° from the reconstruction plane

FIGURE 6.48: Cylinder reconstruction with observer at 2m and at 20° from the reconstruction plane

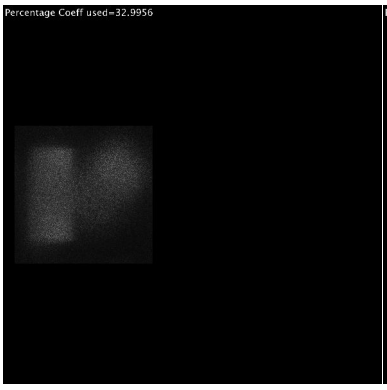

FIGURE 6.49: Cylinder reconstruction with observer at 4m and at -20° from the reconstruction plane

FIGURE 6.50: Cylinder reconstruction with observer at 4m and at 0° from the reconstruction plane

FIGURE 6.51: Cylinder reconstruction with observer at 4m and at 20° from the reconstruction plane

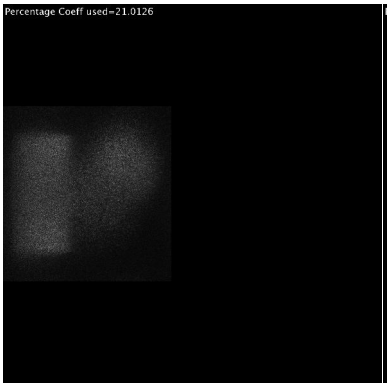

FIGURE 6.52: Cylinder reconstruction with observer at 6m and at -20° from the reconstruction plane

FIGURE 6.53: Cylinder reconstruction with observer at 6m and at 0° from the reconstruction plane

FIGURE 6.54: Cylinder reconstruction with observer at 6m and at 20° from the reconstruction plane

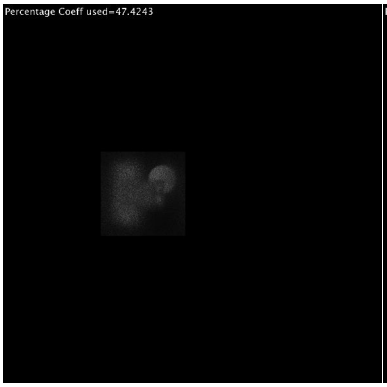

FIGURE 6.55: Sphere reconstruction with observer at 2m and at -20° from the reconstruction plane

FIGURE 6.56: Sphere reconstruction with observer at 2m and at 0° from the reconstruction plane

FIGURE 6.57: Sphere reconstruction with observer at 2m and at 20° from the reconstruction plane

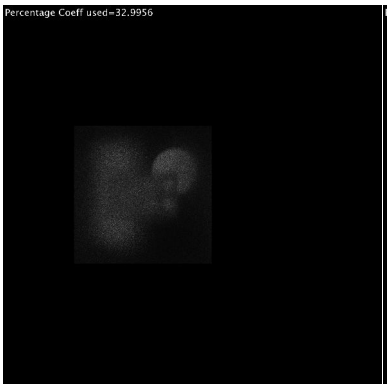

FIGURE 6.58: Sphere reconstruction with observer at 4m and at -20° from the reconstruction plane

FIGURE 6.59: Sphere reconstruction with observer at 4m and at 0° from the reconstruction plane

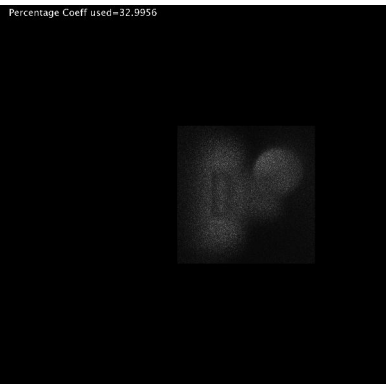

FIGURE 6.60: Sphere reconstruction with observer at 4m and at 20° from the reconstruction plane

FIGURE 6.61: Sphere reconstruction with observer at 6m and at -20° from the reconstruction plane

FIGURE 6.62: Sphere reconstruction with observer at 6m and at 0° from the reconstruction plane

FIGURE 6.63: Sphere reconstruction with observer at 6m and at 20° from the reconstruction plane

of the coefficient pruning ratio for comparing the partial and complete numerical reconstructions.

For our experiments we have generated a hologram with 3 solid objects called as the 3shapes hologram. We performed MSE and PSNR calculations for the reconstructions obtained by *perfect reconstruction* or *dot product* approach and *optimized convolution* approach. We found that the quality is within acceptable range (PSNR $>$ 40dB). We reiterated that in order to obtain the same quality as *perfect reconstruction* the eye simulation needs to be done in a better way numerically. We later showed the efficiency of the algorithm to reduce the coefficients needed for reconstruction based on the position of the viewer. It was observed that there is an almost exponential decrease in the % coefficients as the observer distance increases away from the hologram.

We have provided several screenshots of the reconstructions at various observer positions.

Chapter 7

Conclusion and Future Work

The ever increasing demand of 3D *life-like* visual reconstructions from display devices, has resulted in several scientists and researchers to employ devices like stereoscopic displays to commercial devices; the disadvantages of which are trifling compared to the mere attraction of viewing something in 3D.

With the understanding of years of research in the field of light propagation, scientists today are studying the subject of holography with a new renewed interest, to be able to develop display systems based on holographic technologies.

In our dissertation we provide a scalable adaptive hologram representation system that can perform reconstruction of holograms based on the position of the observer, referred to as the view-dependent hologram reconstruction setup. This representation exploits two existing theories of diffraction gratings and propagation of light, namely the *Grating equation* and *Angular spectrum propagation on tilted planes*.

The choice of this type of representation system arose from the need to somehow reduce (*prune*) portions of the hologram based on the position of the observer. The field around the hologram contains a large amount of information. This 3D complex field contains all the optical and physical information of the object that is gathered during the hologram generation process. Using the angular spectrum propagation on titled planes method, we take cross-sections of this 3D field and propagate them to the observer planes.

Wavelet transforms are used for the purpose of pruning the holograms. The essential condition for an ideal wavelet in this setup was one having *good* space and frequency localizations. Our first contribution in this respect is to show why this is necessary and we compare the Gabor wavelet and the Fresnelet. We show experimentally that Gabor wavelets are able to suppress the unwanted orders created in the reconstruction process without the need for spatial filtering. Gabor wavelets are more computationally complex

than Fresnelets, hence optimization of the Gabor wavelet transform using multi-core or multi-processor architectures becomes necessary. The good localization properties of the Gabor wavelet bases in space and frequency domain make them an easy choice for view-based representation techniques for digital hologram reconstruction. The max Gabor transform used, is inherently not a reversible transform, but can be made reversible by making the Gabor wavelet admissible based on certain assumptions. The max-Gabor transform was capable of extracting the localized frequency information from the hologram.

In our following contribution we used the Morlet wavelet for our view-dependent hologram reconstruction setup. Beginning with the Gabor basis function, we overcame the problem of inherent non-admissibility in the Gabor wavelet by eliminating the DC term in all the Morlet wavelet function decompositions in the multiresolution analysis. We explained the design, discretization and implementation of Morlet wavelets for the view-dependent compression system in detail. Using a *client-server* architecture, we can generate and store *off-line*, the sub-holograms for each discretized observer point in the observer plane. Each sub-hologram can be transmitted and reconstructed in real-time by tracking the observer.

In out third contribution we exploit another wavelet: Shannon wavelet. This wavelet is well localized in space but poorly localized in frequency. The advantage of this wavelet is the immense speed-up that can be achieved by generating and transmitting the sub-holograms based on the position of the observer *on-the-fly*. Such a setup is based on the assumption that there is only one observer and the pruning depends on the dynamics of the scene and size of the hologram. The reductions in complexity and the storage space saved by this method is too good not to overlook.

As with any research there is always room for improvement and development in the future.

- The view-based reconstruction setup is currently performed numerically. The limitations of the SLMs along with the lower angles of diffraction from the holograms, we are unable to reconstruct holograms optically. In the future with the help of advances SLMs have pixel pitches $< 1\mu m$, we can obtain larger angles of viewing to implement this technique optically.

- Further wavelet study is needed to identify newer and better wavelets to prune the hologram. Currently our setup involves the usage of only one wavelet at a time. Moreover the wavelets can be selected on the fly for transforming and pruning the coefficients based on the physical characteristics. For example, the Morlet wavelet

can be used when multiple viewers are involved and can be switched to Shannon wavelets when there is only one observer.

- Holograms containing truly immersive contents with wider viewing angles ($> 20^o$) need to be generated for testing and validation of the holographic setup that we have described. Using a larger assortment of test cases, we can experimentally understand the selection of the wavelets based on the dynamics of the scene.

- Compression of the pruned coefficients is another field that has not been covered in detail in our work. We have limited our experiments to basic entropy coding methods (Huffmann coding), but there is wide array of compression methods that need to be exploited. The correlation between the real and imaginary parts of the complex pruned information is not good, and a study needs to be carried out to find an efficient coding method to compress such data. The correlation can be obtained between the pruned information of neighboring views. This needs to be studied further and exploited.

- In terms of quality assessment, we have performed the comparison in terms of MSE and PSNR of the reconstructions obtained between the original reconstructions (golden references) and wavelet transformed reconstruction, because the application of these metrics to the holograms themselves will not predict the visual quality of the reconstructions. Digital holography for 3D display systems is a nascent field and an in-depth study into the quality metrics of holographic displays needs to be carried out.

Appendix A

Angular Spectrum Rotation

In this section we describe the principle of angular spectrum rotation based on [48].

In our experiments we *tilt the aperture* and then propagate the the wavefront. What this means is that we take a cross-section of the 3D field near the hologram plane by the angular spectrum rotation algorithm based on the position of the observer, and then propagate this cross-section to the observer position as shown in figure(A.1). This involves a coordinate rotation in the Fourier domain.

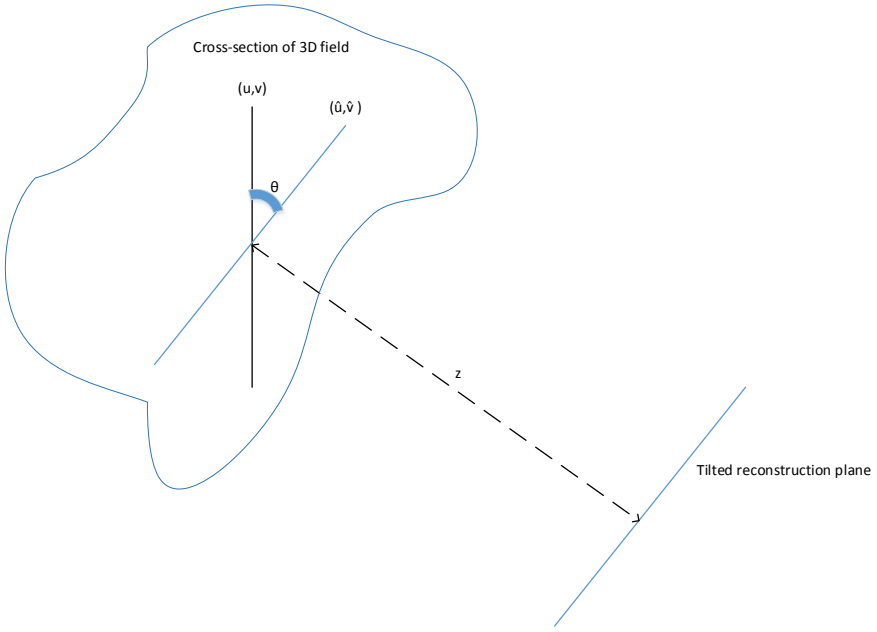

FIGURE A.1: Angular Spectrum Rotation

Let $U(x, y, 0)$ be the light field incident on the hologram plane at $z = 0$. The spectrum of which is given as $A(x, y; 0)$. To understand the spectrum better we shall first define the Fourier and Inverse fourier transform of $U(x, y, 0)$.

$$\begin{aligned} G(u, v) &= \mathcal{F}\{U(x, y, 0)\} \\ &= \iint_{-\infty}^{\infty} U(x, y, 0) \exp[-i2\pi(ux + vy)]dxdy \end{aligned} \tag{A.1a}$$

$$\begin{aligned} U(x, y, 0) &= \mathcal{F}^{-1}\{G(u, v)\} \\ &= \iint_{-\infty}^{\infty} G(u, v) \exp[i2\pi(ux + vy)]dudv \end{aligned} \tag{A.1b}$$

Equation(A.1b) is interpreted as a superposition of plane waves and can be rewritten as:

$$U(x, y, 0; u, v) = G(u, v) \exp[i2\pi(ux + vy)] \tag{A.2}$$

The same plane wave with a complex amplitude A and wavevector k can be defined as

$$U(x, y, 0; k) = A \exp[i\frac{2\pi}{\lambda}(k_x x + k_y y)] \tag{A.3}$$

where

$$k = \frac{2\pi}{\lambda} \begin{bmatrix} k_x & k_y & k_z \end{bmatrix} \tag{A.4}$$

Therefore $|k| = \frac{2\pi}{\lambda}$ and $k_x^2 + k_y^2 + k_z^2 = 1$, and

$$k = 2\pi \begin{bmatrix} u & v & w(u, v) \end{bmatrix} \tag{A.5}$$

with $w(u, v) = (\lambda^{-2} - u^2 - v^2)^{1/2}$

To obtain the cross-section based on the position of the viewer we can use a coordinate transform matrix T such that the new wave vector after rotation is given as

$$k = T^{-1}\hat{k} \tag{A.6}$$

where

$$\hat{k} = 2\pi \begin{bmatrix} \hat{u} & \hat{v} & \hat{w}(u, v) \end{bmatrix} \tag{A.7}$$

where T^{-1} is of the form

$$T^{-1} = \begin{bmatrix} a_1 & a_2 & a_3 \\ a_4 & a_5 & a_6 \\ a_7 & a_8 & a_9 \end{bmatrix} \tag{A.8}$$

We now need to associate the Fourier frequencies in the hologram coordinates (u, v) with those in the cross-section coordinates $(\hat{u}, \hat{v})$.

$$u = \alpha(\hat{u}, \hat{v}) = a_1\hat{u} + a_2\hat{v} + a_3\hat{w} \tag{A.9a}$$

$$v = \beta(\hat{v}, \hat{v}) = a_4\hat{u} + a_5\hat{v} + a_6\hat{w} \tag{A.9b}$$

Hence the new spectrum coeffcients of the cross-section is given as

$$\hat{A} = A(\hat{u}, \hat{v}) = G(\alpha, \beta) \tag{A.10}$$

Looking at equation(A.9) it can be easily deduced that the non-linearity with not result in integer values of α and β. Hence a weighted interpolation is done on these values to obtain integer values. Also the inverse transform of $\hat{A}$ will not give the perfect results. A Jocaobian needs to be included to correct the non-linearity and it is given as

$$J(\hat{u}, \hat{v}) \approx (a_1a_5 - a_2a_4) \tag{A.11}$$

Hence the new set of coeffcients for the cross-section is given as

$$\hat{A}_J = \hat{A}.J(\hat{u}, \hat{v}) \tag{A.12}$$

Replacing equation(A.12) in equation(2.23) will propagate the cross-section to the observer position.

Appendix B

Interactive interface for view-dependent display system

B.1 Introduction

In this Appendix we explain the GUI for the view-dependent representation of the holograms and how to calibrate the display.

In the first section we will discuss about the view-based representation and reconstruction GUI in detail. In section B.2 we shall provide a description for an example scene and give the various parameters that are needed for the generation of the reconstruction using the view-based representation and reconstruction GUI. We will then show how to calibrate the display in section(B.3).

B.2 Description of the GUI

Figure (B.1) shows the GUI for the view based representation and reconstruction system.

The basic controls and features of the GUI are explained as follows:

- Holograms are loaded using (1) button *Load Hologram*. Complex holograms can be loaded by toggling (6) *Complex* checkbox.
- The parameter file that is unique to every scene and display device is loaded using (2) *Parameter file*. This file is needed when working with the Kinect sensor.
- To perform the reconstruction, there is a possibility to perform a direct reconstruction from the hologram on a plane (9) *Recon* and (11) *Recon Kinect* or by

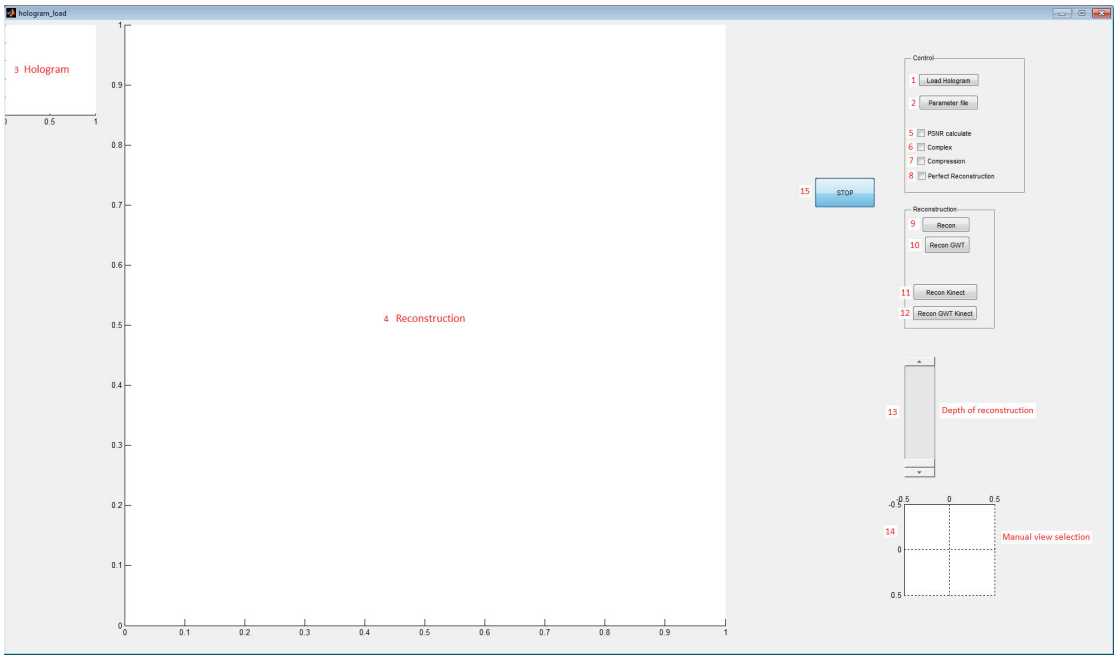

FIGURE B.1: GUI for view based representation of holograms

using wavelet transforms for view based representation for diffractions at a point or an aperture (10) *Recon GWT* and (12) *Recon GWT Kinect*.

- The GUI functions in two modes:
  - Mouse interface mode (9) and (10)
  - Kinect interface mode (11) and (12)

- The reconstruction depth can be varied on the fly in the Kinect interface mode using (13).
- The observer postion at a fixed depth of reconstruction can obtained using (14) in the mouse interface mode.
- The simulation can be stopped forcefully in the kinect interface mode using (15) button *STOP*.
- The loaded hologram is display in window (3).
- The reconstruction is obtained in window (4).
- PSNR can be calculated by comparing the original reconstruction and wavelet transformed partial reconstructions using the checbox (5) *PSNR Calculate*.
- To toggle between *dot product* approach and *convolution* approach of reconstructions, we use the checkbox (8) *Perfect Reconstruction*.

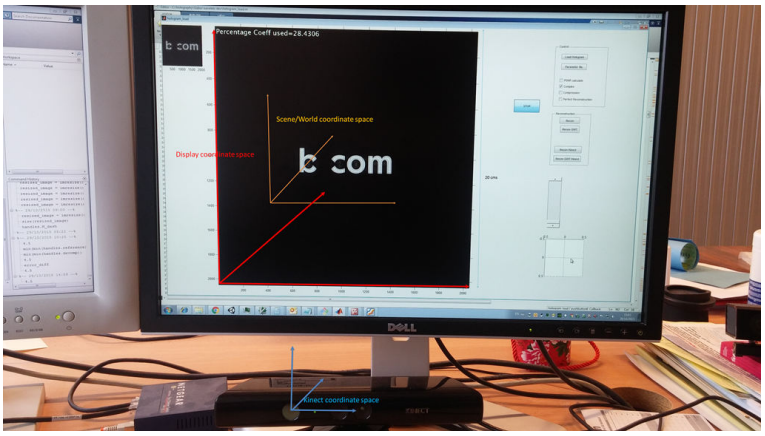

FIGURE B.2: Coordinate planes in Kinect mode

- Compression using uniform quanization and Huffmann coding is obtained using checkbox (7) *Compression*.

B.3 Calibration of the display (*Kinect only*)

For using the software in Kinect mode an intial calibration of the display is carried out. There are 3 coordinate planes that are considered for the calibration process.

- Kinect coordinate plane
- Scene or World coordinate plane
- Display coordinate plane

The figure(B.2) shows the setup of the display system and shows the 3 coordinate planes.

The user position is obtained in the Kinect coordinate plane. We need to be able to transform these coordinates to the display coordinate plane and then calculate the user position in the scene/world coordinate plane as shown in figure(B.3).

B.3.1 The parameter file

The figure(B.4) describes the parameter file.

The parameter file gives us the values to populate the matrices `M_disp` and `M_world`. The various elements of the parameter file are obtained from the parameters of the scene.

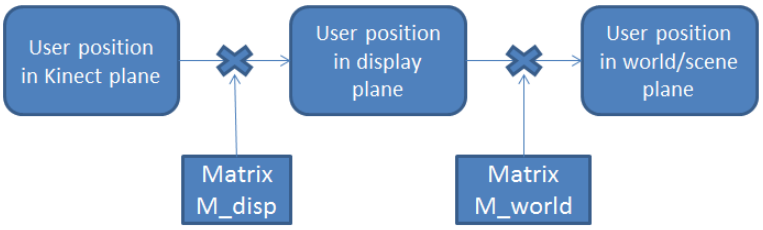

FIGURE B.3

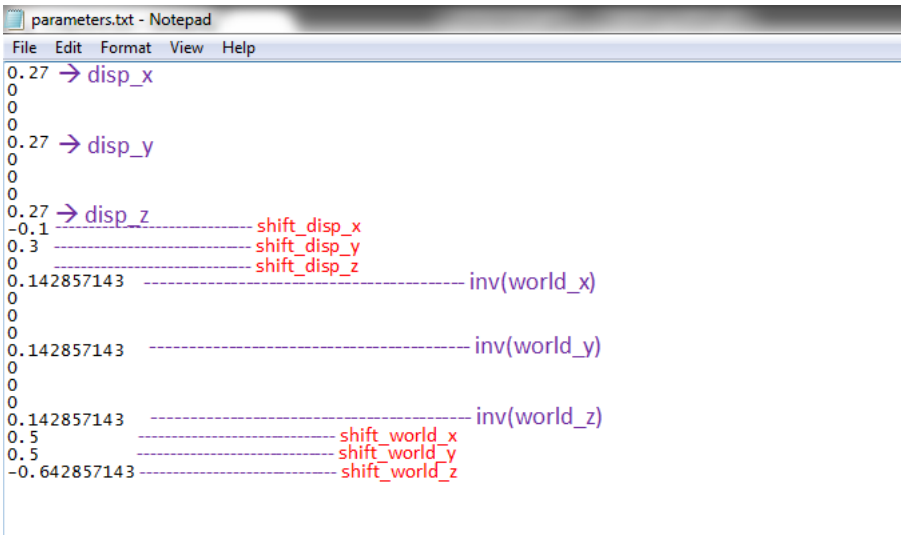

FIGURE B.4: A parameter file

$$\text{M\_disp} = \begin{bmatrix} disp\_x & 0 & 0 & shift\_disp\_x \\ 0 & disp\_y & 0 & shift\_disp\_y \\ 0 & 0 & disp\_z & shift\_disp\_z \\ 0 & 0 & 0 & 1 \end{bmatrix} \tag{B.1}$$

$$\text{M\_world} = \begin{bmatrix} inv(world\_x) & 0 & 0 & shift\_world\_x \\ 0 & inv(world\_y) & 0 & shift\_world\_y \\ 0 & 0 & inv(world\_z) & shift\_world\_z \\ 0 & 0 & 0 & 1 \end{bmatrix} \tag{B.2}$$

B.3.1.1 Measuring the display parameters

The first 12 elements of the parameter file are the display parameters.
The first 9 elements of the parameter file represent the xy and z components of the display plane vector. The origin of the display plane is the left bottom of the display

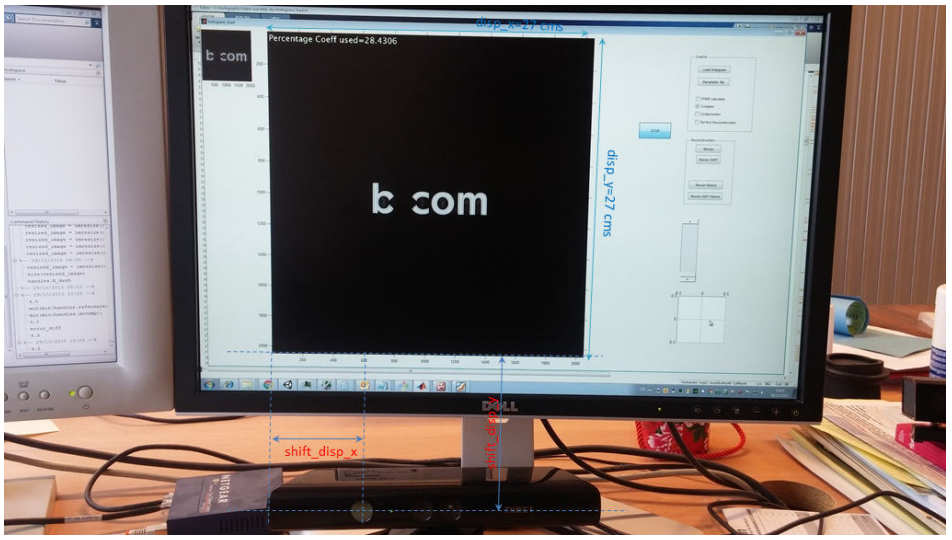

FIGURE B.5: Measuring the display parameters

as shown in figure(B.2). The next 3 elements are the distances in meters (x,y and z) between the origins of the Kinect plane and the display plane. The figure(B.5) shows how to measure these parameters.

B.3.1.2 Measuring the Scene/World parameters

The last 12 elements of the parameter file are obtained from the scene.
Elements 13 through 21 are the x,y and z components of the scene/world plane vector. They are stored as their inverses for computational ease. The origin is considered to be at the left bottom of the scene as in the case of the display. The last 3 elements are the shifts of the scene origin to the center of the scene. The figure(B.6) shows the mesurements for the scene parameters in Unity.

B.3.2 Verification of the reconstruction

For verifying that the reconstruction in the software is correct, we compare the reconstructions in Unity with the reconstructions in our software for the same parameters. The figure(B.7,B.8) and figure(B.9,B.10) shows the comparison at 2 different observer positions.

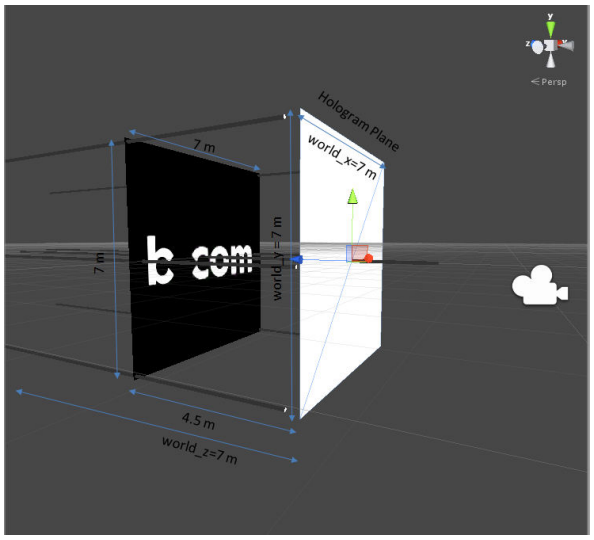

FIGURE B.6: Measuring the scene parameters

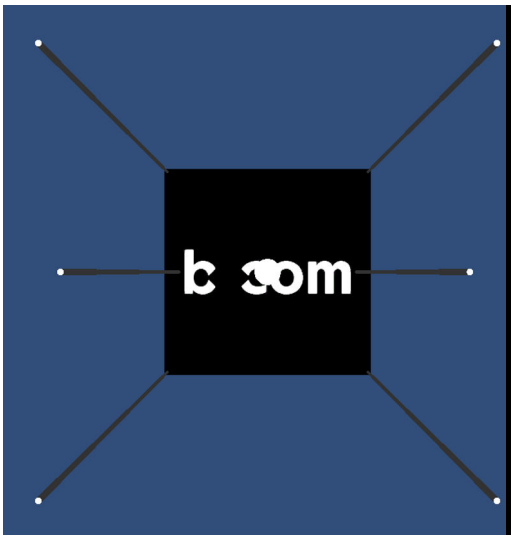

FIGURE B.7: User position at 3.5m from the hologram at 0 degrees (Unity)

FIGURE B.8: User position at 3.5m from the hologram at 0 degrees (Software)

B.4 Conclusion

In this chapter we have explained in detail the GUI of the software that was developed for the view based reconstruction system. We have explained the calibration of the display system when used with the Kinect and how to measure the scene/world parameters and display parameters to obtain the tranform matrices. Later we have verified the outputs obtained by our software with the output obtained from *Unity*.

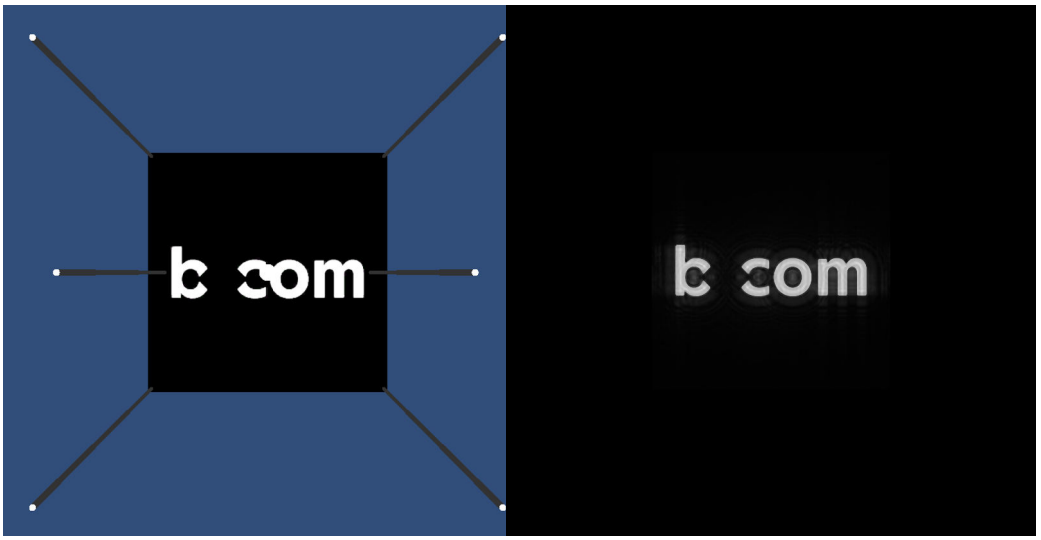

FIGURE B.9: User position at 4.5m from the hologram at 0 degrees (Unity)

FIGURE B.10: User position at 4.5m from the hologram at 0 degrees (Software)

Bibliography

[1] Fahri Yaras, Hoonjong Kang, and Levent Onural. State of the art in holographic displays: A survey. *Journal of Display Technology*, 6(10):443–454, October 2010.

[2] Dennis Gabor. A new microscopic principle. *Nature*, 161, 1948.

[3] Dennis Gabor. Microscopy by reconstructed wavefronts. *Royal Society proceedings*, 197, 1949.

[4] Dennis Gabor. Microscopy by reconstructed wavefronts. *Physics Society proceedings*, 64, 1951.

[5] Stephan Reichelt, Ralf Hussler, Gerald Ftterer, and Norbert Leister. Depth cues in human visual perception and their realization in 3d displays. *Three-dimensional Imaging, Visualization and Display proceeding SPIE*, 7690, 2010.

[6] Leith EN and Upatnieks J. Reconstructed wavefronts and communications theory. *Optical Society of America*, 52, 1962.

[7] Leith EN and Upatnieks J. Wavefront reconstruction with diffused illumination and three-dimensional objects. *Optical Society of America*, 54, 1964.

[8] A. W. Lohmann, D. P. Paris, and H. W. Werlich. A computer generated spatial filter, applied to code translation. *Appl. Opt.*, 6(6):1139–1140, Jun 1967. doi: 10.1364/AO.6.001139. URL http://ao.osa.org/abstract.cfm?URI=ao-6-6-1139.

[9] A. W. Lohmann and D. P. Paris. Computer generated spatial filters for coherent optical data processing. *Appl. Opt.*, 7(4):651–655, Apr 1968. doi: 10.1364/AO.7.000651. URL http://ao.osa.org/abstract.cfm?URI=ao-7-4-651.

[10] L. P. Iaroslavskii and N. S. Merzliakov. *Methods of digital holography*. Moscow, Izdatel'stvo Nauka, In Russian., 1977.

[11] O. Bryngdahl and F. Wyrowski. *Digital Holography: Computer generated holograms*. Progress in optics XXVIII, 1990.

[12] J. W. Goodman and R. W. Lawrence. Digital image formation from electronically detected holograms. *Appl. Phys.*, 11(77), 1967. URL http://dx.doi.org/10.1063/1.1755043.

[13] Ulf Schnars and Werner Juptner. Digital recording and numerical reconstruction of holograms. *MEASUREMENT SCIENCE AND TECHNOLOGY*, 2002.

[14] U. Schnars and W. Jüptner. Direct recording of holograms by a ccd target and numerical reconstruction. *Appl. Opt.*, 33(2):179–181, Jan 1994. doi: 10.1364/AO.33.000179. URL http://ao.osa.org/abstract.cfm?URI=ao-33-2-179.

[15] P.Hariharan. *Optical Holography Principles, Techniques and Applications*. Cambridge University Press, 1996.

[16] Y.N.Denisyuk. Optika. *Optika I Spectroskopiya*, (522), 1963.

[17] Joseph W. Goodman. *Introduction to Fourier Optics*. Roberts and Company, 2005.

[18] U.Schnars and W.Jueptner. *Digital Holography: Digital Hologram Recording, Numerical Reconstruction and Related Techniques*. Springer, 2005.

[19] I.Yamaguchi and T.Zhang. Phase shifting digital holography. *Optics letters*, 1997.

[20] D.Grewell and A.Benatar. Diffractive optics as beam shaping elements. *Optical Engineering*, 2007.

[21] S.Marchesini. A unified evaluation of iterative projection algorithms for phase retrieval. *Physics Optics*, (12), 2006.

[22] J.R Fienup. Reconstruction of an object from the modulus of its fourier transform. *Optics Letters*, (3), 1978.

[23] N.C.Gallagher and B.Liu. Method for computing kinoforms that reduces image reconstruction error. *Applied Optics*, (12), 1973.

[24] J.Turunen and F.Wyrowski. *Diffractive optics for industrial and commercial applications*. Akademic Verlag,Berlin, 1997.

[25] R.W.Gerchberg and W.O.Saxton. A practical algorithm for the determination of the phase from image and diffraction plane pictures. *Optik*, (35), 1972.

[26] Chang and Jiang. Holographic image projection on tilted planes by phase-only computer generated holograms using fractional fourier transforms. *Journal of display technology*, (2), 2014.

[27] H.Kang, C.Ahn, and S.Lee. Computer generated 3d holograms of depth annotated images. *SPIE Optics and Photonics*, (2), 2005.

[28] Y.Sato and Y.Sakamoto. Calculation method for reconstruction at arbitrary depths in cgh with fourier transform optical system. *SPIE Optics and Photonics*, (2), 2012.

[29] K.Bauchert, S.Serati, and A.Furman. Advances in liquid crystal spatial light modulators. *SPIE*, 4734, 2002.

[30] A. Michalkiewicz, M. Kujawinskaa, T. Kozackia, X. Wangb, and P. J. Bosb. Holographic three-dimensional displays with liquid crystal on silicon spatial light modulator. *SPIE*, 5531, 2004.

[31] Y. Frauel, T. J. Naughton, O. Matoba, E. Tajahueerce, and B. Javidi. Three-dimensional imaging and processing using computational holographic imaging. *IEEE*, 94, 2006.

[32] T.Ito, T.Shimobaba, H.Godo, and M.Horiuchi. Holographic reconstruction with 10 micro meter pixel pitch reflective lcd by use of a led reference light. *IEEE*, 10(5), 2003.

[33] G.Lippmann. La photographie integral. *C.R Hebd. Seances Acad. Sci.*, (146), 1908.

[34] David E. Roberts and Trebor Smith. *Lens Array Print Techniques.* http://lenticulartechnology.com/files/2014/02/Integral-History.pdf, 2014.

[35] K.Choi, J.Kim, Y.Lim, and B.Lee. Full parallax viewing-angle enhanced computer-generated holographic 3d display system using integral lens array. *Optical Society of America*, (13), 2005.

[36] A.O.Yontem and L.Onural. Integral image based 3d display of holographic data. *Optical Society of America*, (22), 2012.

[37] David E. Roberts and Trebor Smith. The history of integral print methods. *An excerpt from: Lens Array Print Techniques*, 2006.

[38] F.Okano, H.Hoshino, H.A.Jun, and I.Yuyama. Real-time pick-up method for a 3d image based on integral photography. *Applied Optics*, (36), 1997.

[39] F.Reinitzer. Beitrge zur kenntniss des cholesterins. *Wiener Monatschr, Fur Chem*, (146), 1888.

[40] J.S.Kollin, S.A.Benton, and M.L.Jepsen. Real-time display of 3d computed holograms by scanning the image of an acousto-optic modulator. *Proceedings SPIE*, (46), 1989.

[41] P.S.Hillaire, S.A.Benton, M.Lucente, and P.M.Hubel. Color images with mit holographic video display. *Proceedings SPIE*, (46), 1989.

[42] M.Stanley, M.A.Smith, P.J.Watson, S.D.Coomber, C.D.Cameroon, C.W.Slinger, and A.D.Wood. 3d electronic holographic display system using 100 megapixel slm. *Proceedings SPIE*, (56), 2004.

[43] J.Neff, R.Athale, and S.Lee. Two dimensional spatial light modulators:a tutorial. *Proceedings IEEE*, (46), 1990.

[44] S.T.Tang, F.H.Yu, J.Chen, M.Wong, H.C.Huang, and H.S.Kwok. Reflective twisted nematic liquid crystal displays. *Journal of applied physics*, (46), 1997.

[45] T.Balogh, P.Kovacs, and A.Barsi. Holovizio 3d display system. *IEEE 3DTV conference*, (56), 2007.

[46] George Green. An essay on the application of mathematical analysis to the theories of electricity and magnetism. *Nottingham, England: T. Wheelhouse*, 1828.

[47] Dr Peter Vickers. The physics and philosophy of kirchhoffs theory of diffraction (on the 130th anniversary of kirchhoffs paper). *Durham University Institute of Advanced Study*, 2012.

[48] Kyoji Matsushima, Hagen Schimmel, and Frank Wyrowski. Fast calculation method for optical diffraction on tilted planes by use of angular spectrum of plane waves. *Optical Society of America*, 20, 2003.

[49] Gokhan Bora Esmer. Computation of holographic patterns between tilted planes. Master's thesis, Bilkent University, 2004.

[50] T.J.Naughton, J.B.McDonald, Y.Frauel, and B.Javidi. Efficient compression of digital holograms for internet transmission of three-dimensional images. *National University of Ireland*, 2008.

[51] T.J.Naughton, Y.Frauel, B.Javidi, and E.Tajahuerce. Compression of digital holograms for 3d object reconstruction and recognition. *Applied Optics*, 2002.

[52] E.Darakis, T.J.Naughton, M.Kowiel, and R.Nasanen. Visually lossless compression of digital hologram sequences. *SPIE*, 2010.

[53] Darakis E and Soraghan JJ. Use of fresnelets for phase-shifting digital compression. *IEEE Transactions in Image Processing*, 15(12), December 2006.

[54] E.Darakis, T.J.Naughton, J.Soraghan, and B.Javidi. Measurement of compression defects in phase-shifting digital holographic data. *SPIE Optical information systems*, 2005.

[55] Y.Xing, B.Pesquet-Popescu, and F.Dufaux. Compression of computer generated hologram based on phase-shifting algorithm. *European workshop on visual information processing*, 2013.

[56] Y.Xing, B.Pesquet-Popescu, and F.Dufaux. Compression of computer generated phase-shifting hologram sequence using avc and hevc. *SPIE Applications of Digital Image Processing*, 2013.

[57] Y.Xing, B.Pesquet-Popescu, and F.Dufaux. Vector quantization of computer generated phase-shifting holograms. *Signals, systems and computers*, 2013.

[58] Y.Xing, B.Pesquet-Popescu, and F.Dufaux. Comparative study of scalar and vector quantization on different phase-shifting digital holographic data representations. *3DTV conference : True vision capture, transmission and display of 3D video*, 2014.

[59] E.Darakis and T.Naughton. Compression of digital hologram sequences using mpeg-4. *SPIE*, 2009.

[60] Angelo Arrifano, Marc Antonini, and Manuela Pereira. Multiple description coding of digital holograms using maximum-a-posteriori. *EUVIPS*, 2013.

[61] Alison Shortt, Thomas Naughton, and Bahram Javidi. Compression of digital holograms of 3d objects using wavelets. *Optics Express*, 14(7), April 2006.

[62] E.Darakis and J.J.Soraghan. Compression of interference patterns with application to phase-shifting digital holography. *Applied Optics*, 2006.

[63] L.T.Bang, Z.Ali, P.D.Quang, J.Park, and N.Kim. Compression of digital hologram for 3d object using wavelet-bandlets transform. *OSA*, 2011.

[64] D.Blinder, T.Bruylants, E.Stijns, H.Ottevaere, and P.Schelkens. Wavelet coding of off-axis holographic images. *SPIE*, 2013.

[65] Levent Onural. Diffraction from a wavelet point of view. *Optics Letters*, 18(11), June 1993.

[66] L.Onural and M.Kocetepe. Family of scaling chirp functions. *IEEE transaction in image processing*, 1995.

[67] Micheal Liebling, Thierry Blu, and Micheal Unser. Fresnelets: New multiresolution waveletbases for digital holography. *IEEE Transactions on Image Processing*, 12 (1):29–43, January 2003.

[68] R.Haussler and H.Stolle. Real-time holography. Technical report, SeeReal Technologies GmbH, Dresden Germany, 2008.

[69] Y.Li, H.Szu, Y.Sheng, and J.Caulfield. Wavelet processing and optics. *IEEE Invited paper*, 1996.

[70] Stephan R, Ralf H, Norbert L, Gerald F, and Armin S. Large holographic 3d displays for tommorow's tv and monitors - solutions, challenges and prospects. *IEEE lasers and electro optics*, December 2008.

[71] Michael Unser. Splines: A perfecr fit for signal and image processing. *IEEE Signal Processing magazine*, November 1999.

[72] J.Benedetto, C.Heil, and D.Walnut. Differentiation and balian-low theorem. *Journal of Fourier analysis and applications*, 1994.

[73] David Barina. Gabor wavelets in image processing. *EU FP7-ARTEMIS*, 2007.

[74] T.S.Lee. Image representation of 2d gabor wavelets. *IEEE transactions on Pattern Analysis and Machine Learning*, 1996.

[75] J.Han and K.Ma. Rotation-invariant and scale-invariant gabor features for texture image retrieval. *Image and vision Computing*, 2007.

[76] D. Gabor. Theory of communication. *Journal of the Institution of Electrical Engineers Part III: Radio and Communication Engineering*, 1946.

[77] Javier.R.Movellan. Tutorial on gabor filters. *http://mplab.ucsd.edu/tutorials/gabor.pdf*, 2008.

[78] Ingrid Daubechies, Jaffard.S, and L.Journes. A simple wilson orthonormal basis with exponential decay. *SIAM Journal of Mathematics*, 1991.

[79] J.Zhong and L.Weng. Holographic research and technologies. *Intech Open*, 2011.

[80] Tony Ezzat, Jake Bouvrie, and Tomaso Poggio. Max-gabor analysis and synthesis of spectrograms. *Center for Biological and Computational Learning, McGovern Institute for Brain Research MIT*, 2006.

[81] Ole Christensen and Torben Jensen. An introduction to the theory of bases, frames and wavelets.

[82] Ingrid Daubechies. *Ten lectures on wavelets*. Society for Industrial and Applied Mathematics, 1992.

[83] L.Cohen. *Wavelets and Signal Processing*. Lokenath Debnath, 2003.

[84] J.Morlet, G.Arens, E.Fourgeau, and D.Giard. Wave propagation and sampling theory part 1: Complex signals and scattering in multi-layered media. *Society of exploration Geo-Physicists*, 1982.

[85] Hans G. Feichtinger and Thomas Strohmer. *Gabor Analysis and Algorithms.* Birkhuser, 1998.

[86] Stefan Mallat. *A wavelet tour of signal processing.* Academic Press, 1999.

[87] Kartik Viswanathan, Patrick Gioia, and Luce Morin. Wavelet compression of holograms: Towards view-dependent frameworks. *SPIE Applications in digital image processing*, 36(8856):1–10, October 2013.

REPRÉSENTATION ET RECONSTRUCTION ADAPTATIVE DES HOLOGRAMMES NUMÉRIQUES

KARTIK VISWANATHAN[1]

CONTENTS

LIST OF FIGURES

RÉSUMÉ

On constate une forte augmentation de l'intérêt porté sur l'utilisation des technologies vidéo 3D pour des besoins commerciaux, notamment par l'application de l'holographie, pour fournir des images *réalistes* , *qui semblent vivantes*. Surtout, pour sa capacité à reconstruire tous les parallaxe nécessaires, afin de permettre de realiser une vision véritablement immersive qui peut être observée par quiconque (humains, machine ou animal). Malheureusement la grande quantité d'information contenue dans un hologramme le rend inapte à être transmis en temps réel sur les réseaux existants. Cette thèse présente des techniques afin de réduire efficacement la taille de l'hologramme par *l'élaguage* de portions de l'hologramme en fonction de la position de l'observateur. Un grand nombre d'informations contenues dans l'hologramme n'est pas utilisé si le nombre d'observateurs d'une scène immersive est limité. Sous cette hypothèse,éléments de l'hologramme peuvent être décomposés pour que seules les parties requises sensibles au phénomène de diffraction vers un point d'observation particulier soient conservés. Les reconstructions de ces hologrammes élagués peuvent être propagés numériquement ou optiquement. On utilise la transformation en ondelettes pour capter les informations de fréquences localisées depuis l'hologramme. La sélection des ondelettes est basée sur des capacités de localisation en espace et en fréquence. Par exemple, les ondelettes de Gabor et Morlet possèdent une bonne localisation dans l'espace et la fréquence. Ce sont des bons candidats pour la reconstruction des hologramme suivant la position de l'observateur. Pour cette raison les ondelettes de Shannon sont également utilisées. De plus l'application en fonction du domaine de fréquence des ondelettes de Shannon est présentée pour fournir des calculs rapides de l'élagage en temps réel et de la reconstruction.

* *Orange Labs, INSA IETR*

1 INTRODUCTION

La technologie holographique d'affichage en trois dimensions est un domaine stimulant qui attire beaucoup l'attention des scientifiques et également du public. La capacité à observer le véritable monde *qui semble vivant* grâce à un support d'enregistrement a grandement attiré l'attention du public et les scientifiques ont depuis longtemps essayé de fournir une solution à ce besoin.

Un des aspects intéressant développé récement et utilisé commercialement dans les cinémas et téléviseurs haut de gamme est le concept de vision stéréoscopique. Mais cette technique est très irritante pour le système visuel humain car la parallaxe de profondeur perçue par le cerveau et l'oeil n'est pas la même. A cause de cet inconfort, cela créé une fatigue oculaire chez un grand nombre de personnes. Pourtant, cette technologie, même si elle n'est pas réellement de la 3D est largement utilisée comme un produit commercial. Cela montre l'intérêt immense du public pour l'affichage 3D.

Au fil des années, de grandes améliorations ont été apportées dans la compréhension du comportement de la lumière et les ingénieurs ont réussi à reproduire les propriétés physiques de la lumière afin de remplir un volume. Ceci est la *vraie* technologie 3D ou 3D immersive. L'holographie est l'une des technologie 3D les plus sophistiquées, où l'on peut enregistrer et relire toute scène 3D en utilisant toutes les propriétés physiques de lumière nécessaires. Cela signifie que la reconstruction d'un hologramme *qui semble vivant* serait donc indépendente de l'observateur (humains, animaux, caméra, etc.). Ils peuvent percevoir la scène comme si la scène se déroulait devant eux.

Aujourd'hui, l'affichage holographique n'est pas aussi avancé que l'affichage stéréoscopique, cependant nous estimons que l'affichage holographique est supérieur et souhaitable même si la technologie est de plus en plus compliquée.En outre il y a le problème inhérent aux restrictions de bande passante des réseaux. Aujourd'hui, le coût de transmission des copies numériques des médias par les cables du réseaux et d'Internet représente un enjeu majeur. Cette thèse est donc consacrée à surmonter les défis de la transmission des hologrammes numériques en *élaguant* certaines portions de l'hologramme d'après certains paramètres physiques tel que la position de l'observateur ou la reconstruction de la partie à observer.

L'élaboration d'un tel écran holographique nécessite une bonne compréhension des propriétés physiques de la lumière. Comment la lumière se propage dans l'espace et comment elle est réfléchie, diffractée et réfractée à partir d'un objet 3D. Cette dispersion de la lumière porte les informations optiques et géométriques de l'objet 3D et remplit cet espace. Les propriétés physiques de ce *champ lumineux* qui remplit l'espace 3D doivent être mesurées afin de regénérer le même champ lumineux dans un autre endroit. Aujourd'hui, ces informations enregistrées sont trop *lourdes* et doivent être efficacement réduites (taillées et compressées) avant de pouvoir être transmises sur les réseaux.

Cette thèse se concentre sur l'efficacité de l'élaguage des hologrammes, suivant la position de l'observateur, à l'aide d'ondelettes. Le choix d'une transformée en ondelettes est crucial puisque les ondelettes conventionnelles ne sont pas adaptées à ce type de système d'affichage.

2 REPRÉSENTATION DES HOLOGRAMMES EN FONCTION DE LA POSITION DE L'OBSERVATEUR

Dans toutes les méthodes de représentation d'hologramme utilisées aujourd'hui, l'hypothèse est que le volume de reconstruction est assez petit. La taille des objets varie de quelques *millimètres* à quelques *centimètres*. Dans une véritable configuration 3D immersive, le volume de reconstruction est de l'ordre du m^3. Cela signifierait de grands hologrammes qui présentent 10^9 pixels et au-delà. Pour cette grande quantité de données holographiques nous proposons une stratégie alternative qui plutôt que d'essayer de coder et de transmettre l'ensemble de l'hologramme ne va traiter uniquement que les informations nécessaires au décodeur pour un ensemble spécifique d'observateurs. Il faut donc une étape intermédiaire où les informations inutiles de l'hologramme seront *élaguées* et les informations restantes seront alors quantifiées, codées et transmises. Dans cette section nous donnerons plus de précisions sur les hypothèses émises pour l'élaguage des portions de l'hologramme.

Nous faisons deux hypothèses ici:

- le volume à reconstruire ou la taille de l'objet sont relativement importants par rapport à la taille de l'observateur
- Il y a un nombre limité d'observateurs

En vertu de ces hypothèses, notre objectif est d'obtenir les portions de l'hologramme qui entraînent une diffraction à la position de l'observateur. La première hypothèse implique de savoir gérer les technologies 3D immersives et la deuxième hypothèse nous permet d'introduire une certaine dégradation des informations dans le but d'obtenir une bonne compression.

L'hologramme résultant obtenu par l'élaguage doit être fidèle c'est-à-dire que la reconstruction obtenue à la position de l'observateur est identique à celle obtenue à partir d'un hologramme complet. Cet hologramme résultant est dénommé comme *sous-hologramme*. Ce concept de sous-hologramme n'est pas nouveau et a déjà été utilisé auparavant dans [1].

3 ONDELETTES POUR REPRÉSENTATIONS DES HOLOGRAMMES

Le critère qu'une ondelette doit remplir est de pouvoir être en mesure d'approximer l'hologramme de façon raisonnable, c'est-à-dire récupérer les informations de fréquence à chaque emplacement de pixel. Les hologrammes ne sont pas des fonctions lisses qui peuvent être approximées facilement. Aussi, pour capturer les grandes variations de fréquence d'un hologramme, il est naturel de s'attendre à trouver une ondelette qui est bien localisée dans l'espace et la fréquence.

Jusqu'à présent les transformées en ondelettes pour les hologrammes sont divisées en deux grandes catégories. La première catégorie est l'ensemble des ondelettes qui remplissent les critères de recevabilité (mathématiquement) et sont en accord avec les principes de l'analyse multi resolution par ondelettes. Le point importante à propos de ces ondelettes est le temps (l'espace) - fréquence des analyses possibles. Tout comme les ondelettes génériques Haar, Meyer, Coifflet, Daub-4 etc. incluses dans cette catégorie.

L'application directe des bancs de filtres utilisés pour la compression d'images a été appliquée aux hologrammes [2], cependant afin d'être adaptée pour la représentation et l'approximation d'hologrammes utilisés dans les systèmes basés sur la position de l'observateur, les ondelettes doivent être adaptées, souvent en assouplissant certaines exigences. Cela est nécessaire lors de la conception de fonctions semblables à des ondelettes en observant la relation étroite entre le phénomène de diffraction optique et de propagation des ondes à l'échelle des ondelettes, c'est-à-dire le paramètre échelle s qui désigne la distance (profondeur) de la propagation. Ce fut d'abord proposé par Onural dans [3]. Cette théorie est intéressante en ce sens seulement si nous sommes prêts à abandonner le cadre de l'analyse multi-résolution en se concentrant sur l'analyse espace - profondeur, plutôt que sur l'analyse temps - fréquence. Il y a certaines questions qui demeurent mathématiquement irrecevables [4]. Cela a été illustré par Onural dans [5], la fonction chirp (chirplet) réalise une transformée qui est réversible mais qui n'est pas mathématiquement recevable. Ces ondelettes forment la deuxième catégorie d'ondelettes.

Dans le même esprit, Fresnel [6] a essayé de compenser l'effet de propagation de front d'onde en utilisant les transformées de Fresnel pour transformer les signaux originaux pendant l'analyse en ondelettes. Cela implique la nécessité d'adapter certaines conditions de l'analyse multirésolution, mais surtout d'assouplir certaines propriétés de l'espace et de la localisation de la fréquence.

D'autre part, garder une bonne localisation en espace et en fréquence se fait au détriment du temps de traitement des informations. C'est le cas des ondelettes de Gabor. L'acceptabilité des hypothèses posées sur l'assouplissement des conditions pour la création des Fresnelets et des ondelettes de Gabor sera discutée prochainement.

Pour un système de représentation basé sur la vue, nous avons besoin d'une fonction d'ondelettes qui permet d'effectuer l'analyse de multi-résolution de l'hologramme en décomposant les positions de l'observateur en plusieurs points de vue, c'est-à-dire que les paramètres configurables de la transformation en ondelette (*échelle, translation etc.*) correspondant à chaque décomposition devra représenter une position unique ou un ensemble de positions de l'observateur.

4 HYPOTHÈSES SUR LES ONDELETTES ET IMPORTANCE DE LA LOCALISATION

En résumé, l'ondelette idéale doit posséder les propriétés suivantes :

- Elle devra être localisée en espace et en fréquence
- Elle devra permettre l'analyse fréquence - espace et non pas l'analyse espace - profondeur
- Elle doit être mathématiquement recevable

Bien que les ondelettes soient un outil puissant pour la compression des données, leur capacité à analyser localement les signaux les rendent particulièrement adaptées pour les reconstructions partielles et adaptatives. Cette fonctionnalité est classiquement utilisée pour dégrader certaines données dans l'espace (ou le temps) et la fréquence selon les exigences de

l'utilisateur ou les paramètres de rendu. Lorsqu'il s'agit de l'holographie, les ondelettes peuvent efficacement contribuer à exploiter un type particulier d'adaptativité, à savoir l'adaptativité suivant le point de vue.

La dégradation (causée par l'adaptativité) est d'autant plus importante que l'holographie numérique peut être exploitée non seulement au niveau de la transmission, mais aussi au niveau de l'affichage, avec à des résolutions qui ne permettraient pas de traiter un hologramme complet. Nous voyons donc que dans des cas particuliers, seulement dans les cas où il n'y a qu'un nombre limité d'utilisateurs autorisés à observer l'hologramme, un bon schéma de compression n'est pas celui qui offre le meilleur ratio de compression, mais celui qui permet de dégrader efficacement le signal de façon à transmettre uniquement les données pertinentes aux différents obsevateurs identifiés.

En effet, en raison des équations de diffraction (grating equation (1)), l'émission de lumièredans la direction θ sera produite uniquement par le contenu de l'hologramme ayant la longueur d'onde λ. Ainsi, en considérant une position d'observation spécifique (voir Figure 1), il y aura seulement un sous-ensemble de données de l'hologramme qui contribuera au champ de lumière atteignant cet observateur. Ce sous-ensemble (que nous appellerons *"sous-hologramme"*) peut être obtenu en sélectionnant les fréquences associées aux angles de l'affichage de l'hologramme à l'observateur. La fréquence à sélectionner dépend de la localisation spatiale de l'hologramme. Il s'agit de décomposer en ondelettes les données de l'hologramme grâce à une ondelette qui présente une *bonne* localisation en espace et en fréquence. C'est le moyen naturel pour extraire des informations sur la localisation et sur les fréquence provenant des données de l'hologramme. Extraire les informations du sous-hologramme pour un point d'observation donné est une adaptation réalisée en simplifiant certains coefficients de l'ondelette.

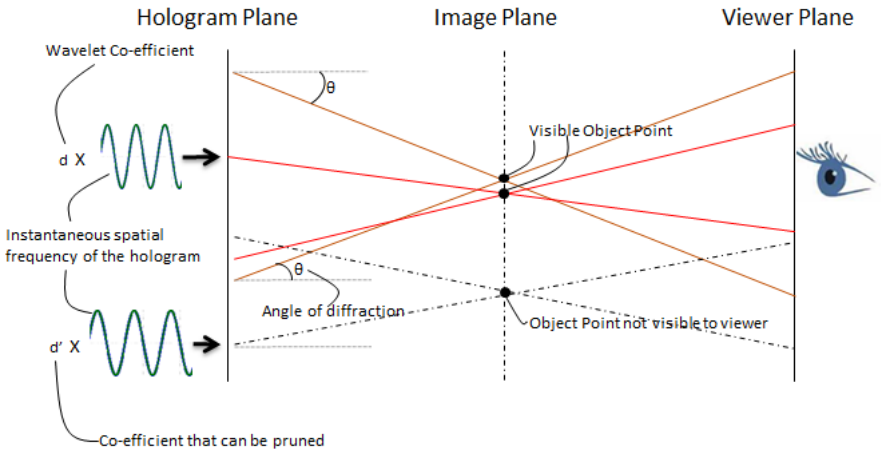

Figure 1: Compression d'hologrammes suivant le point d'observation

$$\sin\theta = \frac{m\lambda}{\Lambda}, \tag{1}$$

où θ est l'angle de diffraction, λ la longueur d'onde, Λ est la période localisée d'un hologramme m est un entier arbitraire.

Nous voyons qu'un coefficient sera pertinent pour un angle de propagation donné si il est lié à la bonne fréquence suivant cette relation, c'est-à-

dire que le spectre de ces ondelettes doit être centré autour de cette valeur. D'autre part, les ondelettes doivent également avoir une bonne localisation en espace, puisque cette diffraction directionnelle est considérée localement, figure(1).

Dans les prochaines sections, nous discuterons de bases d'ondelettes qui offrent une "bonne" localisation et qui sont les mieux adaptées pour ce type de représentation.

5 FRESNELETS ET ONDELETTES DE GABOR: UNE COMPARAISON

5.1 Fresnelets et leurs lacunes

Les Fresnelets [6] sont l'une des ondelettes utilisées pour la représentation compacte d'hologrammes. Nous montrons que cette ondelette n'est pas bien localisée en espace et en fréquence et ne peut donc pas constituer une bonne base pour la représentation compacte des hologrammes pour un système dépendant de la position de l'observateur.

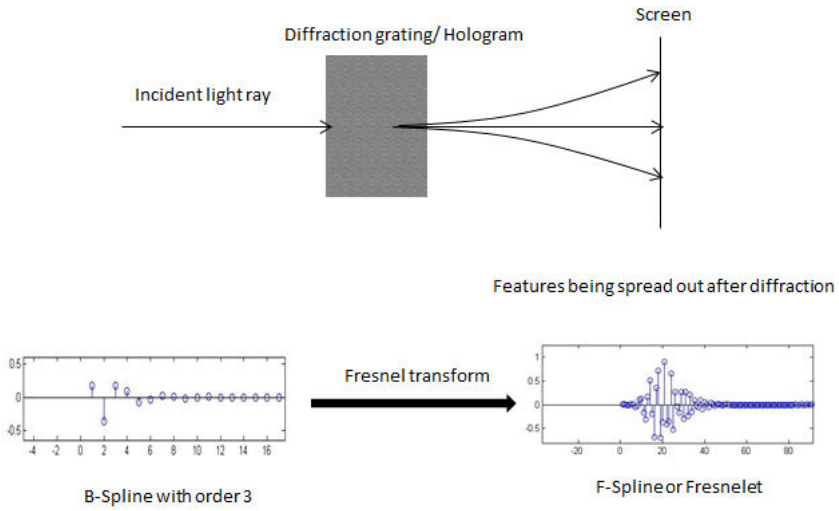

Figure 2: B-Splines et diffraction

L'étalement spatial de la base d'ondelettes (dû à la conversion de Fresnel de B-splines) n'est pas bien adapté pour des techniques de représentation d'hologramme basées point de vue , figure (2).

Une autre façon d'interpréter l'étalement spatial est présentée ci-après. À l'aide de l'incertitude relative liée à la transformée de Fresnel [6] , la limite du produit du temps par la largeur de la bande passante est donnée comme le produit du carré de la variance pour des fonctions complexes.

$$\sigma_g^2 \sigma_{\tilde{g}}^2 \leqslant \frac{\tau^4}{16\pi^2} \tag{2}$$

où σ_g^2 est la variance du signal $g(x)$, $\sigma_{\tilde{g}}^2$ la variance du signal issue de la transformée de Fresnel $\tilde{g}(x)$. Nous remarquons que la meilleure localisation dans l'espace-fréquence est obtenue lorsque nous obtenons le produit d'une

fonction chirp du formulaire $e^{\alpha x^2}$ par une fonction gaussienne, qui peut être interprétée comme son enveloppe. Comme indiqué dans [6]. Lorsque le paramètre τ (qui est directement proportionnel à la distance de propagation) augmente, l'étalement spatial de cette enveloppe s'accroît davantage. Puisque la fonction chirp des fréquences varie de façon monotone quand nous nous éloignons de l'origine, des fréquences pertinentes devront être alors prises en compte. Puisque la fonction chirp est celle qui donne les meilleurs résultats pour ce qui est de l'incertitude, nous voyons que ces étalements de fréquence se produiront pour toute fonction arbitraire. Si nous devions utiliser les coefficients des odelettes qui sont générés après une transformée de Fresnel, les informations obtenues sur les fréquences ne pourraient pas être distinguées. De ce fait, la capacité à localiser ces ondelettes est faible. Ces ondelettes ne sont alors plus très utiles pour la représentation d'hologrammes suivant la position de l'observateur.

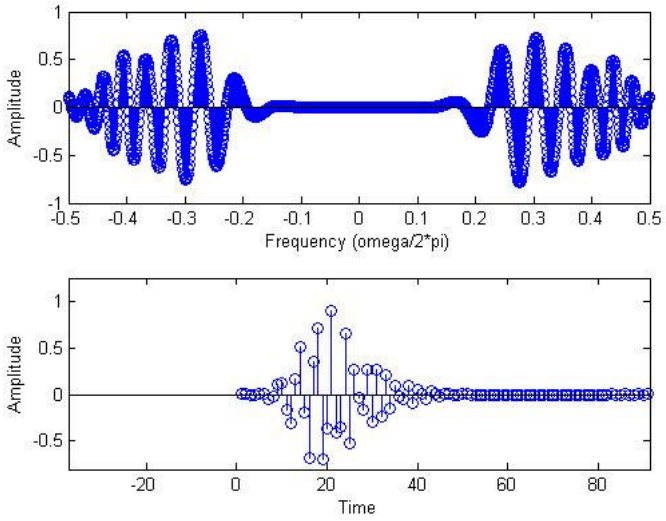

Figure 3: Base Fresnelet montrant la fréquence (en haut) et la représentations du domaine temporel pour la partie réelle de la plus petite échelle. Remarquez l'étalement de la base dans le temps (spatiale)

Bien qu'il ait été théoriquement prouvé que les Fresnelets ne présentent pas une bonne localisation en temps et en fréquence, on peut montrer que, dans la pratique, elles pourront être choisies de façon à être suffisamment proches de fonctions qui possèdent cette propriété. Ceci est contré par l'argument suivant.

Dans [7] Il est montré que les B-splines convergent asymptotiquement vers une fonction de Gabor puisque le degré tend vers ∞. Les fonctions de Gabor sont des fonctions gaussiennes qui sont modulées avec une fréquence porteuse sinusoïdale. Cela signifie que les B-splines tendent à converger vers $e^{j2\pi mbx}g(x-na)$, dans le même temps l'ordre de la B-spline va tendre vers ∞.

Si nous faisons l'hypothèse que la limite de la base de Gabor est une base de Riesz, alors nous pouvons utiliser le théorème de Bailen-low [8] et en déduire que la base n'est pas bien localisée en temps et en fréquence; les

séries approximées de fonctions de B-Spline ne se comporteront alors pas mieux, peut importe la façon dont elles s'approchent de la limite :

$$(\int_{\mathbb{R}} |\, xg(x) \,|^2 \, dx)(\int_{\mathbb{R}} |\, \gamma\hat{g}(\gamma) \,|^2 \, d\gamma) = \infty \tag{3}$$

L'équation(3) montre qu'il n'y a pas de fenêtre de fonction bien-localisée (ou Gabor atom) g ni dans le temps ni dans la fréquence pour avoir un Gabor frame (base de Riesz).

Il a été prouvé dans [6] que la Fresnelet forme également une base de Riesz. Ces Fresnelets qui sont ces transformées de Fresnel de B-splines, vont en fait augmenter l'étalement de la fréquence, et par conséquent, on peut dire que les Fresnelets ne peuvent satisfaire le théorème de Bailen-Low (3). Il ne peut donc pas y avoir une bonne localisation dans en espace et en fréquence. La figure (3) montre l'étalement de la fréquence de l'information pour une Fresnelet de degré 3. Un tel étalement des Fresnelets dans les domaines spatial et fréquenciel n'est pas bien adapté à l'application de la compression d'hologramme suivant le point d'observation.

5.2 Ondelettes de Gabor

Les ondelettes de Gabor sont de plus en plus utilisées dans le domaine de la modélisation de la vision biologique. Les ondelettes de Gabor sont utilisées pour réaliser la mise à l'échelle, la rotation et la translation. Elles sont donc très bien adaptées pour mesurer les fréquences spatiales locales d'hologrammes. Le théorème d'incertitude joue un rôle important dans la localisation en temps-fréquence. Il est connu que la fonction gaussienne est celle qui fournit les meilleures limites sur l'incertitude. Les fonctions de Gabor sont des fonctions gaussiennes qui sont modulées avec une fonction sinusoïdale.

La fonction de Gabor est représentée à l'aide de 2 opérateurs :

- Opérateur de modulation $E_b \mid (E_b g)(x) := e^{i2\pi bx}, b > 0$
- Opérateur de translation $T_a \mid (T_a g)(x) := g(x-a), a > 0$

$$\{E_b T_a g\} = e^{i2\pi bx} g(x-a) \tag{4}$$

les ondelettes de Gabor sont composées de 4 paramètres: modulation (b), translation (a), Echelle (s), rotation (θ) et les ondelettes sont notées $g_{s,\theta,a,b}(x)$. Nous voulons que le produit $ab < 1$ afin d'empêcher la formation d'une frame de Gabor et permettre de contourner le théorème de Balian-Low.

Nous utilisons la transformée en ondelettes de Gabor 2D, qui fournit des meilleurs résultats que les ondelettes de Gabor en 1D, voir [9]. Mathématiquement, la fonction de Gabor 2D permet la meilleure localisation espace-fréquence uniquement dans sa forme complexe, car une fonction 2D complexe contient dans une projection en quadrature, une composante de cosinus appelée pair-symétrique ainsi qu'une composante de sinus impair-symétrique [10].

La figure 4 montre une ondelette de Gabor bien localisée et centrée en fréquence sur 2π.

Une fois que nous avons les coefficients de l'ondelette de Gabor, nous pouvons les utiliser pour les techniques d'élagage basées sur la position de l'observateur comme expliqué dans la section (4). Il a également été observé que les bases des ondelettes de Gabor sont bien localisées dans la domaine spatial par rapport aux Fresnelets comme illustré dans la figure(4).

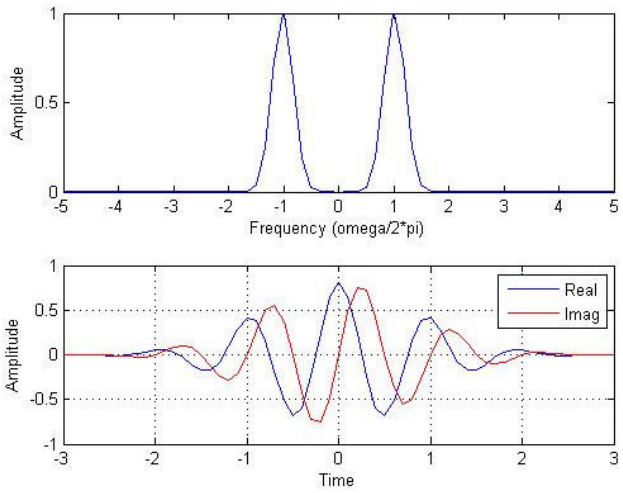

Figure 4: Ondelette de Gabor montrant la fréquence (en haut) et la représentations du domaine temporel

En utilisant ces bases d'ondelettes, on améliore l'approximation d'une zone locale de l'hologramme ce qui résulte en une meilleure extraction des caractéristiques pour la reconstruction de l'hologramme suivant la position de l'observateur.

Les ondelettes de Gabor 2D permettent naturellement la suppression des ordres de diffraction indésirables. L'ondelette de Gabor utilisée pour notre expérience est celle donnée dans [10].

La figure 5 montre la fonction ψ pour 5 valeurs de s entre 2π et $\frac{\pi}{4}$ radians et pour des valeurs de rotation à intervalles de 18 degrés.

$$\psi(\frac{x-a}{s}, \frac{x-b}{s}, \theta) = \frac{1}{\sqrt[4]{\pi}}\sqrt{\frac{2\pi}{\gamma}}\exp\{-\frac{(2\pi/\gamma)^2[(x-a)^2+(y-b)^2]}{2s^2}\} \exp\{j2\pi\frac{(x-a)Cos\theta+(y-b)Sin\theta}{s}\} \quad (5)$$

s représente l'échelle de la fonction d'ondelettes, θ représente la rotation, a et b représentent la translation de l'ondelette. γ est sélectionné pour être égal à $\pi\sqrt{2/\ln 2}$.

La transformée en ondelette de Gabor utilisée ici est également appelée la transformée de *Max-Gabor*. Nous effectuerons les opérations de convolution entre l'hologramme et les ondelettes à échelle spécifique s. Nous obtenons la transformée en ondelette de Gabor pour chaque valeur de s et θ déterminée grâce aux paramètres de translation a et b pour un hologramme. Le maximum de la transformée en ondelette de Gabor 2D est obtenu lorsque la magnitude du coefficient d'ondelette est maximale pour chaque s et θ, pour chaque valeur de a et b dans l'hologramme. Cela est illustré dans la figure(6). Ceci est le *ridge* de la transformée en ondelette de Max-Gabor. Il a été montré que le coefficient d'ondelettes construit de cette manière est égal à l'onde produite par l'objet au plan hologramme multipliée par une constante [10]. Cette méthode a également montré qu'il y a une suppression naturelle de l'ordre zéro et des images réelles sans la nécessité de filtrage spatial.[10]

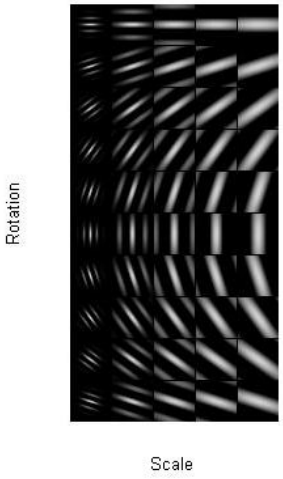

Figure 5: Ondelette de Gabor 2D pour 5 échelles différentes et 10 rotations différentes

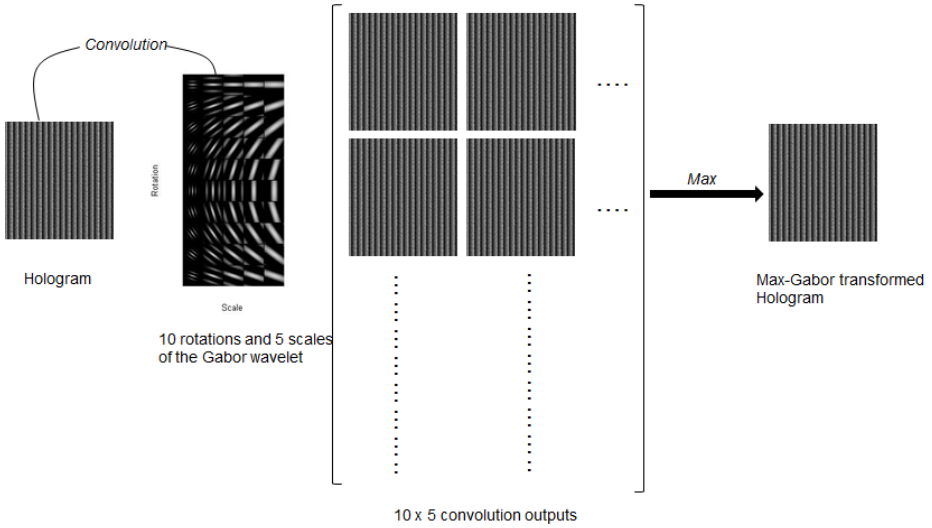

Figure 6: La transformée de Max-Gabor

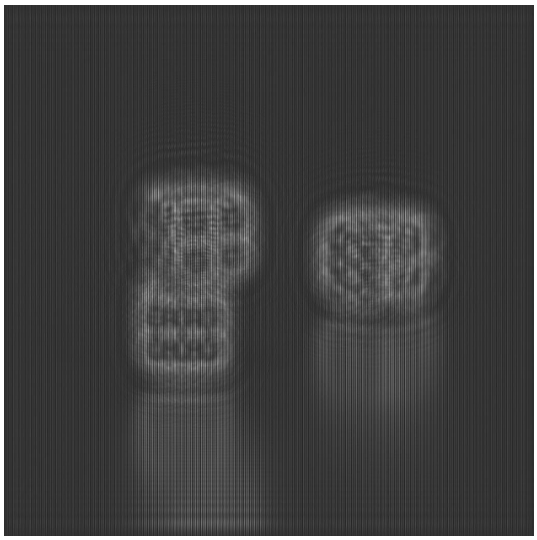

Figure 7: Hologramme d'une image de dés

5.3 Expériences

En utilisant les deux ondelettes présentées jusqu'ici (Fresnelets et ondelettes de Gabor), nous avons obtenu la reconstruction d'un hologramme. L'hologramme est celui d'une image simple (2D) de dés. Il n'y a donc qu'une seule vue qui puisse être reconstruite. L'hologramme est généré numériquement dans la configuration hors de l'axe avec une différence de 10 degrés entre l'onde de référence et l'onde de l'objet, Figure (7). Pour les ondelettes de Gabor nous avons utilisé la méthode angular spectrum afin d'effectuer la reconstruction. Pour les Fresnelets, on utilise la transformée de Fresnel, car la transformée en Fresnelet effectue intrinsèquement la propagation de Fresnel, voir section 5.1.

Les ondelettes de Gabor sont capables de supprimer les ordres indésirables si l'on a calculé les coefficients d'ondelette au ridge de la transformée. Cf. figure (9). La sortie d'une image transformée par Fresnelet (8) montre que des ordres indésirables de diffraction ont été générés.

Le code pour les deux transformations est écrit en MATLAB©et les résultats sont générés sur un PC doté d'un processeur Xeon©E5-1620 CPU fonctionnant à 3,6 Ghz avec 8 Go de RAM. La résolution de la photo permettant la création de l'hologramme (7) est de 1024x1024 pixels. Le code de Fresnelets dans sa forme non optimisée effectue la conversion en 25 secondes alors que le code non optimisé des ondelettes de Gabor en 2D, prend environ 4 minutes de temps de calcul. Cela est dû au fait que pour chaque angle de rotation et chaque échelle de l'ondelette de Gabor, on produit une image transformée. Plus tard, le maximum du coefficients de Gabor est trouvé pour obtenir les valeurs au *ridge* de la transformée.

Dans les sections suivantes, nous examinerons les reconstructions d'hologrammes qui ne sont pas des images simples en 2D, c'est-à-dire que nous devrons être en mesure de reconstruire à partir de l'hologramme toutes les coupes transversales dans le champ 3D. Les deux ondelettes ci-dessus ne sont pas très bien adaptées pour ce type de reconstruction. Les Fresnelets ne conviennent pas à cause de leur propriété de localisation et la transformée de *Max-Gabor* effectue l'opération d'élagage en sélectionnant le coefficient max-

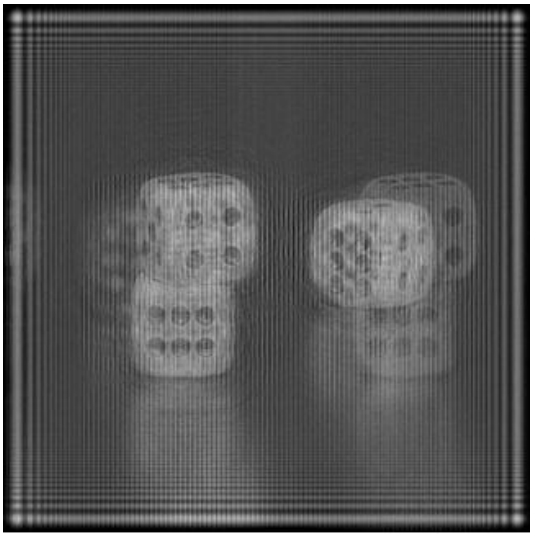

Figure 8: Reconstruction de l'hologramme à partir d'une Fresnelet. Remarquez que les ordres indésirables sont visibles dans la reconstruction

Figure 9: Reconstruction d'un hologramme à partir d'une transformée de Gabor en utilisant la méthode angular spectrum. Notez que les ordres non désirés sont supprimés

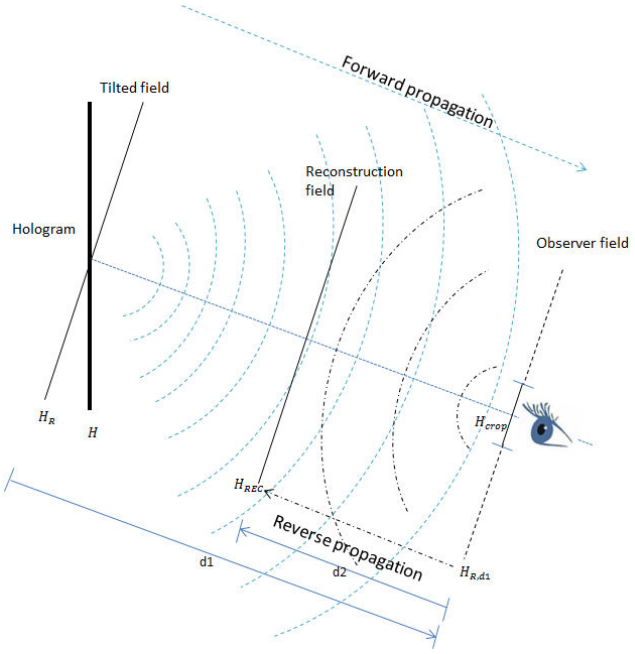

Figure 10: Illustration de propagation du champ lumineux pour la reconstruction

imal de chaque plage de fréquences, ce qui signifie qu'un grand nombre d'informations potentiellement pertinentes pour la reconstruction de certaines vues est perdu. Nous examinerons comment faire des reconstructions sur des plans inclinés puis nous discuterons de 2 techniques d'élagage à savoir l'approche *dot-produit* et l'approche *convolution*.

6 RECONSTRUCTION SUIVANT LE POINT D'OBSERVATION

Pour une reconstruction générale des hologrammes, nous effectuerons les étapes comme indiqué dans la figure(10).

H représente l'hologramme et $\hat{H}$ est sa transformée de Fourier. Les fréquences de Fourier sont désignées par (u, v) pour les directions x et y respectivement. Le vecteur d'onde est défini par:

$$k = 2\pi \begin{bmatrix} u & v & w \end{bmatrix} \tag{6}$$

où,

$$w = (\lambda^{-2} - u^2 - v^2)^{\frac{1}{2}} \tag{7}$$

La rotation du spectre angulaire est utilisée pour obtenir une coupe transversale du champ d'onde $\hat{H}_R$, parallèle au champ d'observation. Les rotations des fréquences sont données par:

$$R = \begin{bmatrix} 1 & 0 & 0 \\ 0 & \cos\theta & -\sin\theta \\ 0 & \sin\theta & \cos\theta \end{bmatrix} \begin{bmatrix} \cos\phi & 0 & \sin\phi \\ 0 & 1 & 0 \\ -\sin\phi & 0 & \cos\phi \end{bmatrix} \tag{8}$$

La rotation du vecteur d'onde est désormais obtenue par

$$\hat{k} = Rk \tag{9}$$

où

$$\hat{k} = 2\pi \begin{bmatrix} \hat{u} & \hat{v} & \hat{w} \end{bmatrix} \tag{10}$$

avec

$$\hat{w} = (\lambda^{-2} - \hat{u}^2 - \hat{v}^2)^{\frac{1}{2}} \tag{11}$$

Le champ incliné (section transversale) est représenté ainsi :

$$\hat{H}_R = \hat{H}(\hat{u}, \hat{v}) \tag{12}$$

La rotation du spectre angulaire utilise uniquement les fréquences nécessaires pour la reconstruction d'un plan incliné particulier. Puis la propagation de ce champ transverse est calculée à l'aide de l'algorithme angular spectrum comme expliqué dans [11]. Dans la figure (10), le champ d'observation est à une distance d_1 du plan d'hologramme incliné. Le champ d'onde au plan d'observation est donné par :

$$\hat{H}_{R,d_1} = \sum_{\hat{u}} \sum_{\hat{v}} H_R . \exp(i\hat{w} d_1) \tag{13}$$

Nous simulons le point de vue de l'observateur par un diaphragme et une lentille. L'opération de filtrage spatial réalisée par l'ouverture du diaphragme L fournit le champ d'onde obtenu dans le plan d'observation en éliminant les rayons qui n'atteignent pas la position de l'œil. Le champ résultant filtré spatialement est défini par :

$$\hat{H}_{crop} = \hat{H}_{R,d_1} . \text{rect}\left(\frac{\hat{u}}{L}, \frac{\hat{v}}{L}\right) \tag{14}$$

La simulation du passage du champ résultant par le biais de la lentille est effectué par une propagation arrière sur le plan de focalisation (plan de reconstruction), comme illustré sur la figure (10).

$$\hat{H}_{rec} = \sum_{\hat{u}} \sum_{\hat{v}} H_{crop} . \exp(i\hat{w}(-d_2)) \tag{15}$$

La transformée inverse de la reconstruction du champ d'onde nous donne la vue observée.

7 LES APPROCHES PAR CONVOLUTION ET PRODUIT SCALAIRE POUR LA REPRÉSENTATION DES HOLOGRAMMES

Représenter les hologrammes consiste à identifier les coefficients qui génèrent le bon champ d'onde à la position de l'observateur. Nous effectuerons les opérations de transformée en ondelettes sur l'hologramme pour sélectionner les coefficients nécessaires. Cela peut se faire de 2 façons:

7.1 L'approche par Produit Scalaire

Comme illustré dans la figure(12), le coefficient en chaque point de l'hologramme est calculé pour le point de vue de l'observateur. Cette approche est appelée *reconstruction parfaite* et nous utiliserons les reconstructions obtenues à partir de cette approche comme référence.

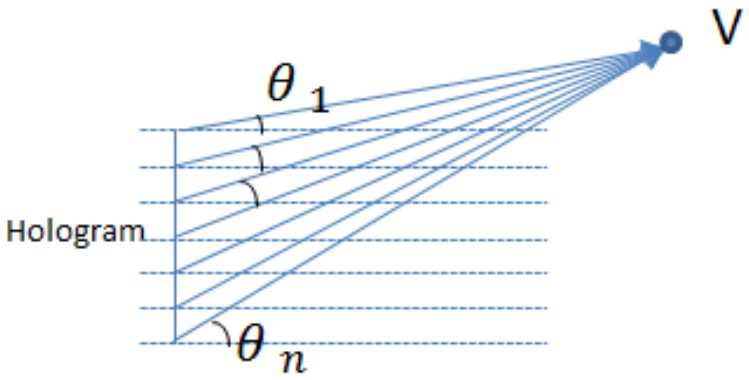

Figure 11: La diffraction au point V de l'hologramme H (produit scalaire)

Examinons l'espace 2D de $\mathbb{R}^2$ contenant un hologramme 1D désigné par H avec n pixels de valeurs complexes indexés par k.

$$H = \{H_1, H_2, H_3, \ldots, H_n\} \tag{16}$$

Soit $X : \mathbb{N} \to \mathbb{R}^2$, une fonction qui associe tous les index $k \in \mathbb{N}$ à la position 2D du pixel de valeur H_k dans $\mathbb{R}^2$. Ainsi le pixel de valeur H_k dans H est situé à la position 2D $X(k)$.

Considérons un point de vue arbitraire V dans l'espace 2D $\mathbb{R}^2$.

Soit $\alpha : \mathbb{R}^2 \to \mathbb{R}^n$, une fonction qui associe V au vecteur de coordonnées polaires

$$\alpha(V) = \theta^V = \{\theta_1, \theta_2, \theta_3, ..., \theta_n\} \tag{17}$$

qui sont les angles générés par le point V pour chaque point $X(k)$ sur l'hologramme comme illustré dans la figure (12).

À partir de ces angles nous pouvons calculer l'ensemble des fréquences dans H qui contribuent au champ de lumière diffracté reçu par V depuis l'hologramme. Afin d'extraire ces fréquences à partir de l'hologramme, nous construisons un ensemble de bases d'ondelettes pouvant capturer ces fréquences.

Soit f, une fonction qui donne la fréquence spatiale localisée à partir d'un angle θ selon l'équation de diffraction.

$f : \mathbb{R} \to \mathbb{R}$

$$f(\theta) = \frac{\sin(\theta)}{\lambda} \tag{18}$$

Nous définissons l'ensemble de ces fréquences

$$f^V = \{f_1, f_2, ..., f_n\} \tag{19}$$

où,

$$f_k = f(\theta_k) \tag{20}$$

Au point $X(k)$ seule la fréquence f_k va générer un champ lumineux à V en raison de l'équation de diffraction (18). Nous voulons obtenir les informations liées à cette fréquence localisée à chaque emplacement $X(k)$.

Considérons une fonction de base ψ qui est une fonction de base d'ondelettes ayant une fréquence centrale f. Pour chaque k dans H, nous pouvons obtenir

une fonction ψ en la translatant de façon à être centrée sur k et en la redimensionnant grâce au facteur d'échelle afin d'avoir une fréquence f_k donnant la fonction ψ_{k,f_k}. Nous définissons ψ^V comme :

$$\psi^V = \{\psi_{1,f_1}, \psi_{2,f_2}, \psi_{3,f_3}, ..., \psi_{n,f_n}\} \tag{21}$$

Pour obtenir chacun des poids d'ondelette (contributions) au champ d'onde diffracté à V, nous effectuons un produit scalaire de H avec chaque ondelette fournissant un ensemble C^V de coefficients d'ondelette. Ces coefficients vont générer le même champ lumineux à la position de l'observateur V que l'hologramme original H.

$$C^V = \{C_1, C_2, \ldots, C_n\} \tag{22a}$$

où,

$$C_k =< H, \psi_{k,f_k} >= \sum_{i=1}^{n} H(i)\psi^*_{k,f_k}(i) \tag{22b}$$

Le sous-hologramme pouvant générer un champ de lumière diffractée au point V est désigné par H^V. L'ensemble ψ^V représente une famille de fonctions d'ondelette qui sont centrées à chaque *k-ème* position sur l'hologramme et ont une fréquence f_k correspondant à la fréquence spatiale localisée en $X(k)$, afin d'obtenir une diffraction en V.

Si cette famille d'ondelettes ψ^V est orthogonale, alors le sous-hologramme H^V peut être obtenu à partir des coefficients C_k par:

$$H^V = \sum_k C_k \psi_{k,f_k} \tag{23}$$

Cette approche est une opération de calcul intensif et les *sous-hologrammes* (coefficients d'hologramme sélectionnés pour un point vue arbitraire) doivent être générés et stockés localement. Pour les cas 1D, le sous-hologramme H^V exige $L \times n$ multiplications complexes et $L \times n$ additions complexes, où L est le nombre de points discrets en ψ_{k,f_k}. En plus d'être une opération de calcul intensif, cette approche aura également besoin d'assez de mémoire pour stocker les vecteurs ψ^V pour chaque point discret dans l'hologramme, il y aura $L \times n$ valeurs. S'il n'y a n points d'observation, la mémoire nécessaire sera de $L \times n \times N$. Aussi le calcul aura besoin de $L \times n \times N$ multiplications complexes et $L \times n \times N$ additions complexes.

7.2 L'approche par Convolution

L'approche par convolution est un moyen rapide d'obtenir les coefficients d'un hologramme nécessaires pour former les sous-hologramme H'^V. Dans ce cas, nous supposons que l'observateur est assez loin de l'hologramme. Cette méthode implique l'utilisation d'une seule ondelette (ψ'^V) pour effectuer l'opération de sélection de fréquence. L'angle de diffraction de l'hologramme est très proche de l'angle suivant lequel le champ d'onde se propage, à savoir la direction générale entre l'hologramme et l'observateur.

La convolution de l'hologramme par la fonction d'ondelettes est notée

$$H'^V = H \circledast \psi'^V \tag{24}$$

Cette méthode est rapide puisque l'opération de convolution peut être réalisée dans le domaine fréquentiel comme une simple opération de multiplication. Mais le sous-hologramme généré par ce moyen ne permet pas

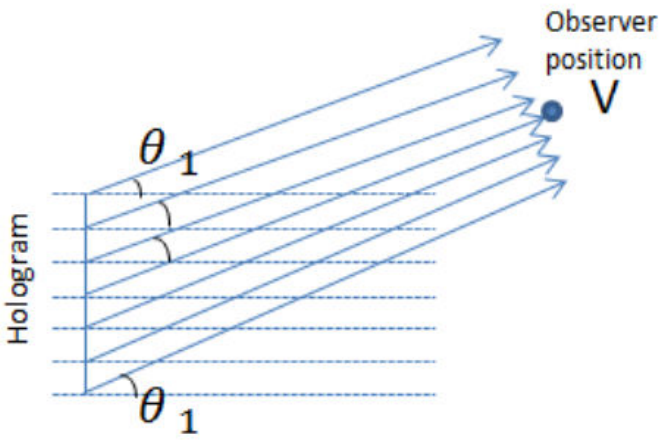

Figure 12: La diffraction au point V de l'hologramme H (la convolution)

une *reconstruction parfaite*. Il y aura une différence marquante dans le PSNR de reconstructions obtenu grâce au produit scalaire (référence) et par convolution. Cette différence est principalement dépendante de la transformée en ondelettes qui est utilisée. Les sections suivantes décrivent 2 ondelettes pour le système de représentation selon la position de l'observateur et comparent les reconstructions pour les 2 approches.

8 L'ONDELETTE DE MORLET

Les *'bonnes'* propriétés de localisation de l'ondelette de Gabor en font un candidat potentiel pour représenter les hologrammes dans un système de compression dépendante du point de vue. Mais encore une fois il y a plusieurs problèmes qui se posent avec les ondelettes de Gabor tels que l'échec sur la condition de recevabilité et un nombre inégal de sinusoïdes entre diverses fréquences [10, 12]. La recevabilité est une condition nécessaire pour obtenir le signal original depuis les coefficients des transformées en ondelettes [13]. L'inégalité du nombre d'oscillations des sinusoïdes au sein de la fonction gaussienne pour différentes fréquences entraîne un poids non uniforme des coefficients sur toutes les fréquences.

Nous avons rempli la condition de recevabilité en s'assurant que certaines conditions soient respectées, voir section (5.2). Nous présentons ici une meilleure méthode en éliminant la valeur DC pour toutes les translations et dilations pour chaque fréquence de la fonction de base de Gabor afin de former l'ondelette de Morlet. Cela permettra d'assurer que la condition de recevabilité est satisfaite. Aussi, nous allons nous assurer qu'il y a un nombre égal d'oscillations de la sinusoïde dans la fenêtre de la fonction gaussienne.

8.1 L'ondelette de Morlet discrétisée

Nous obtenons l'ondelette de Morlet en éliminant la valeur DC à partir de la base de la fonction de Gabor, en discrétisant l'ondelette de façon à ce que les critères de Nyquist soient validés et en s'assurant que le nombre

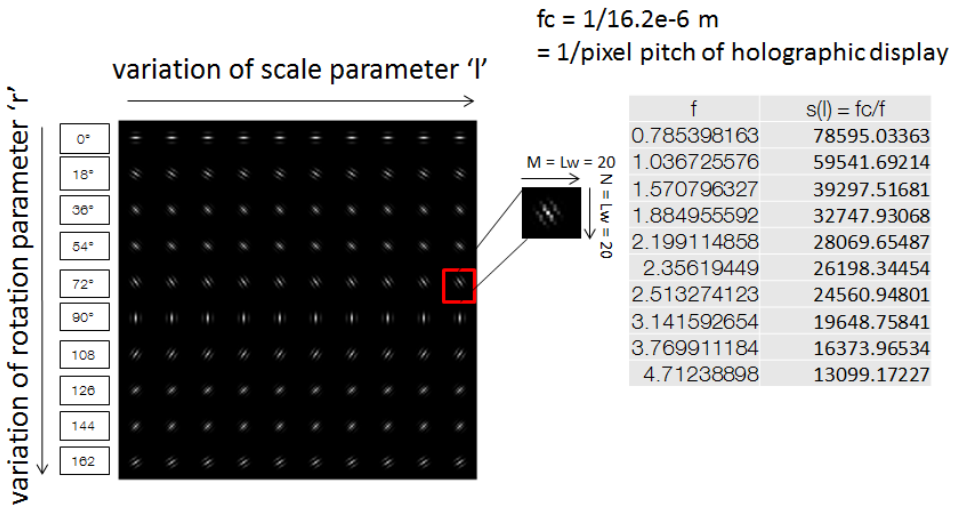

f	s(l) = fc/f
0.785398163	78595.03363
1.036725576	59541.69214
1.570796327	39297.51681
1.884955592	32747.93068
2.199114858	28069.65487
2.35619449	26198.34454
2.513274123	24560.94801
3.141592654	19648.75841
3.769911184	16373.96534
4.71238898	13099.17227

Figure 13: Discrétisation d'ondelette de Morlet

de sinusoïdes dans la fenêtre gaussienne soit le même. Le résultat est une ondelette de Morlet définie par :

$$\psi_{l,r}[m,n] = \exp\left(-\frac{f_c^2}{s_l^2\pi^2}(m^2+n^2)\right) \cdot \exp\left(2\pi^2\frac{f_c}{s_l\pi}j(m\cos(\Theta r)+n\sin(\Theta r))\right), \quad (25)$$

s

Les crochets représentent des paramètres discrets, où $-\frac{M}{2} \leqslant m < \frac{M}{2}, -\frac{N}{2} \leqslant n < \frac{N}{2}$ où M et N représentent les étalements des fonctions d'ondelettes dans le domaine spatial et sont des entiers. $l > 0$ et entier. $\Theta = \frac{\pi}{K}$ et $-K \leqslant r \leqslant K$ où K est le nombre total de rotations discrètes avec $K > 0$ entier. Il s'agit d'une fonction d'ondelettes qui est centrée sur f_c, mise à l'échelle par un paramètre discret l et orientée par le paramètre discret r.

La figure (13) montre la famille d'ondelettes de Morlet obtenue en faisant varier le paramètre discret d'orientation r et le paramètre discret d'échelle l.

Pour les deux approches (convolution et produit scalaire), nous nous assurons que l'opération est exécutée sur la taille physique exacte L de l'hologramme. Dans nos implémentations nous avons ré-échantillonné des portions de l'hologramme qui subissent une convolution ou des produits scalaires en fonction de la fréquence de la transformée en ondelette qui est utilisée. Le ré-échantillonnage effectue automatiquement une opération de filtrage passe-bas pour éliminer toutes les fréquences supérieures à $\frac{f_s}{2}$ où f_s est la fréquence d'échantillonnage.

9 L'ONDELETTE DE SHANNON

En vertu des hypothèses restrictives, nous avons besoin d'obtenir un sous-hologramme à la volée (*on the fly*) en effectuant l'élagage dans le domaine de la fréquence. Les hypothèses sont les suivantes:

- Il n'y a qu'un seul observateur

- La scène 3D doit être de taille importante, de grande résolution, et elle doit se trouver à une distance importante entre l'hologramme et l'observateur, etc. Ceci ne nous laisse qu'une petite fenêtre dans le plan d'observation

Avec la restriction d'avoir une grande scène ou une scène *immersive*, il n'est pas possible d'utiliser l'opération de convolution d'une fonction d'ondelettes unique pour obtenir les coefficients exacts de l'hologramme qui peuvent générer un champ vers un point arbitraire dans l'espace de l'observateur. C'est parce que la convolution nous permettra de ne recueillir que les coefficients de l'hologramme qui génèrent un champ dans la direction générale de l'observateur.

En testant diverses fonctions de fenêtre à la place de la fenêtre gaussienne (ondelettes de Morlet), nous avons constaté que l'utilisation de sinus cardinaux apporte des résultats intéressants qui indiquent que pour notre application, la localisation spatiale est primordiale et que le besoin d'une bonne localisation en fréquences peut être assoupli pour avoir une meilleure qualité de reconstruction. En outre, la transformée de Fourier de la fenêtre sinc (qui est une ondelette de Shannon) est une fonction fenêtre rectangulaire de Heaviside, qui permet d'accélérer le fenêtrage dans le domaine de la fréquence. Par conséquent, nous avons utilisé les ondelettes de Gabor et de Shannon dans notre mise en œuvre et comparé les résultats, voir Figure(14).

L'ensemble de la famille discrétisée d'ondelettes de Shannon est donnée par

$$\psi_k[u] = \sqrt{f_b[k]}(\mathrm{sinc}(f_b[k]u).\exp(j2\pi f_c[k]u)) \tag{26}$$

9.1 Equation d'ondelette de Shannon en 2D

La famille des ondelettes de Shannon 2D qui transforment l'hologramme pour générer une diffraction à V est donnée par

$$\begin{aligned}\psi_{k_x,k_y}[u,v] = f_b[k_x,k_y](\mathrm{sinc}(f_b[k_x,k_y](u+v))\\ .\exp(j2\pi f_c[k_x,k_y](u\cos\theta_{k_x,k_y} + v\sin\theta_{k_x,k_y})))\end{aligned} \tag{27}$$

La discrétisation est effectuée de la même façon que l'ondelette de Morlet, où le nombre de points de fenêtres discrètes L_w est maintenu constant pour toutes les fonctions d'ondelette et le produit scalaire est effectué par réechantillonnage afin que la partie de l'hologramme ait toujours le même L_w nombre de points discrets. Comme mentionné précédemment, ceci permet de réaliser un filtrage passe-bas naturel et toutes les fréquences au-dessus de $\frac{f_s}{2}$ (où f_s est la fréquence d'échantillonnage) seront automatiquement exclues.

10 RÉSULTATS

10.1 Reconstruction de l'hologramme *b<>com* dé

Dans cette section nous présenterons certains résultats pour le logo_dés hologramme. La scène est décrite comme:

- Pixel pitch = 8.1 µm
- Longeur d'onde = 11.08 µm

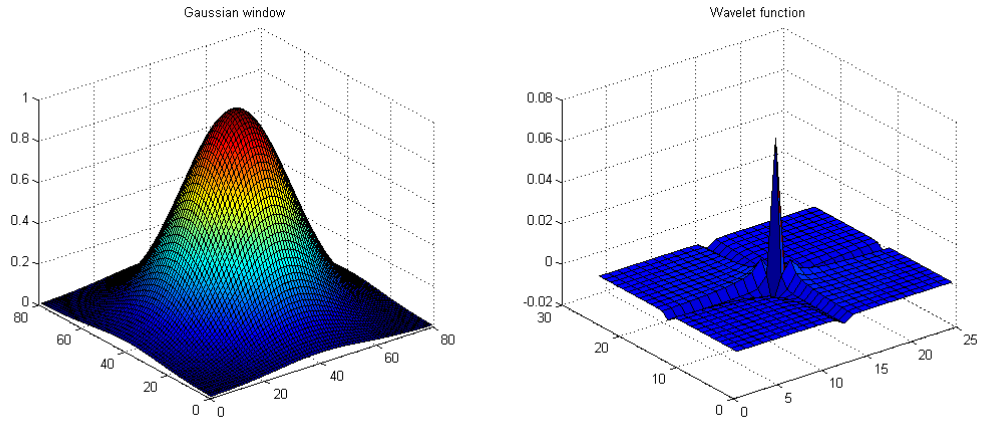

(a) Fenêtre gaussienne et fonction d'ondelettes de Morlet

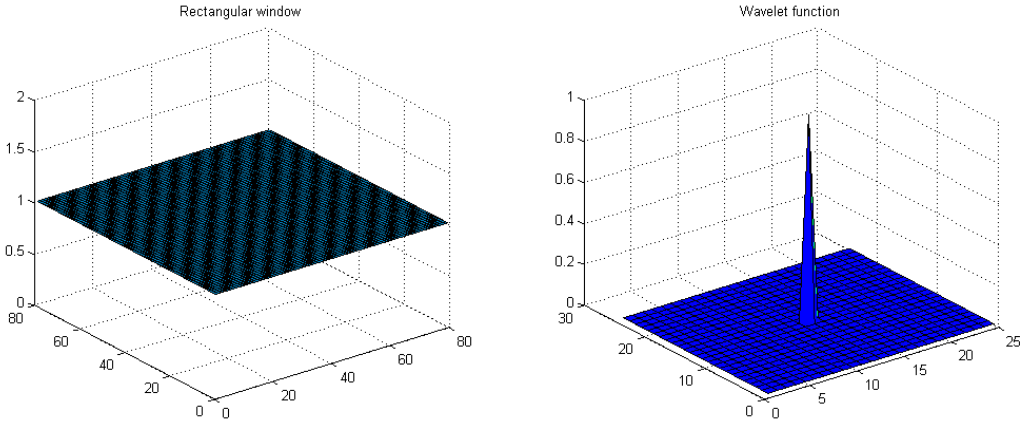

(b) Fenêtre rectangulaire et fonction d'ondelettes de Shannon

Figure 14: Fonctions fenêtre

- Dimensions = 2048x2048 pixels

La scène contient un dé qui est présent dans le plan de l'hologramme et un logo de *b<>com* à 0,0025m du dé derrière le plan de hologramme. C'est un objet de taille relativement petite. C'est pourquoi nous simulons l'observateur de façon à ce qu'il se trouve au maximum à 0,0025m à l'avant de l'hologramme. Il a été observé qu'à cette distance, seulement environ 25% des coefficients sont nécessaires pour la reconstruction de l'hologramme en simulant une ouverture de l'œil de 0,001m. Nous effectuons une comparaison avec l'approche par produit scalaire qui est notre référence et qui est détaillée dans la section (7).

L'hologrammee logo_dés est illustré sur la figure (15,16).

10.1.1 *Qualité de la reconstruction suivant sur le nombre de coefficients utilisés*

La figure (17) montre la variation de la qualité de la reconstruction en fonction des différentes tailles de fenêtre pour une fonction d'ondelettes de Shannon. Il doit être noté que dans le cadre de cette analyse, la simulation de l'ouverture de l'œil s'effectue avec un carré présentant 25% coefficients. Les différents groupes de coefficients retenus pour la reconstruc-

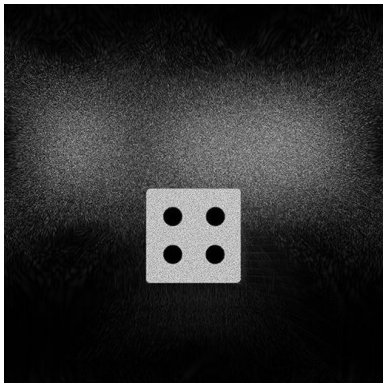

Figure 15: Amplitude de l'hologramme logo_dice

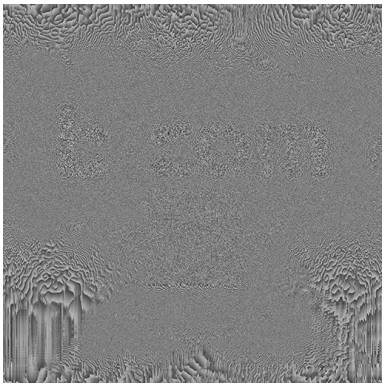

Figure 16: Phase de l'hologramme logo_dice

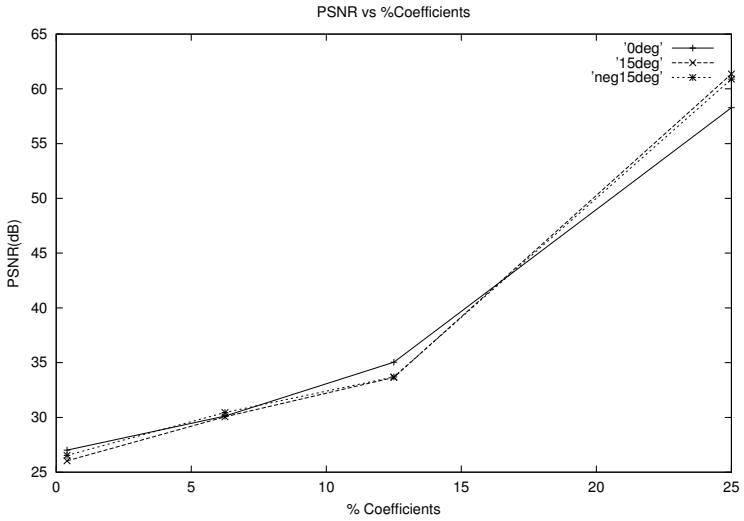

Figure 17: PSNR vs %Coefficients

tion (dans le plan de l'hologramme) sont $0,4\%, 6,25\%, 12,5\%, 25\%$ respectivement. Comme le nombre de coefficients augmente, le PSNR s'améliore comme illustré sur la figure (17).

10.1.2 *Dégradation de la qualité*

Ces expériences permettent d'évaluer la dégradation de la qualité pour le spectateur placé loin de la position d'émission (cas d'un retard ou de l'incertitude dans l'estimation de position). La figure(18) donne la qualité de la reconstruction pour des postes d'observation écartés de la position vers laquelle est émis l'hologramme par un angle maximal de 30 degrés. On remarque que la qualité se dégrade brutalement.

10.1.3 *Codage des coefficients selectionés*

Dans cette expérience nous comparons les ondelettes de Shannon et de Morlet suivant la référence, c'est-à-dire le résultat des produits scalaires appelé

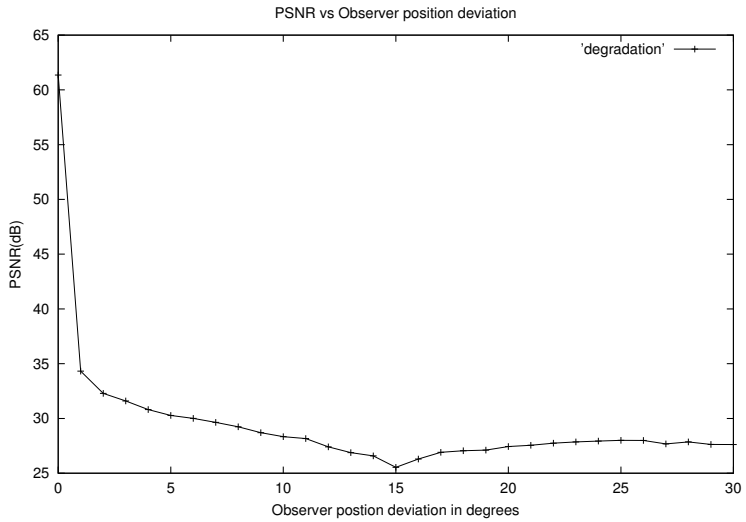

Figure 18: Dégradation de qualité

aussi reconstruction parfaite. Dans la figure (19) RD-plot sont obtenus à l'aide de 25% des coefficients pour des angles de visualisation de 0º et 15º, pour une résolution de l'hologramme de 2048x2048 pixels et pour 4 valeurs de quantification 3,5,6 et 8 bits. La quantification linéaire est effectuée sur les coefficients. *c.r* représente le ratio de compression entre l'hologramme transformé et l'hologramme original non-compressé, *bpp* (bits par pixel) est obtenu après le codage entropique des coefficients de la transformée et *dB* est le PSNR entre la référence ou reconstruction parfaite et l'hologramme transformé optimisé à l'aide des ondelettes de Shannon et des ondelettes de Morlet en utilisant l'approche par convolution. Il peut être observé qu'une quantification de 5 bits est suffisante pour obtenir une bonne approximation des coefficients. L'ondelette de Shannon offre les résultats de meilleure qualité car la fenêtre de filtrage spatial se rapproche très fortement de sa transformée de Fourier. Si la fenêtre gaussienne (Morlet wavelet) est utilisée, alors il y a une baisse dans la qualité, mais le résultat reste visuellement attrayant.

11 DESCRIPTION DE L'INTERFACE GRAPHIQUE

La mise en œuvre GUI pour le système d'affichage 3D est décrite dans cette section. La figure (20) montre l'interface graphique de l'utilisateur pour l'affichage en fonction du système de reconstruction.

Les contrôles et les fonctionnalités de l'interface graphique sont expliqués comme suit :

- Les hologrammes sont chargés à l'aide de (1) Bouton *Load Hologram*. Les hologrammes complexes peuvent être chargés en activant la case à cocher (6) *Complex*.
- Le fichier de paramètres qui est unique pour chaque scène et le périphérique d'affichage sont chargés à l'aide de (2) *Parameter file*. Ce fichier est requis lorsque vous travaillez avec le capteur Kinect.

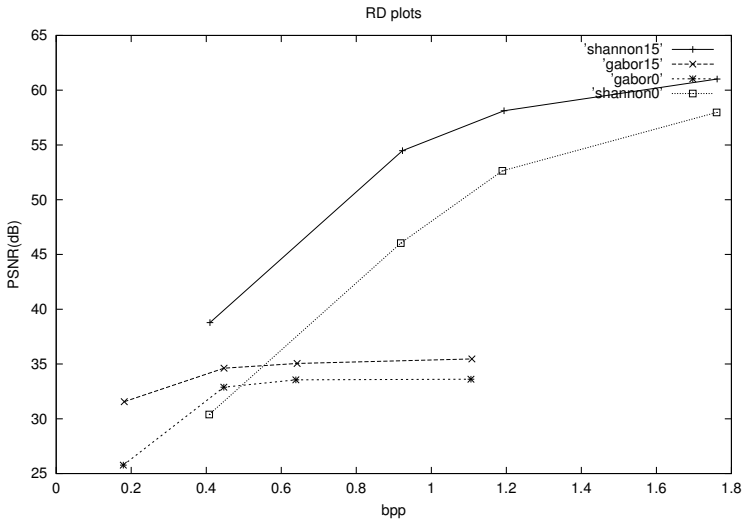

Figure 19: RD-plots avec Q=3,5,6,8 bits

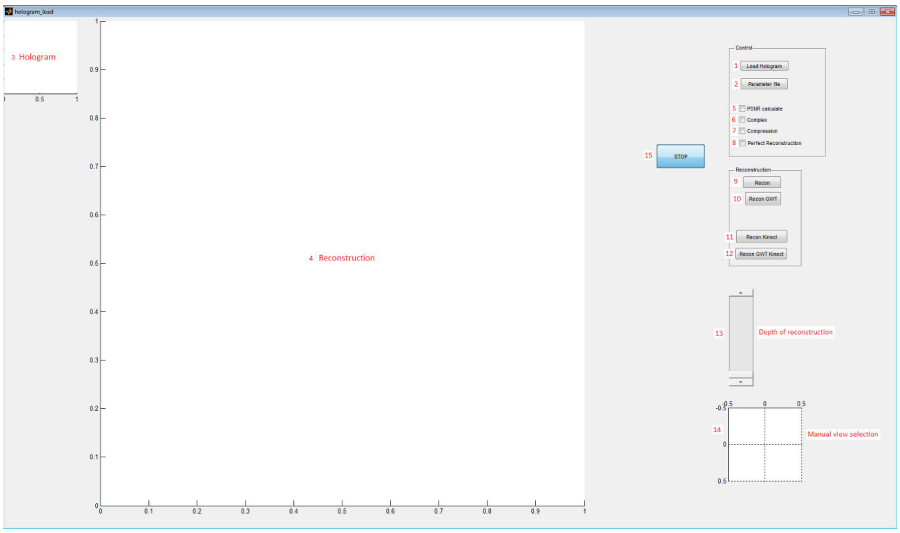

Figure 20: Interface graphique pour la représentation des hologrammes basée sur la position de l'observateur

- Pour effectuer la reconstruction, il est possible d'effectuer une reconstruction directe de l'hologramme sur un plan (9) *Recon* et (11) *Recon Kinect* ou en utilisant les transformées en ondelettes pour une représentation basée sur la position de l'observateur en utilisant la diffraction vers un point ou une ouverture (10) *Recon GWT* et (12) *Recon GWT Kinect*.
- Les fonctions de l'interface graphique présentent deux modes:
  - Mouse interface mode (9) et (10)
  - Kinect interface mode (11) et (12)
- La profondeur de reconstruction peut être modifiée en temps réel dans le mode d'interface en utilisant Kinect (13).
- La position de l'observateur à une profondeur fixe de reconstruction peut être obtenue en utilisant (14) dans le mouse interface mode.
- La simulation peut être arrêtée de force dans le kinect interface mode en utilisant le bouton (15) *STOP*.
- L'hologramme est chargé dans la fenêtre d'affichage (3).
- La reconstruction est obtenue dans la fenêtre (4).
- Le PSNR peut être calculé en comparant la reconstruction d'origine et les transformées en ondelette des reconstructions partielles à l'aide de la case à cocher (5) *PSNR Calculate*.
- Pour basculer entre l'approche *produit scalaire* et l'approche *convolution* des reconstructions, nous utilisons la case à cocher (8) *Perfect Reconstruction*.
- La compression en utilisant une quantification uniforme et le codage de Huffman est obtenue en utilisant la case à cocher (7) *Compression*.

12 CONCLUSION ET TRAVAUX PROCHAIN

La demande croissante de dispositifs d'affichage de reconstitutions visuelles 3D *qui semblent vivantes*, a poussé plusieurs scientifiques et chercheurs à employer des dispositifs tels que les appareils commerciaux d'affichage stéréoscopique; les désavantages sont minimes par rapport à la simple attraction de visualisation en 3D.

Avec la compréhension apportée par des années de recherche dans le domaine de la propagation de la lumière, les chercheurs d'aujourd'hui étudient la question de l'holographie avec un nouveau regain d'intérêt, afin d'être en mesure d'élaborer des systèmes d'affichage basés sur les technologies holographiques.

Ce mémoire présente un système de représentation d'hologramme adaptatif et scalable qui peut effectuer la reconstruction d'hologrammes en fonction de la position de l'observateur. Cette représentation exploite deux théories existantes de diffraction et de propagation de la lumière, à savoir les équations de *Grating equation* et *la propagation Angular Spectrum sur les plans inclinés*.

Le choix de ce type de système de représentation découle de la nécessité de réduire (*élaguer*) des portions de l'hologramme suivant la position

de l'observateur. Le champ autour de l'hologramme contient une grande quantité d'information. Ce champ complexe 3D contient toutes les informations optiques et physiques de l'objet, celles-ci sont recueillies au cours de la génération des hologrammes. À l'aide de la méthode angular spectrum de propagation sur plan incliné , nous prenons des coupes transversales de ce champ 3D afin de les propager vers le plan de l'observateur.

Les ondelettes sont utilisées à des fins d'élagage des hologrammes. La condition essentielle pour les ondelettes idéales est une *bonne* localisation en fréquence et en espace. Ce mémoire a tenu à expliquer en premier lieu pourquoi ces conditions sont nécessaires et à comparer les ondelettes de Gabor et les Fresnelets. Il est montré expérimentalement que les ondelettes de Gabor sont capables de supprimer les ordres indésirables créés dans le processus de reconstruction sans la nécessité de réaliser un filtrage spatial. Les ondelettes de Gabor nécessitent un nombre plus important de calculs complexes que les Fresnelets, d'où la nécessité d'optimiser l'opération de la transformée en ondelettes de Gabor en utilisant des processeurs multi-core ou des architectures multi-processeurs. Les *bonnes* propriétés de localisation des ondelettes de Gabor dans les domaines fréquentiel et spatial en font un choix évident pour la représentation des hologrammes numériques suivant la position d'observation. La transformée de Max-Gabor utilisée est intrinsèquement non réversible, mais peut être rendue réversible sous certaines hypothèses. La transformée de Max-Gabor a permis d'extraire les informations de fréquences localisées de l'hologramme.

Puis, il a été montré comment utiliser l'ondelette de Morlet pour la représentation des hologrammes numériques en fonction de la position de l'observateur. En commençant par la fonction de base de Gabor, nous avons surmonté le problème inhérent de non-admissibilité de l'ondelette de Gabor en éliminant la valeur DC dans toutes les décompositions de fonctions d'ondelettes de Morlet pendant l'analyse multirésolution. Nous avons détaillé la conception, la discrétisation et la mise en œuvre des ondelettes de Morlet pour le système de compression basé point de vue. À l'aide d'une architecture *client-serveur*, nous pouvons générer et stocker *hors ligne* les sous-hologrammes pour chaque point d'observation dans le plan d'observation discrétisé. Chaque sous-hologramme peut être transmis et reconstruit en temps réel grâce au suivi de l'observateur.

Enfin nous avons exploité une autre ondelette : l'ondelette de Shannon. Cette ondelette est bien localisée dans l'espace mais mal localisée en fréquence. L'avantage de cette ondelette est la réduction importante du temps de calculs permettant de générer et transmettre à la volée le sous-hologramme en fonction de la position de l'observateur. Une telle configuration est fondée sur l'hypothèse qu'il n'y a qu'un seul observateur, et que l'élagage dépend de la dynamique de la scène et de la taille de l'hologramme. Les réductions en termes de complexité et d'espace de stockage économisé par cette méthode sont trop importantes pour être négligées.

Comme dans tout projet de recherche il y a toujours des points d'amélioration et des pistes de développement dans l'avenir.

- La reconstruction des hologrammes selon le point d'observation est actuellement effectuée numériquement. Les limitations des SLMs pour les angles inférieurs de diffraction de l'hologramme ne nous permettent pas de reconstruire les hologrammes optiquement. Dans l'avenir, avec l'aide d'avancées dans la technologie SLM ayant des pas de pixels $< 1\mu m$, nous pourrons alors obtenir de grands angles d'affichage permettant la mise en œuvre optique de cette technique.

- Une étude plus poussée des ondelettes est nécessaire pour identifier de nouvelles ondelettes plus performantes pour élaguer l'hologramme. Actuellement, notre configuration implique l'utilisation d'une seule ondelette à la fois. En outre, les ondelettes peuvent être sélectionnées *on-the-fly* pour la transformée et l'élagage des coefficients en fonction des caractéristiques physiques. Par exemple, les ondelettes de Morlet peuvent être utilisées lorsque plusieurs spectateurs sont impliqués et peuvent être commutées au besoin en ondelettes de Shannon quand il n'y a qu'un seul observateur.
- Les hologrammes contenant des scènes vraiment immersives avec des angles de vision ($> 20^o$) doivent être générés pour effectuer des tests et valider le système holographique décrit dans ce mémoire. Grâce à l'utilisation d'une plus grande base de données de test, nous pourrions comprendre expérimentalement comment sélectionner les ondelettes suivant la dynamique de la scène.
- La compression des coefficients élagués est un autre domaine qui n'a pas été traité en détail dans ce travail. Nous avons limité nos expériences aux méthodes de codage entropique (codage de Huffmann), mais il existe un large éventail de méthodes de compression qui pourraient d'être exploitées. La corrélation entre les parties réelle et imaginaire de l'information complexe élaguée n'est pas bonne, et une étude doit être menée pour trouver une méthode de codage efficace pour comprimer ces données. Une corrélation peut être obtenue entre les coefficients issus de l'élagage des informations provenant de plusieurs points de vue proches les uns des autres. Ceci gagne à être étudié plus en détail et exploité.
- En termes d'évaluation de la qualité, nous avons effectué la comparaison en termes de MSE et PSNR de reconstructions obtenues entre les reconstructions d'origines (références) et la reconstruction d'un hologramme obtenue en utilisant une transformée en ondelettes. L'application de ces mesures aux hologrammes eux-mêmes ne peut pas prédire la qualité visuelle des reconstructions. L'holographie numérique pour les systèmes d'affichage 3D est un domaine naissant et une étude approfondie sur la mesure de la qualité de l'affichage holographique doit être effectuée.

REFERENCES

[1] R.Haussler and H.Stolle. Real-time holography. Technical report, SeeReal Technologies GmbH, Dresden Germany, 2008.

[2] Alison Shortt, Thomas Naughton, and Bahram Javidi. Compression of digital holograms of 3d objects using wavelets. *Optics Express*, 14(7), April 2006.

[3] Levent Onural. Diffraction from a wavelet point of view. *Optics Letters*, 18(11), June 1993.

[4] Y.Li, H.Szu, Y.Sheng, and J.Caulfield. Wavelet processing and optics. *IEEE Invited paper*, 1996.

[5] L.Onural and M.Kocetepe. Family of scaling chirp functions. *IEEE transaction in image processing*, 1995.

[6] Micheal Liebling, Thierry Blu, and Micheal Unser. Fresnelets: New multiresolution waveletbases for digital holography. *IEEE Transactions on Image Processing*, 12(1):29–43, January 2003.

[7] Michael Unser. Splines: A perfecr fit for signal and image processing. *IEEE Signal Processing magazine*, November 1999.

[8] J.Benedetto, C.Heil, and D.Walnut. Differentiation and balian-low theorem. *Journal of Fourier analysis and applications*, 1994.

[9] J.Zhong and L.Weng. Holographic research and technologies. *Intech Open*, 2011.

[10] T.S.Lee. Image representation of 2d gabor wavelets. *IEEE transactions on Pattern Analysis and Machine Learning*, 1996.

[11] Joseph W. Goodman. *Introduction to Fourier Optics*. Roberts and Company, 2005.

[12] Ole Christensen and Torben Jensen. An introduction to the theory of bases, frames and wavelets.

[13] Ingrid Daubechies. *Ten lectures on wavelets*. Society for Industrial and Applied Mathematics, 1992.

INSA de RENNES
Service des Formations

AVIS DU JURY SUR LA REPRODUCTION DE LA THESE SOUTENUE

Titre de la thèse:
Adaptive representation and reconstruction of digital holograms

Nom Prénom de l'auteur : VISWANATHAN KARTIK

Membres du jury :
- Monsieur DUFAUX Frédéric
- Madame MORIN Luce
- Monsieur BASKURT Atilla
- Monsieur GIOIA Patrick
- Monsieur ANTONINI Marc

Président du jury : Monsieur Atilla BASKURT

Date de la soutenance : 01 Décembre 2016

Reproduction de la these soutenue

Thèse pouvant être reproduite en l'état
~~Thèse pouvant être reproduite après corrections suggérées~~

Fait à Rennes, le 01 Décembre 2016

Signature du président de jury

A. Baskurt

Le Directeur,

M'hamed DRISSI

Résumé

On constate une forte augmentation de l'intérêt porté sur l'utilisation des technologies vidéo 3D pour des besoins commerciaux, notamment par l'application de l'holographie, pour fournir des images réalistes, qui semblent vivantes. Surtout, pour sa capacité à reconstruire tous les parallaxes nécessaires, afin de permettre de réaliser une vision véritablement immersive qui peut être observée par quiconque (humains, machine ou animal). Malheureusement la grande quantité d'information contenue dans un hologramme le rend inapte à être transmis en temps réel sur les réseaux existants. Cette thèse présente des techniques afin de réduire efficacement la taille de l'hologramme par l'élagage de portions de l'hologramme en fonction de la position de l'observateur. Un grand nombre d'informations contenues dans l'hologramme n'est pas utilisé si le nombre d'observateurs d'une scène immersive est limité. Sous cette hypothèse, éléments de l'hologramme peuvent être décomposés pour que seules les parties requises sensibles au phénomène de diffraction vers un point d'observation particulier soient conservés. Les reconstructions de ces hologrammes élagués peuvent être propagés numériquement ou optiquement. On utilise la transformation en ondelettes pour capter les informations de fréquences localisées depuis l'hologramme. La sélection des ondelettes est basée sur des capacités de localisation en espace et en fréquence. Par exemple, les ondelettes de Gabor et Morlet possèdent une bonne localisation dans l'espace et la fréquence. Ce sont des bons candidats pour la reconstruction des hologrammes suivant la position de l'observateur. Pour cette raison les ondelettes de Shannon sont également utilisées. De plus l'application en fonction du domaine de fréquence des ondelettes de Shannon est présentée pour fournir des calculs rapides de l'élagage en temps réel et de la reconstruction.

Abstract

With the increased interest in 3D video technologies for commercial purposes, there is renewed interest in holography for providing true, life-like images. Mainly for the hologram's capability to reconstruct all the parallaxes that are needed for a truly immersive views that can be observed by anyone (human, machine or animal). But the large amount of information that is contained in a hologram make it quite unsuitable to be transmitted over existing networks in real-time. In this thesis we present techniques to effectively reduce the size of the hologram by pruning portions of the hologram based on the position of the observer. A large amount of information contained in the hologram is not used if the number of observers of an immersive scene is limited. Under this assumption, parts of the hologram can be pruned out and only the requisite parts that can cause diffraction at an observer point can be retained. For reconstructions these pruned holograms can be propagated numerically or optically. Wavelet transforms are employed to capture the localized frequency information from the hologram. The selection of the wavelets is based on the localization capabilities in the space and frequency domains. Gabor and Morlet wavelets possess good localization in space and frequency and form good candidates for the view based reconstruction system. Shannon wavelets are also employed for this cause and the frequency domain based application using the Shannon wavelet is shown to provide fast calculations for real-time pruning and reconstruction.

INSA RENNES

N° d'ordre : 16ISAR 22 / D16 - 22

Institut National des Sciences Appliquées de Rennes
20, Avenue des Buttes de Coëmes • CS 70839 • F-35708 Rennes Cedex 7
Tel : 02 23 23 82 00 - Fax : 02 23 23 83 96